INFORMATION TO USERS

This manuscript has been reproduced from the microfilm master. UMI films the text directly from the original or copy submitted. Thus, some thesis and dissertation copies are in typewriter face, while others may be from any type of computer printer.

The quality of this reproduction is dependent upon the quality of the copy submitted. Broken or indistinct print, colored or poor quality illustrations and photographs, print bleedthrough, substandard margins, and improper alignment can adversely affect reproduction.

In the unlikely event that the author did not send UMI a complete manuscript and there are missing pages, these will be noted. Also, if unauthorized copyright material had to be removed, a note will indicate the deletion.

Oversize materials (e.g., maps, drawings, charts) are reproduced by sectioning the original, beginning at the upper left-hand corner and continuing from left to right in equal sections with small overlaps. Each original is also photographed in one exposure and is included in reduced form at the back of the book.

Photographs included in the original manuscript have been reproduced xerographically in this copy. Higher quality 6" x 9" black and white photographic prints are available for any photographs or illustrations appearing in this copy for an additional charge. Contact UMI directly to order.

UMI

A Bell & Howell Information Company
300 North Zeeb Road, Ann Arbor MI 48106-1346 USA
313/761-4700 800/521-0600

THE UNIVERSITY OF OKLAHOMA

GRADUATE COLLEGE

A STUDY OF SEMIACTIVE CONTROLS AND APPLICATIONS

A DISSERTATION

SUBMITTED TO GRADUATE FACULTY

in partial fulfillment of the requirements for the

degree of

DOCTOR OF PHILOSOPHY

By

JAE-SOO LEE

Norman, Oklahoma

1998

A STUDY OF SEMIACTIVE CONTROLS

AND APPLICATIONS

A DISSERTATION

APPROVED FOR THE SCHOOL OF AEROSPACE AND

MECHANICAL ENGINEERING

BY

deceased

Dr. William Neff Patten
(Committee Chairman)

Harold Stalford

Dr. Harold Stalford

Kevin A Grasse

Dr. Kevin. A. Grasse

Feng-Chyuan Lai

Dr. Feng-Chyuan Lai

Robert Anex

Dr. Robert Anex

ACKNOWLEDGMENTS

I would like to express my very sincere appreciation to Dr. William Neff Patten for his ideas, guidance and support through this work, and for serving as the chairman of his advisory committee. He left us for the better life on November 23, 1998

I also wish to express my gratitude to Dr. Harold Stalford, Director of School of Aerospace and Mechanical Engineering, Dr. Kevin A. Grasse, Chairman of Department of Mathematics, Dr. Feng-Chyuan Lai, Associate Professor of School of Aerospace and Mechanical Engineering and Dr. Robert Anex, Assistant Professor of School of Aerospace and Mechanical Engineering for serving as committee members and for their sincere evaluation of this dissertation.

Thanks to my colleagues of Controls Laboratory at the University of Oklahoma, especially Young-Kern Kang and Jeff Kuehn. I would like to thank to Mrs. Susan Wierimaa for her kindness. In addition, I thank to Sung Hun Chung for his contributions to excellent drawings.

There is no word to express my appreciation to my father-in-law and mother-in-low for their understanding and supports to complete this work. I would like to thank my mother, brothers and sister for their sacrifice, understanding and endless love. I am deeply indebted to my wife, Ye-La Min, my daughters, Vivien and Kaylee and son, Brian, for their encouragement, patience and love.

TABLE OF CONTENT

LIST OF FIGURES

LIST OF TABLES

NOMENCLATURE

A_p	Effective face area of the piston	m^2
A_{pipe}	Area of connection tubes of two chambers of SAVA	m^2
A_v	Orifice opening area of the valve	m^2
A_{vmax}	Maximum valve opening area	m^2
A_{vmin}	Minimum valve opening area	m^2
c_1	#1 linear damping coefficient of TDOF system	N/m/sec
c_2	#2 linear damping coefficient of TDOF system	N/m/sec
c_{eq}	Equivalent damping coefficient due to viscous friction F_f	N/m/sec
C_d	Discharge coefficient	-
C_H	Flow coefficient for the linear flow through the valve orifice	-
d	An equivalent diameter of valve orifice opening	m
D_h	Hydraulic diameters of the valve opening	m
diag	Diagonal matrix	-
F_d	Damping force	N
F_f	Viscous friction force between the piston and the cylinder walls of SA	N
F_h	Hydraulic force due to pressure difference	N
F_i	Hydraulic inertia force	N
k_1	Spring stiffness #1 of TDOF system	N/m
k_2	Spring stiffness #2 of TDOF system	N/m

l_e	Effective length of fluid that affects the inertia force	m
m_1	Mass #1 of TDOF system	kg
m_2	Mass #2 of TDOF system	kg
N_{Re}	Reynolds number	-
N_{Remax}	Maximum Reynolds number	-
P_1, P_2	Actuator chamber pressure	N/m^2
Q	Volumetric flowrate	m^3/sec
Q_t	Volumetric flowrate of turbulent flow	m^3/sec
sgn	Signum function	-
V_1, V_2	Volume of the actuator's each chamber	m^3
V_t	Total volume of the actuator chamber	m^3
X_d	System input, displacement	m
β	Bulk modulus of fluid	N/m^2
ΔP	Differential pressure between chambers of SAVA	N/m^2
ν	Kinematic viscosity of fluid	m^2/s
ρ	Density of fluid	kg/m^3
ρ_b, ρ_u	Control gains of the bistate controller and/or clipped optimal	-

ABSTRACT

This dissertation is devoted to three objectives: (1) the development of a method to estimate the damping characteristics of a hydraulic semiactive vibration absorber (SAVA), (2) the determination of bi-state control gains for a SAVA controller, and (3) the selection of an effective control scheme (among various control algorithms) for the closed loop operation of a system equipped with a SAVA.

The work begins with the validation of the hydraulic behavior of SAVA via experiment using both single- and two-degree-of-freedom test setups. The work demonstrates that the behavior of the SAVA remains closely tied to the Reynolds number of flow through a valve orifice. In addition the results indicate that for an exact analysis of SAVA, the frictional force between the piston body and the cylinder body should also be included.

The dissertation next reports the results of an investigation of how best to craft a Lyapunov control for the SAVA system. An analytical way to determine the control gains of a bi-state controller is presented. The stability of the SAVA system is also considered and it is shows that, given a bounded disturbance, the SAVA system will remain stable. Finally, the work reports experimental verification of a bi-state controller using a two-degree-of-freedom (TDOF) system.

Finally, the dissertation reports on a comparative analysis of various control architectures for the SAVA system. The work contrasts the performance of heuristic as well as analytical control algorithms.

While significant advances have been made in the study of semiactive hydraulic systems, there is still a need to further explore the issue of how to control a semiactive actuator. One key question that has hereto for remained unanswered is; among the many control rules posed for use with semiactive system, which gives the best performance. The purpose of this dissertation is to provide a comprehensive answer to that question. That task was accomplished here. To the author's knowledge, this is the first time. A comprehensive comparison of competing semiactive bistate controllers has appeared in the open literature.

아버지 어머니께

CHAPTER ONE

INTRODUCTION

This introduction chapter provides the reader first with a broad overview of the field of semiactive control practice. The first three sections of the chapter describe (1) in terms the hardware that comprises a semiactive control actuator, (hardware), (2) the history of the development of control algorithms for semiactive systems, and (3) a general history of semiactive applications in engineering. The chapter closes with an outline of the remaining chapters in the dissertation.

1.1 Hydraulic Model for Semiactive Vibration Absorbers

The greatest advantage to using semiactive dampers (SA) involves their low-level requirement of electrical power. SA systems are an ideal compromise between passive systems (which are inherently stable) and require no power and active systems (which are fully adjustable, but prove to instabilities and which require a significant power source). There are certain limitations to the effectiveness of a SA system when compared to active systems. Those limitations can be overcome to some extent by selecting a best methodology for the operation of the device.

The basic hardware first used in a hydraulic semiactive vibration absorber was initially suggested by Krasnicki [1979]. Wu et al. [1993] was among the first group of

investigators to give specific details of the hardware needed to realize a semiactive actuator. That design consisted of accumulators and a two-stage four port servo valve with (typical to active control systems) and a complicated system of check valves.

A SAVA operates with low levels of electrical power for signal processing and modulation of the valve orifice area. There is no need for line power, or a hydraulic pump. The force output of a SAVA may be varied by instantaneously modulating the area of the valve orifice. SAVA systems are particularly attractive to real applications, because the hardware required is inexpensive, technically simple, and readably available. The SAVA design has been shown to be an effective means of reducing the vibration of (1) structures [Patten et al. 1994a,b, 1996a,b], as well as (2) vehicles [Mo et al. 1996b].

The hydraulic SAVA consists of a two-chambered cylinder, a valve and piping that join the two chambers of the cylinder. Both chambers of the cylinder are filled with hydraulic fluid. (The layout of SAVA is shown in Figure 1.1).

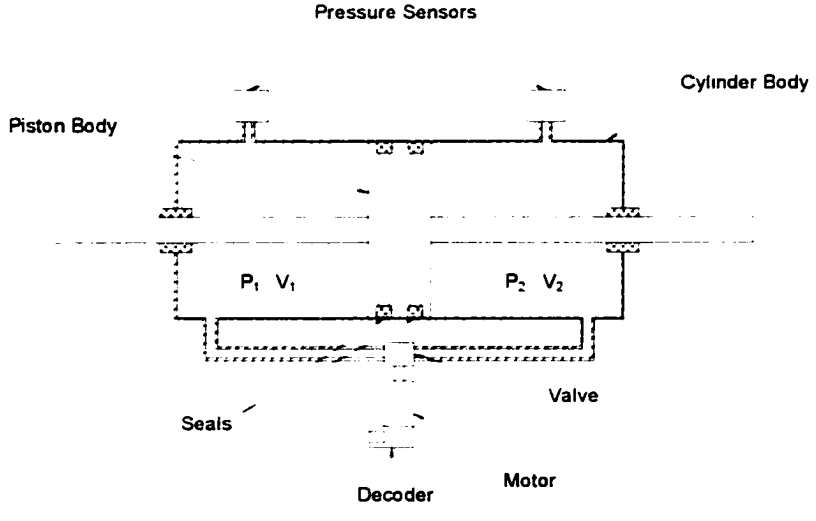

Figure 1.1 Schematic representation of SAVA

1.2 SAVA Control Algorithms

The purpose of a SAVA is to mitigate the dynamic response of the structure it is attached to. In order to provide mitigation, the valve of the SAVA is regulated using feedback signals obtained from sensors attached to the structure and the actuator. It has been said that there are as many different SAVA control schemes as there are investigator conducting SAVA research.

SAVA control schemes can be classified into two broad design categories; namely, continuous and discontinuous control. Both design strategies have advantages and disadvantages. The choice of which controller approach should be employed for a given application depends on the performance desired. The performance of different control schemes should be confirmed and compared for a particular application.

One typical approach to the discontinuous control of semiactive dampers is the "on-off" method, which is used to throttle the SAVA between minimum and maximum force levels. Krasnicki [1979], Miller and Nobles [1990] provide typical examples of "on-off" controllers for the suspension systems of vehicles. The drawback to the use of an "on-off" control is that it provides strong discontinuities that occur during switching, which can in turn cause unwanted control noise, harshness and component accelerations.

Optimal control designs have been applied to semiactive control systems for a number of years [Hrovat et al. 1981, Butsuen, 1989, Hac, 1992]. Optimal solutions are generally impractical however because they are computationally intensive, requiring

highly sophisticated computer hardware systems for real time operation. One "suboptimal" approach to the control of SAVA systems that has found utility is the "clipped optimal" controller introduced by Hrovat et al. [1988], Karnopp [1983] and Margolis [1983]. That technique when combined with feedback linearization produces a continuous control force as long as the demanded force from the SAVA is dissipative. When the desired force is nondissipative, the actuator is turned off.

The "on-off" control approach proves suitable for hydraulic valves with both high-speed performance, as well as their nonlinear characteristics. For example a bistate controller (based on the Lyapunov function candidates) is effective when certain nonlinear characteristics are encountered. Lyapunov stability theory represents a powerful mathematical tool for both the analysis and synthesis of nonlinear control systems. Despite the usefulness of the Lyapunov theory, little work has been done to demonstrate the effectiveness of that approach to semiactive systems. The work reported here provides a clear indication of the effectiveness of the Lyapunov control approach to semiactive system.

Patten et al. [1996b] proposed a bistate control algorithm for SAVA based on a Lyapunov approach in which the switching conditions were determined by the sign of a derived switching function. Leitmann [1994] applied the same approach to the control of a generalized (and linearized) semiactive actuator. As in other approaches to the design of control systems, one finds that the "gains" of the "on-off" control must be tuned to yield best results. Kalman and Bertram [1960] first demonstrated that a bistate control algorithm does not represent the optimal solution.

1.3 Historical Background

One of the first technical treatments of the performance of a hydraulic shock absorber is found in a paper by James and Ullery [1932]. There, the relationship between relief valve and temperature (to improve vehicle-riding comfort) was investigated. Much later, Segel and Lang [1981] presented a physics based model of a shock absorber with 82 parameters. That model proved too complex for computation and thus unsuitable for practical application. Wallaschek [1990] presented a method for the harmonic and stochastic linearization in shock absorber dynamics that produced a simple mathematical model with a small number of physical parameters.

The concept of semiactive (SA) force generation was first proposed by Crosby and Karnopp [1973]. They suggested that an active force generator be replaced by a continually-controllable damper. The assumptions made by those authors have provided the basis of a number of subsequent published works in which SA system control was investigated. Margolis et al. [1975] and Krasnicki [1979, 1980] demonstrated their control schemes using both analysis and experiment. Their results indicated that a SA suspension provides superior vibration isolation when compared to a conventional passive suspension.

Most of the work done to date on SA systems has been aimed the development of low cost adjustable shock absorbers for automobiles. Karnopp [1983] and Margolis [1983] suggested a semiactive controller for the two-degree-of-freedom (TDOF) quarter car model of an automotive suspension system; that control law is now referred

to as "clipped optimal" (CO). Previously, semiactive control schemes were applied to single-degree-of-freedom automotive chassis models [Crosby and Karnopp, 1973, Krasnicki, 1979, Margolis, 1982].

Alternative control algorithms for semiactive dampers have been proposed by Crosby and Karnopp [1973], Hrovat et al. [1988], Miller and Nobles [1990] and Patten et al. [1996a,b]. Specifically, Crosby and Karnopp [1973] and Hrovat et al. [1988] used a damper whose damping force could be modulated continuously. Miller and Nobles [1990] and Patten et al. [1996a,b] used an "on-off" type controllers.

Only a few researchers have applied semiactive dampers to structures for the reduction of structure vibration. For example, Hrovat et al. [1983] proposed a semiactive tuned mass damper (TMD) for structure control. Later, Singh et al. [1997] investigated the application of a sliding-mode control for the active and semiactive control schemes to structures subjected to seismic excitations. Symans et al. [1997] tested a multi-story, scale-model, building structure with a semiactive damper. That work assumed a piece wise linear damping behavior.

A few investigators (e.g., Leitmann [1994], Patten et al. [1993, 1996a]) have demonstrated the application of the Lyapunov method to semiactive control. That method produces a bistate controller. An important problem associated with the synthesis of a Lyapunov controller is the selection of the Lyapunov functions. This dissertation will explore that difficulty.

1.4 Outline of the Dissertation

The hydraulic semiactive device developed by Patten et al. [1993, 1994, 1996a,b] consists of an external bypass loop containing a motor-controlled valve. Consequently, its mathematical model that describes the device is nonlinear. The work conducted by this researcher has indicated that it is extremely important to analyze the hydraulic characteristics of SAVA with as much precision as possible. A hardware design procedure for a hydraulic SAVA is presented in Chapter Two. The purpose of Chapter Two is to verify the mechanistic model of a SA damper via experiments.

A semiactive bistate control scheme, based on a Lyapunov synthesis, is investigated in Chapter Three. The effectiveness of the SAVA system is investigated by applying it to a seismic structure. The analytical results are also verified via experiments.

In Chapter Four, the performance of various bang-bang type controllers are compared to the Lyapunov control when applied to seismic structure. Simulation is used to compare the relative effectiveness of each control scheme. The comparisons are made for differing arrangements of the actuator topology.

In Chapter Five, a similar comparative analysis is conducted for a semiactive vehicle suspension. In the last chapter, recommendations for future work are offered, and conclusions regarding the various compared control algorithms are offered.

CHAPTER TWO

DESIGN PARADIGM FOR SAVA

2.1 Introduction

This chapter describes a hardware design procedure for hydraulic semiactive vibration absorbers (SAVA). The work involved fills a significant gap in the literature, since very little information exists on the actual selection of hardware for a SAVA system. The selection of SAVA hardware is based on two performance criteria: (1) the desired passive damping for a nominal configuration and (2) the bandwidth of the adjustable damper that is needed to achieve a particular objective. The methods used to select SAVA hardware are demonstrated using both a single-degree-of-freedom (SDOF) and a two-degree-of-freedom (TDOF) system.

The testing of SAVA devices suggests that a rational preselection of the hardware can save an enormous amount of time and effort by minimizing the time normally required to tune the control-system design. A poor preselection of components can quite often waste the benefit originally expected from the closed loop operation of the system. The following text describes the simple procedures that, when followed, produce a reasonable selection of the SAVA hardware. Once selected, then the system can be tuned for near optimum performance. Examples of the experimental testing used to verify and iteratively refine a hardware design are included in the text here.

2.2 Theoretical Background

The following paragraphs point out certain issues that ought to be considered when selecting a nominal SAVA hardware design. The approach relies on the notion that, while a multi-component automotive chassis, for example, is required to operate over a broad band of frequencies; an adjustable damper should effect the dynamics of the critical modal frequencies of the system in a beneficial way. Moreover, the basic design of the SAVA system should provide performance equal to or better than a standard damper, when the SAVA operated in its passive mode. The work begins with the characterization of the flow through the valve orifice. When the valve is open, the flow through the system may be either laminar or turbulent. If the piping is large enough (and if the valve affords no constriction when open), then laminar flow will prevail. In that case, the damping provided by the device is linearly related to the difference in pressure drop across the valve orifice. For the more general case of turbulent flow, the damping exhibits a nonlinear characteristic. In order to assure that the hardware for such a design provides nominal levels of performance, the designer must first establish a target hardware configuration.

Laminar flow through the valve orifice is first considered. In this case, the flow inside the pipe can be expressed as [Yeaple, 1996]:

Laminar flow

$$Q_P = \frac{\pi d^4}{128 \rho \nu L} \Delta P \tag{2.1}$$

where ν represents the kinematic viscosity of the fluid, ρ represents the average density of fluid and L represents the characteristic length of the flow chamber. This equation is known as the Hagen-Poiseuille equation, where the actual flow through the valve can be assumed as:

$$Q_L = C_H Q_P \tag{2.2}$$

where C_H represents the flow coefficient for the linear flow through the valve orifice. When the velocity of flow through the valve is high (or the ratio of the area between valve orifice and inner pipe is small) the flow rate through the valve orifice can be expressed as

Turbulent flow

$$Q_T = sgn(\Delta P) C_d A_V \sqrt{\frac{2 \Delta P}{\rho}} \tag{2.3}$$

Here, Q_T represents a volumetric flow rate of turbulent flow, while ΔP represents the pressure difference across the valve (or orifice) and ρ represents the average fluid density. Here, *sgn* represents the standard signum function. C_d is defined as the

discharge coefficient for a given valve where $0 \le C_d \le 1$. The hydraulic force due to pressure differences occurring inside a hydraulic cylinder can be expressed as

$$F_h = A_p \Delta P \tag{2.4}$$

where A_p is the effective face area of a piston (see Figure 2.1).

The fluid to be incompressible, then the flow through the valve must equal the flow out of (or into) one of the two piston chambers;

$$Q_{piston} = A_p \dot{s} . \tag{2.5}$$

which suggests that

$$A_p \dot{s} = \begin{cases} Q_L & \text{(laminar)} \\ Q_T & \text{(turbulent)} \end{cases} \tag{2.6}$$

Substitution of Equations (2.1) and (2.3), and solving for ΔP yields

$$F_h = A_p \Delta P = \begin{cases} c_L \dot{s} & \text{(laminar)} \\ c_T \dot{s}^2 & \text{(turbulent)} \end{cases} \tag{2.7}$$

where

$$\begin{cases} c_L = \dfrac{128 \rho v L A_p^2}{\pi d^4 C_H} \\ c_T = \dfrac{\rho A_p^3}{2 A_v^2 C_d^2} \end{cases} \tag{2.8}$$

Here, d represents the equivalent diameter of the valve orifice opening.

If the flow is considered compressible, then it can be shown [Merritt, 1967, Watton, 1989] that the hydraulic continuity requires that

$$\Delta\dot{P} = \frac{\beta(V_1 + V_2)}{V_1 V_2}(A_p \dot{s} - Q_{pipe}) \tag{2.9}$$

where

$$Q_{pipe} = \begin{cases} Q_L & \text{(laminar)} \\ Q_T & \text{(turbulent)} \end{cases} \tag{2.10}$$

Here, V_1 and V_2 represent the volumes of each chamber of the actuator (Figure 2.1). The Reynolds number can be used to distinguish between laminar and turbulent flow. Specifically, the Reynolds number for flow through a valve is defined as

$$N_{Re} = \frac{Q_{pipe} D_h}{\nu A_v} \tag{2.11}$$

where D_h is the hydraulic diameter of the valve orifice opening [Yeaple, 1996] and A_v is orifice opening area of the valve. The Reynolds number for transition from laminar to turbulent flow through a valve has been established by Dulay et al [1988] as.

$$N_{Re\ transition} \approx 100. \tag{2.12}$$

The hydraulic inertia force of the fluid inside the hydraulic cylinder of SAVA can be calculated as [Dulay et al, 1988, Audenino and Belingardi, 1995]

$$F_i = m_e \ddot{z}(t) = \rho l_e A_{pipe} \ddot{z}(t) \tag{2.13}$$

where l_e is the effective length of fluid that affects the inertia force, which can then be determined from the experimental results of the SAVA. This value can be ascertained when comparing the test result and simulation of a given system.

The continuity equation of incompressible flow between the pipe and the cylinder body can be represented (see Figure 2.1) as;

$$A_{pipe}\dot{z}(t) = A_p\dot{s}(t). \tag{2.14}$$

The inertia force of the hydraulic cylinder can therefore be expressed relative to the piston body as

$$F_i = \rho l_e A_p \ddot{s}(t). \tag{2.15}$$

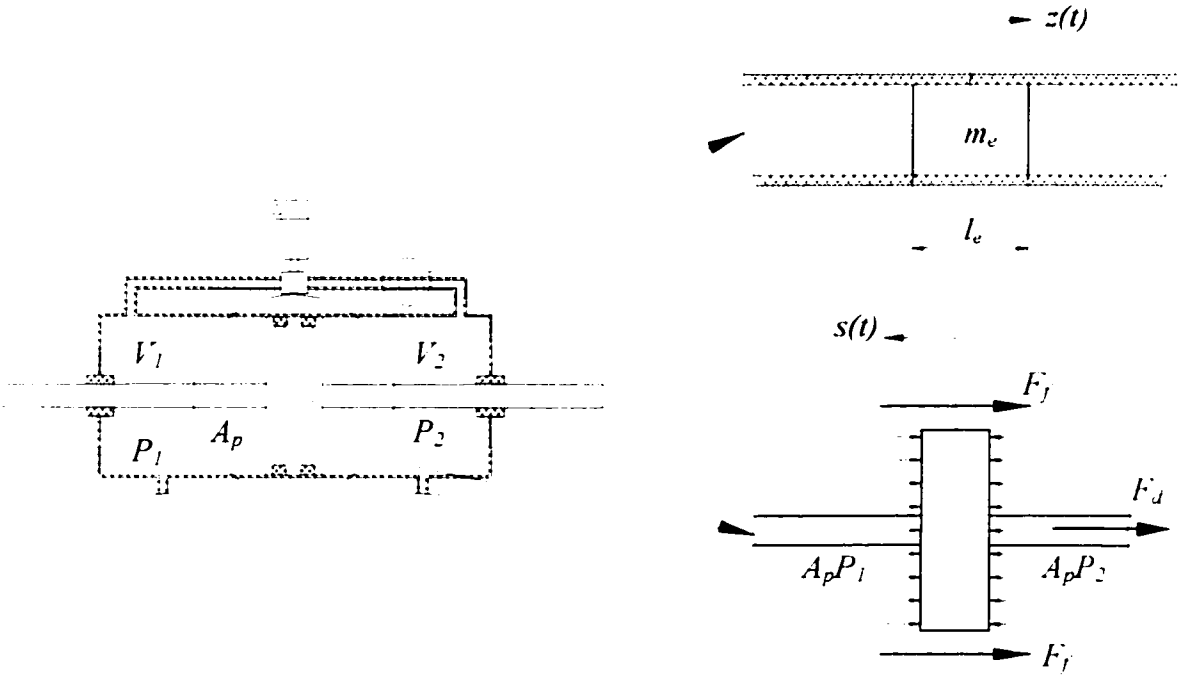

Figure 2.1 Schematic representation of force distribution of SAVA

Viscous friction force

A frictional force may exist between the piston and the cylinder walls of the SAVA actuator. It can be assumed that the flow through the clearance between the piston body and the cylinder body is Newtonian. The friction force exerted by the piston motion can then be calculated according to the relation

$$F_f = A_f \tau = \frac{A_f \rho \nu}{\delta} \dot{s} \tag{2.16}$$

where A_f represents the effective contact area of the piston body with the respect to the cylinder body, while δ represents the clearance between the piston body and the cylinder body. This frictional force exerts an equivalent damping force F_f proportional to the velocity

$$F_f = c_{eq} \dot{s} \tag{2.17}$$

where

$$c_{eq} = \frac{A_f \rho \nu}{\delta} \tag{2.18}$$

In light of the above, then the total hydraulic damping force of the cylinder can be represented as

$$F_d = A_p (P_1 - P_2) + F_f + F_i = F_h + F_f + F_i \tag{2.19}$$

In the sections that follow, various test procedures are described that were used to verify the characteristics of the semiactive hydraulic hardware.

2.3 Experimental Setup

Two different test rigs configuration were used to verify the SAVA actuator dynamics. Both configurations are discussed next.

2.3.1 A single-degree-of-freedom SAVA test rig

The single-degree-of-freedom (SDOF) test rig is shown in Figure 2.2.

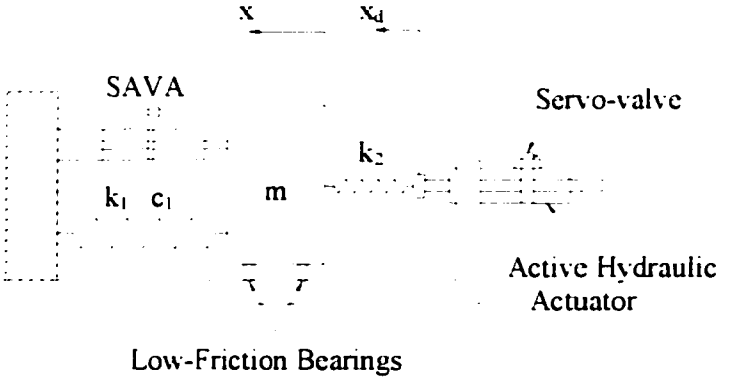

Figure 2.2 Schematic representation of test rigs of SDOF

The equation of motion for the system shown in Figure 2.2 is

$$m\ddot{x} + c_1\dot{x} + (k_1 + k_2)x = F_1 + k_2 x_1 \tag{2.20}$$

The hydrodynamic coupling equation of SAVA is [Patten, 1994b, 1996a]

$$\Delta\dot{P} = \frac{\beta(V_1 - V_2)}{V_1 V_2}\{A_p\dot{x} - Q_{pipe}\} \tag{2.21}$$

where β is the bulk modulus. Defining $X = \{x, \dot{x}\}^T$, then the state equation for the system takes the form.

$$\dot{X} = AX + Bg(X) + E\,X_d \tag{2.22}$$

where

$$A = \begin{bmatrix} 0 & 1 \\ -\dfrac{k_1 + k_2}{m} & -\dfrac{c_1 + c_{eq}}{m} \end{bmatrix} \tag{2.23 a}$$

$$B = \begin{bmatrix} 0 & -\dfrac{A_p}{m} \end{bmatrix}^T, \quad E = \begin{bmatrix} 0 & \dfrac{k_2}{m} \end{bmatrix}^T, \quad g(X) = \Delta P \tag{2.22 b, c}$$

A two-degree-of-freedom test rig was also used in the verification effort. That rig is described next.

2.3.2 A two-degree-of-freedom SAVA test rig

Figure 2.3 represents the experimental setup for the TDOF system:

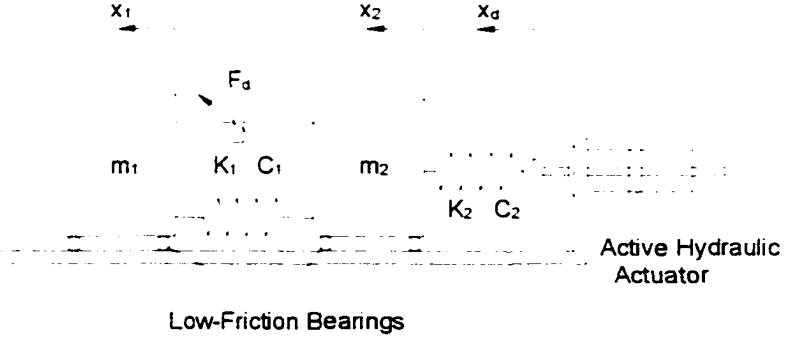

Figure 2.3 Schematic representation of TDOF test rigs.

Here, two masses are mounted on low-friction bearings. The equations of motion for system are

$$m_1 \ddot{x}_1 = -k_1(x_1 - x_2) - c_1(\dot{x}_1 - \dot{x}_2) - F_d$$
$$m_2 \ddot{x}_2 = k_1(x_1 - x_2) + c_1(\dot{x}_1 - \dot{x}_2) - k_2(x_2 - x_d) - c_2(\dot{x}_2 - \dot{x}_d) + F_d \quad (2.24)$$

The hydrodynamic coupling equation is

$$\Delta\dot{P} = \frac{\beta(V_1 + V_2)}{V_1 V_2}\{A_p(\dot{x}_1 - \dot{x}_2) - Q_{pipe}\}. \quad (2.25)$$

Defining

$$X = \{x_1 \quad x_2 \quad \dot{x}_1 \quad \dot{x}_2\}^T, \quad X_d = \begin{Bmatrix} x_d \\ \dot{x}_d \end{Bmatrix} \quad (2.26)$$

then

$$\dot{X} = AX + Bg(X) + EX_d \quad (2.27)$$

where

$$A = \begin{bmatrix} 0 & 0 & 1 & 0 \\ 0 & 0 & 0 & 1 \\ -\frac{k_1}{m_1} & \frac{k_1}{m_1} & -\frac{c_1 + c_{eq}}{m_1} & \frac{c_1 + c_{eq}}{m_1} \\ \frac{k_1}{m_2} & -\frac{k_1 + k_2}{m_2} & \frac{c_1 + c_{eq}}{m_2} & -\frac{c_1 + c_{eq} + c_2}{m_2} \end{bmatrix} \quad (2.28\text{ a})$$

$$B = \begin{bmatrix} 0 & 0 & -\frac{A_p}{m_1} & \frac{A_p}{m_2} \end{bmatrix}^T, \quad E = \begin{bmatrix} 0 & 0 & 0 & \frac{k_2}{m_2} \\ 0 & 0 & 0 & \frac{c_2}{m_2} \end{bmatrix}^T \quad (2.28\text{ b, c})$$

A discussion of the model verification process follows next.

2.4 Model Verification

The material presented here is intended to provide an indication of the extent to which the hydraulic SAVA model predicts the actual process dynamics. Both the single-degree-of-freedom the two-degree-of-freedom test rigs were employed. Each test presents the open loop response of the system for the open valve condition (A_v A_{vmax}) and the condition when the valve is partially closed (A_v = 33% of A_{vmax}). The physical parameters of SAVA are given in Table 2.1. The hydraulic fluid was pre-charged in order to reduce the effect of entrained air in the fluid.

Table 2.1 Physical parameters of SAVA

Description	Notation	Unit	Values
Effective piston area	A_p	m^2	1.0433×10^{-3}
Valve fully open area	A_{vmax}	m^2	1.8096×10^{-5}
Volume # 1	V_1	m^3	1.043×10^{-3}
Volume # 2	V_2	m^3	1.043×10^{-3}
Stroke	-	M	0.1016
Pre-charged pressure	P_o	N/m^2	1.03×10^{6}
Damping coefficient	c_{eq}	N/m/sec	545

2.4.1 Single-degree-of-freedom

The parameters that define the SDOF test rig are given in Table 2.2. A sinusoidal disturbance input was used for the experiment.

Table 2.2 Physical parameters of SDOF system

Description	Notation	Unit	Values
Mass	m	Kg	141
Spring stiffness # 1	k_1	N/m	28000
Spring stiffness # 2	k_2	N/m	125270
Damping coefficient	c_1	N/m/sec	100

Tests were conducted with the valve set at the following two conditions:

Case 1: Valve Fully Open ($\theta = 0°$)

Figures 2.4 through 2.15 depict the measured versus simulated response of the SDOF to open loop inputs with the valve fully open. The data shown there represents the steady-state responses of the SDOF system. Figures 2.4 through 2.7 depict the comparisons between experiment and simulation when the input disturbance is $x_1 = 0.005\sin(6\pi t)$. Here, the Reynolds number of fluid flow through the valve changes with the respect to the variation of relative velocity of SAVA, but the maximum Reynolds number ($N_{Remax} \leq 100$) indicates that the flow in this case is laminar ($\omega = 3$Hz).

Figures 2.4 and 2.5 depict the force-displacement and acceleration-displacement response. The corresponding differential pressures in each chamber of the actuator are shown in Figure 2.6 relative to the initial charge pressure (i.e., 1.03×10^6 N/m^2).

The statistical average of the measured force-velocity data (Figure 2.7) indicates a direction dependent characteristic. A simulation, with and without the inertia effect is also shown there.

A second test using 4Hz sinusoidal input was conducted for comparison purposes. The response data is shown in Figures 2.8 through 2.11. The computed Reynolds number for this case was N_{Remax} = 284 (turbulent flow). The force-velocity response (Figure 2.11) again indicates that the model provides near fidelity when fluid inertia is included. The force-velocity response (measured versus simulated) for a 5Hz input is shown in Figure 2.15. The three tests confirm the accuracy of the proposed model of the SAVA.

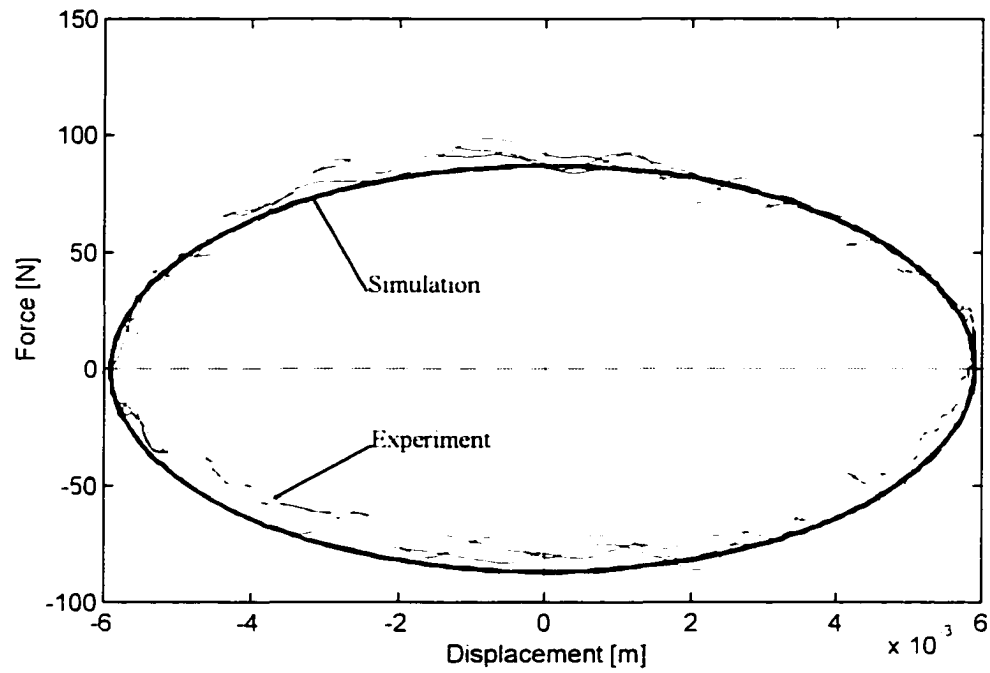

Figure 2.4 Comparison of force-displacement responses when the valve is fully open with disturbance input, $x_d = 0.005\sin(6\pi t)$, $C_H = 0.45$.

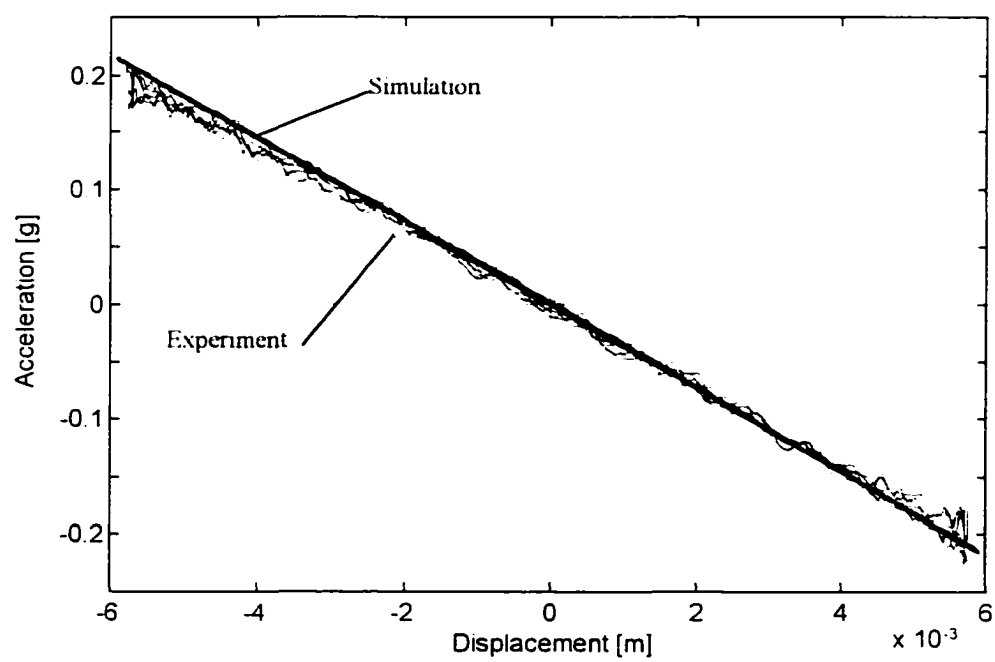

Figure 2.5 Comparison of acceleration-displacement responses when the valve is fully open with disturbance input, $x_d = 0.005\sin(6\pi t)$, $C_H = 0.45$.

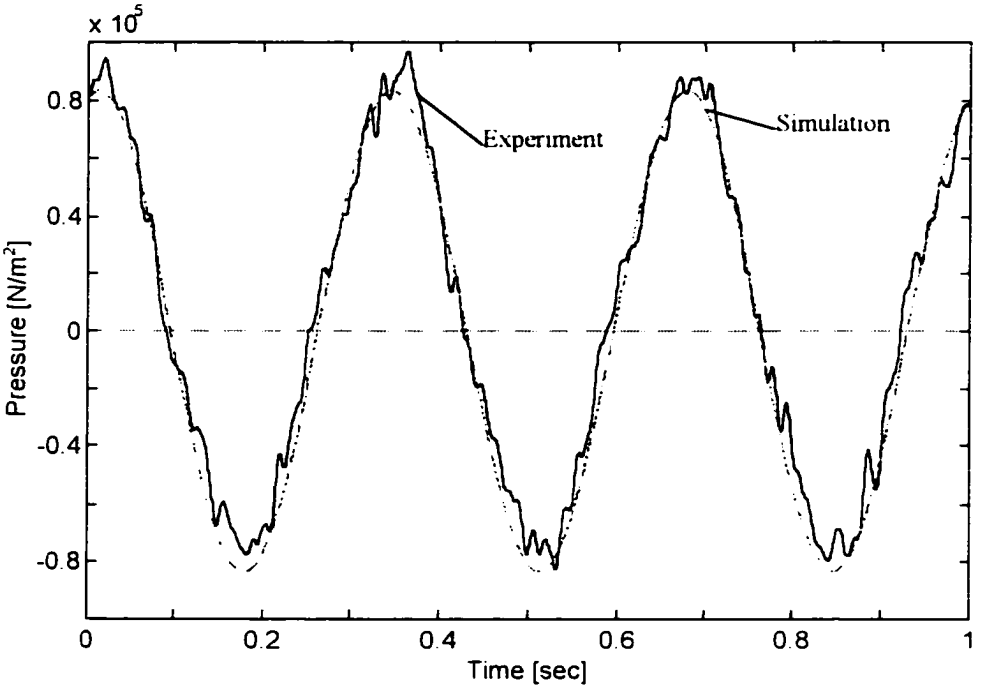

Figure 2.6 Comparison of the variation of differential pressure when the valve is fully open with disturbance input, $x_d = 0.005\sin(6\pi t)$, $C_H = 0.45$.

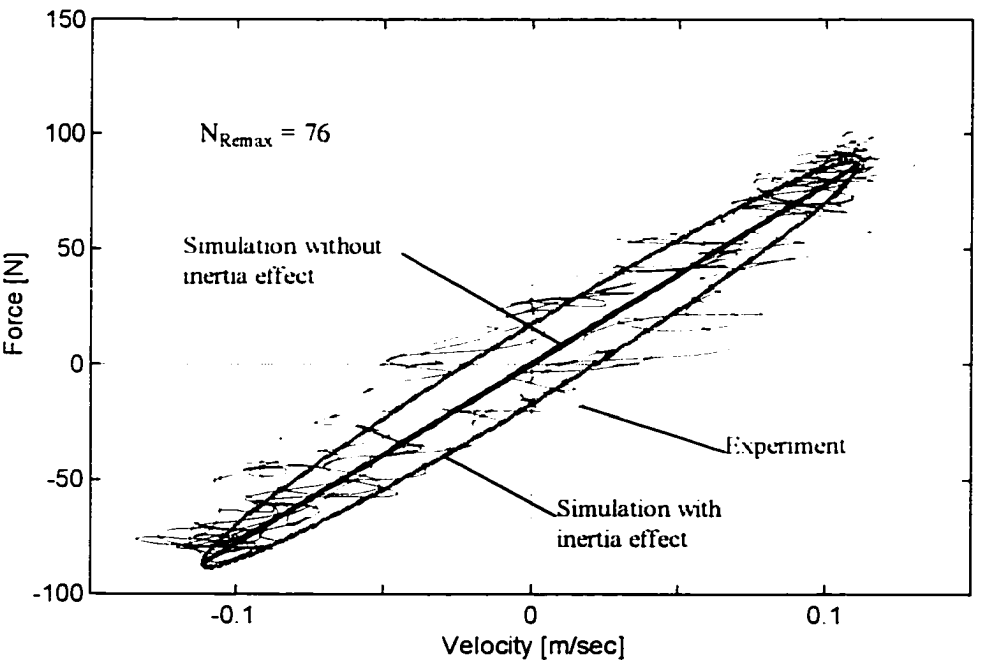

Figure 2.7 Comparison of the inertia effect when the valve is fully open with disturbance input, $x_d = 0.005\sin(6\pi t)$, $C_H = 0.45$.

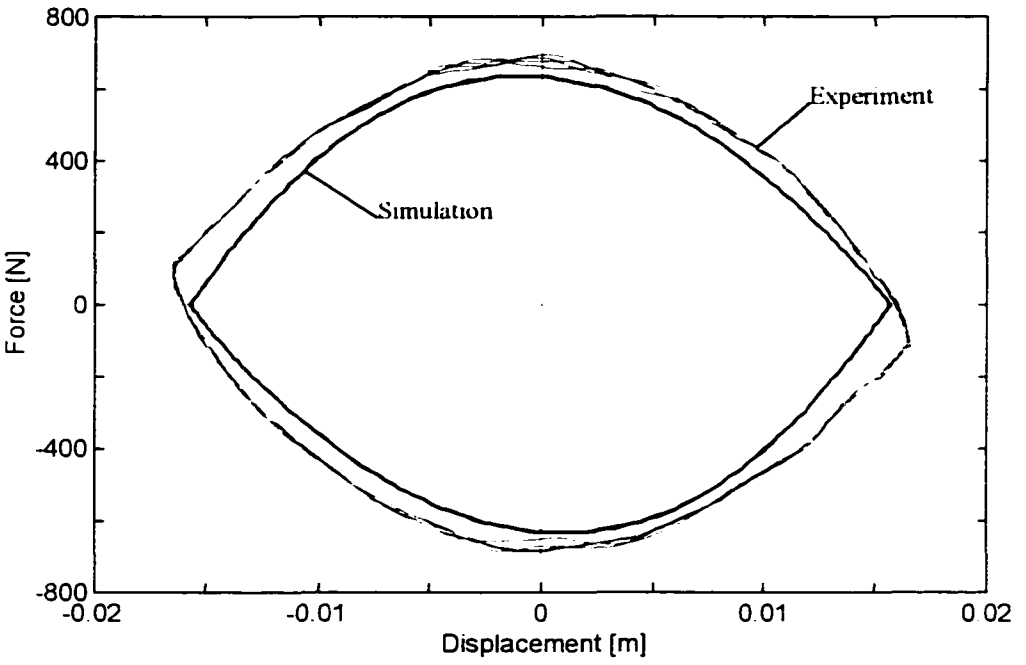

Figure 2.8 Comparison of force-displacement responses when the valve is fully open with disturbance input, $x_d = 0.01\sin(8\pi t)$, $C_d = 0.65$

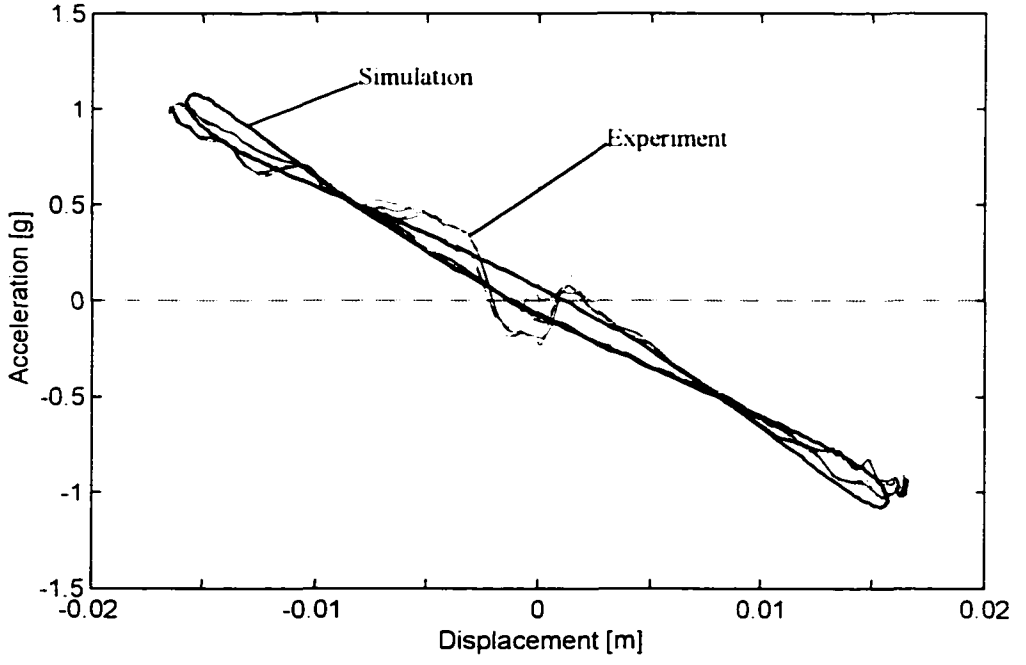

Figure 2.9 Comparison of acceleration-displacement responses when the valve is fully open with disturbance input, $x_d = 0.01\sin(8\pi t)$, $C_d = 0.65$.

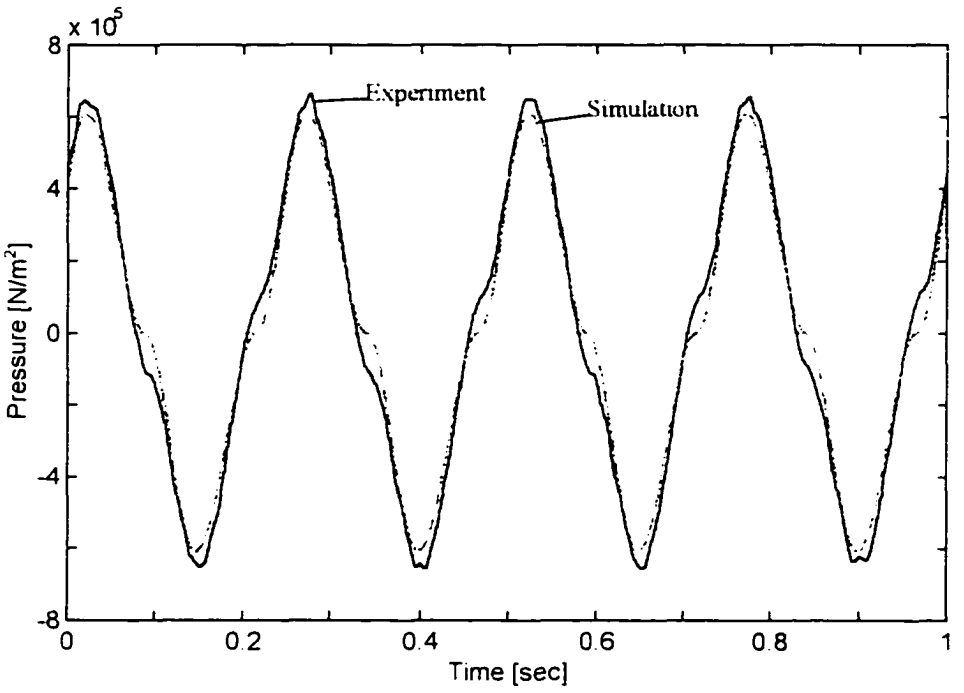

Figure 2.10 Comparison of the variation of differential pressure when the valve is fully open with disturbance input, $x_d = 0.01\sin(8\pi t)$, $C_d = 0.65$.

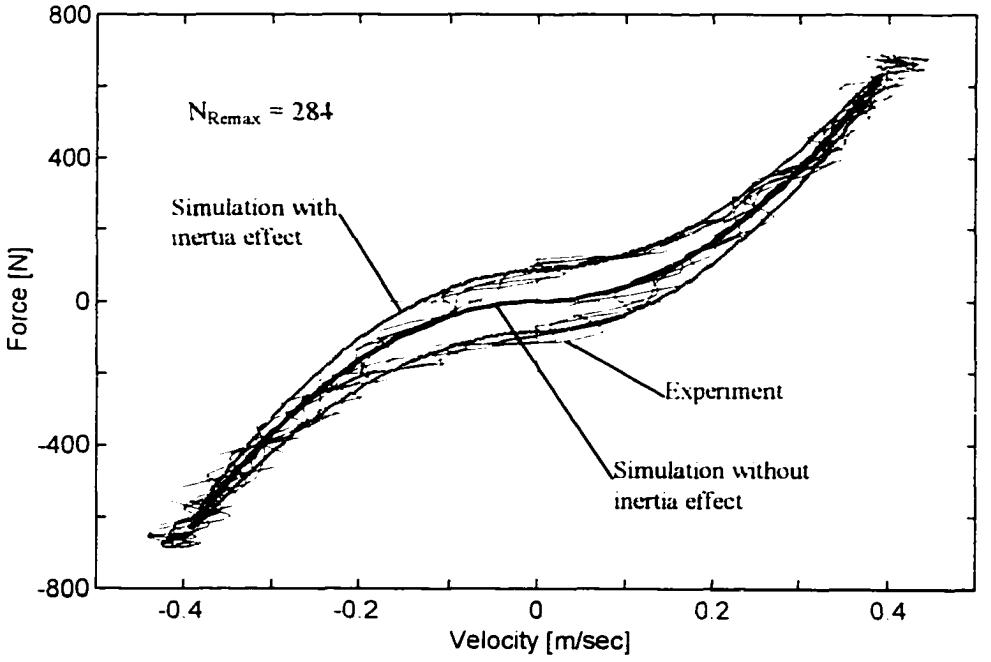

Figure 2.11 Comparison of the inertia effect when the valve is fully open with disturbance input, $x_d = 0.01\sin(8\pi t)$, $C_d = 0.65$.

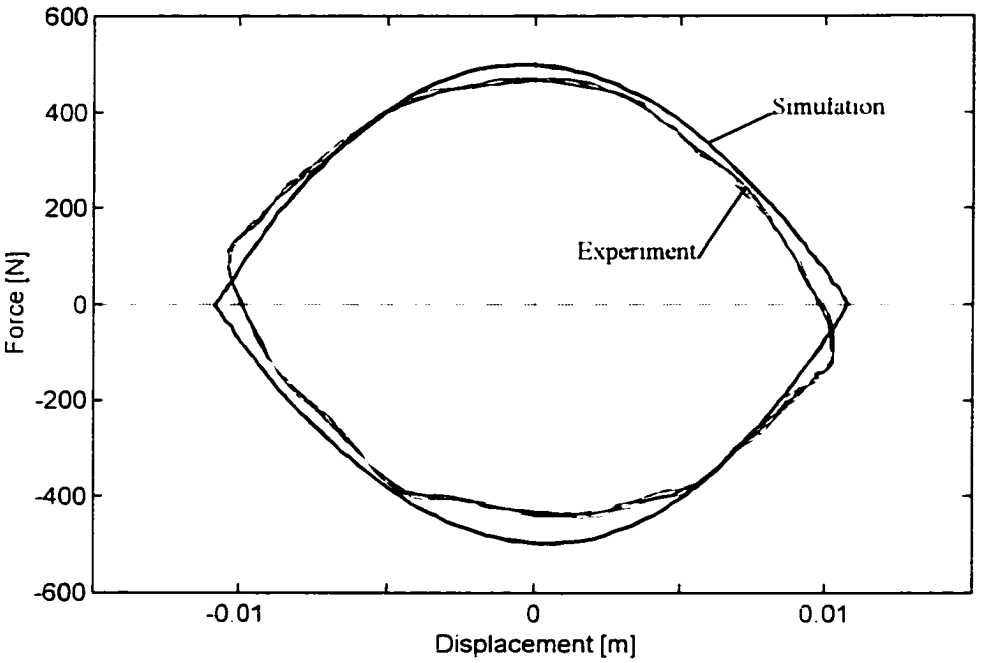

Figure 2.12 Comparison of force-displacement responses when the valve is fully open with disturbance input, $x_d = 0.005\sin(10\pi t)$, $C_d = 0.65$.

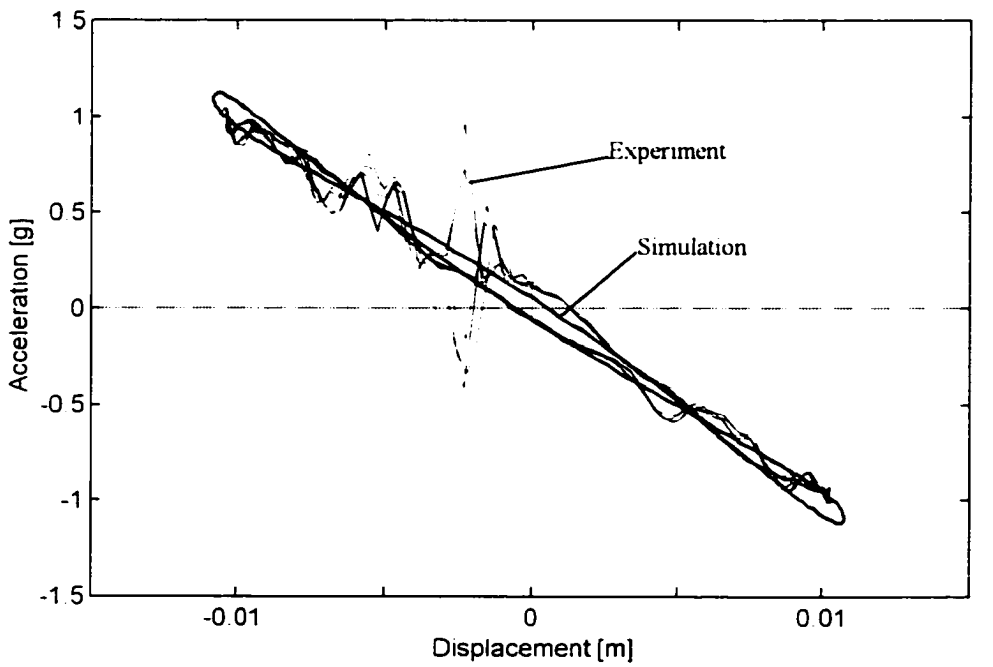

Figure 2.13 Comparison of acceleration-displacement responses when the valve is fully open with disturbance input, $x_d = 0.005\sin(10\pi t)$, $C_d = 0.65$.

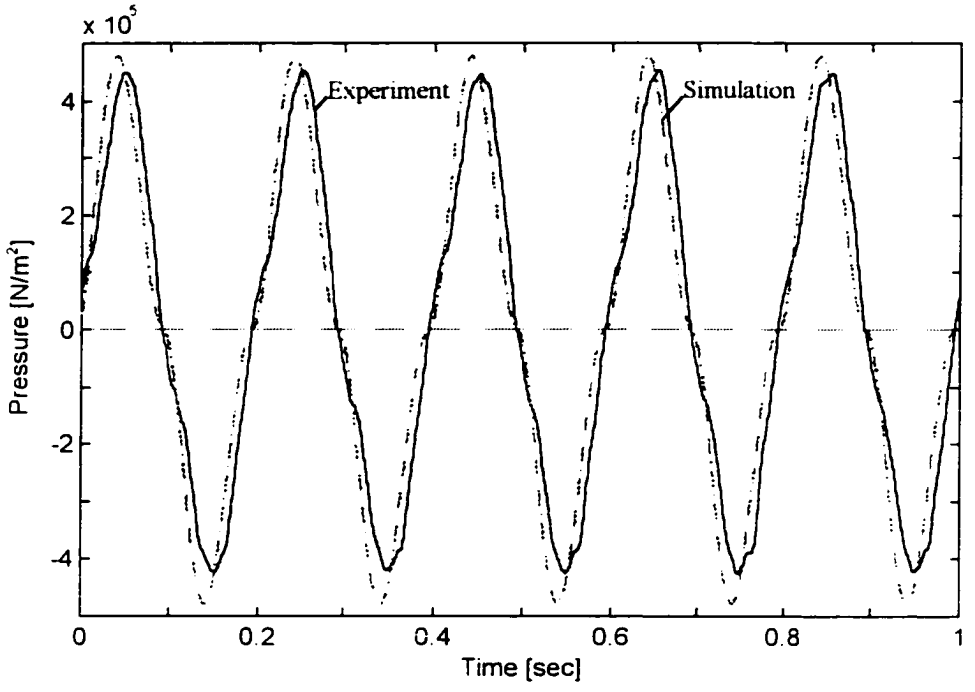

Figure 2.14 Comparison of the variation of differential pressure when the valve is fully open with disturbance input, $x_d = 0.005\sin(10\pi t)$, $C_d = 0.65$.

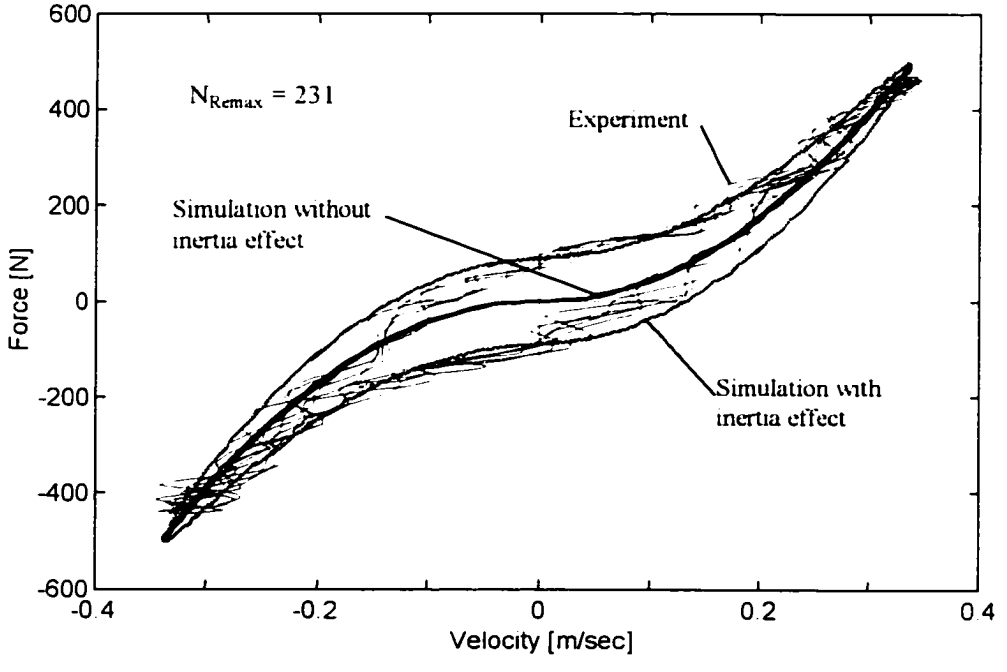

Figure 2.15 Comparison of the inertia effect when the valve is fully open with disturbance input, $x_d = 0.005\sin(10\pi t)$, $C_d = 0.65$.

Case 2: Valve Partially Open ($\theta = 30°$)

Case 1 (above) described the open loop characteristics of the valve with the orifice set to fully open. Case 2 represents the system responses obtained when the valve held at 30° from the fully open position. The force-velocity relationships are compared in Figures 2.16 through 2.18 for three different sinusoidal inputs. Figures 2.19 through 2.21 represent the time history of the system responses to a disturbance x_d $0.005\sin(10\pi t)$. Figures 2.19 reveals the force-displacement of the system for 5Hz input. Figure 2.20 depicts the acceleration-force and Figure 2.21 shows the differential pressure versus time.

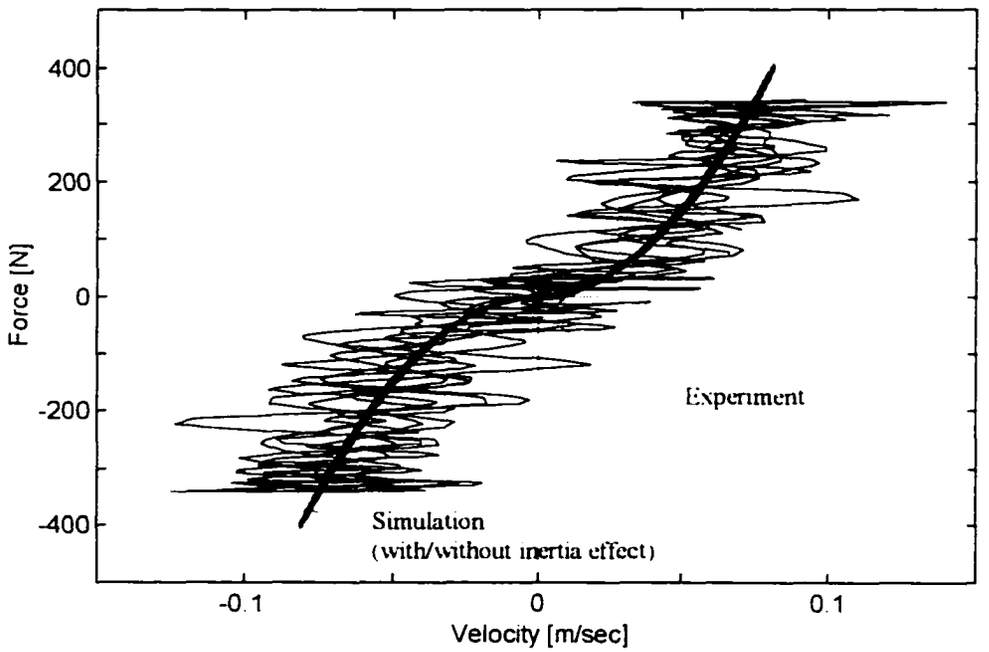

Figure 2.16 Force-velocity diagrams when the valve is partially open (A_v = 4.0×10^{-6} m^2, θ = 30°) with disturbance input, x_d = $0.005\sin(6\pi t)$, C_d = 0.842.

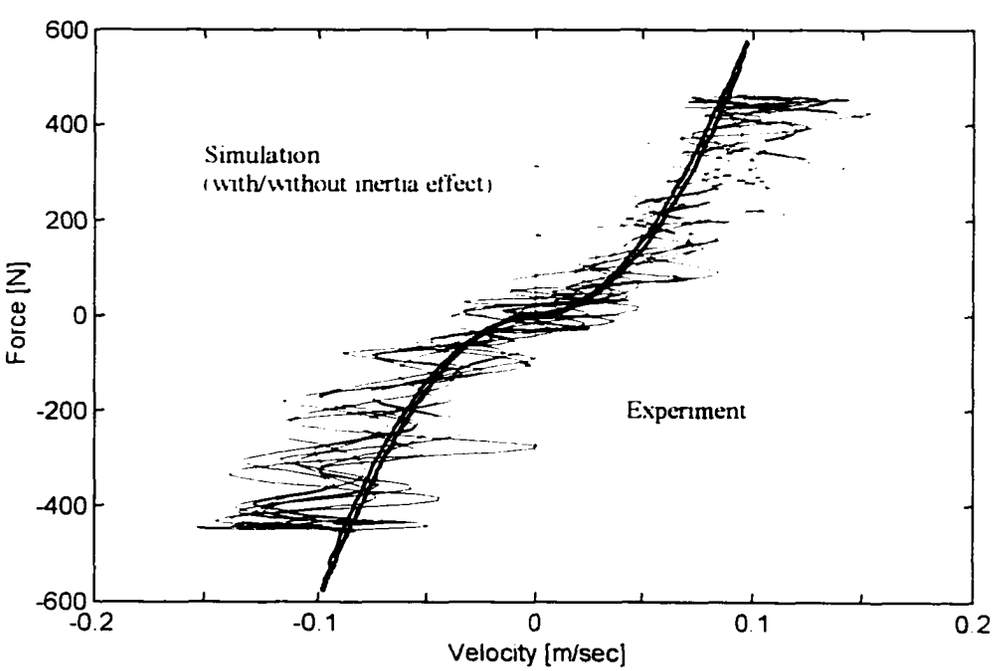

Figure 2.17 Force-velocity diagrams when the valve is partially open (A_v = 4.0×10^{-6} m^2, θ = 30°) with disturbance input, x_d = $0.005\sin(8\pi t)$, C_d = 0.842.

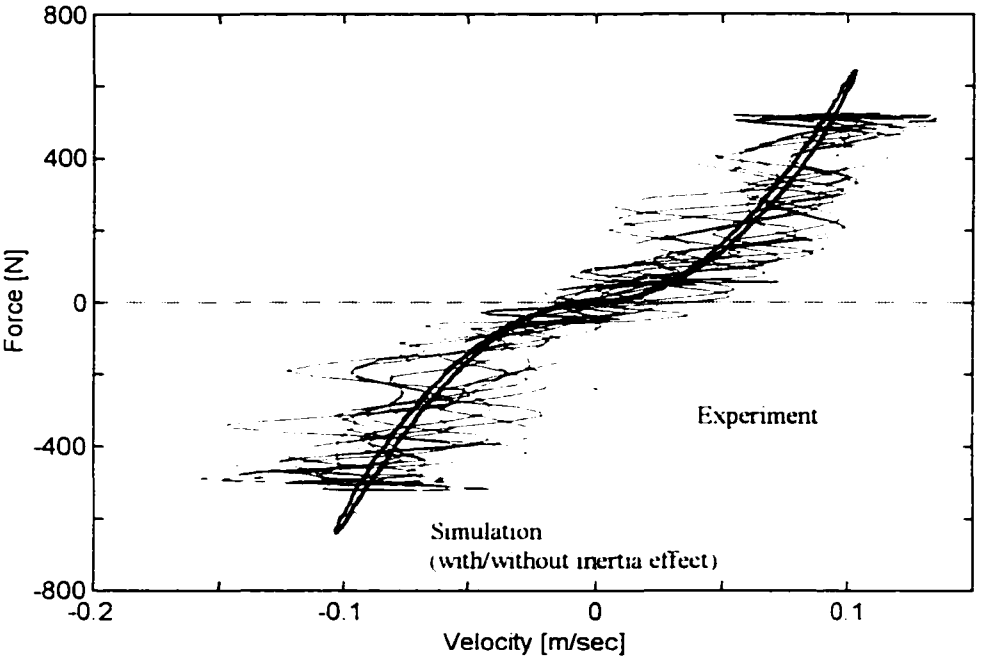

Figure 2.18 Force-velocity diagrams when the valve is partially open (A_v = 4.0×10^{-6} m^2, θ = 30°) with disturbance input, x_d = $0.005\sin(10\pi t)$, C_d = 0.842.

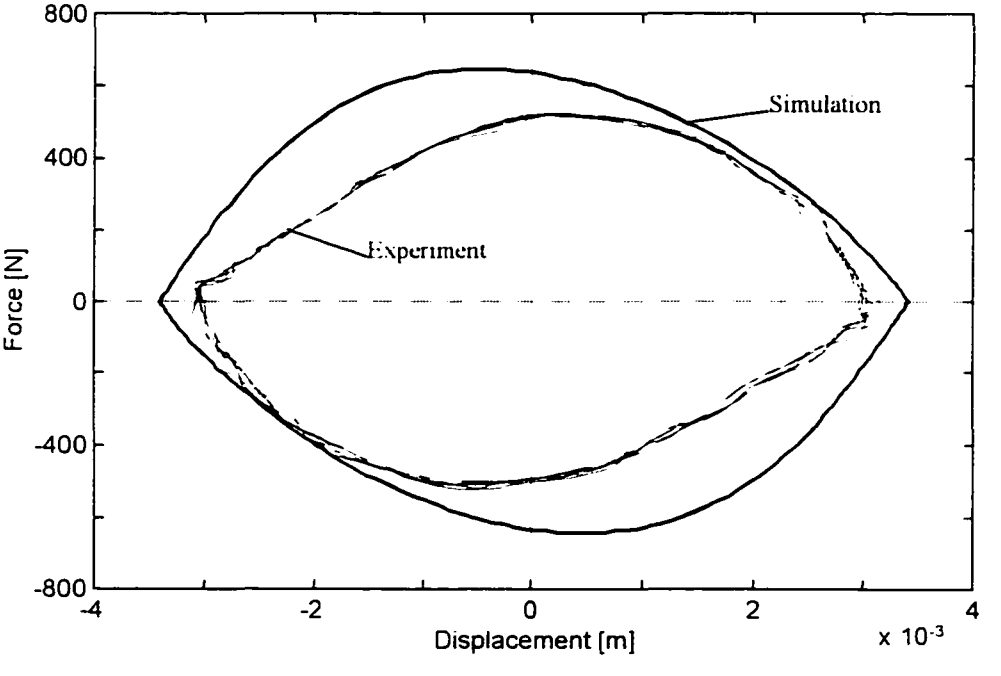

Figure 2.19 Comparison of force-displacement responses when the valve is partially open (A_v = 4.0×10^{-6} m^2, θ = 30°) with disturbance input, x_d = $0.005\sin(10\pi t)$, C_d = 0.842.

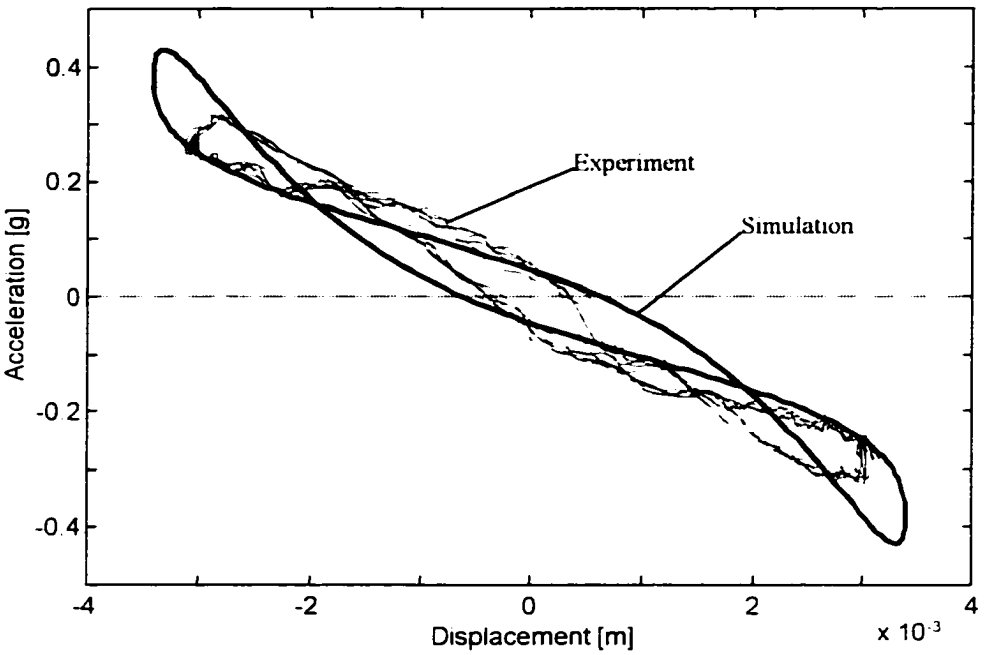

Figure 2.20 Comparison of acceleration-displacement responses when the valve is partially open ($A_v = 4.0\times10^{-6}\ m^2$, $\theta = 30°$) with disturbance input, $x_d = 0.005\sin(10\pi t)$, $C_d = 0.842$.

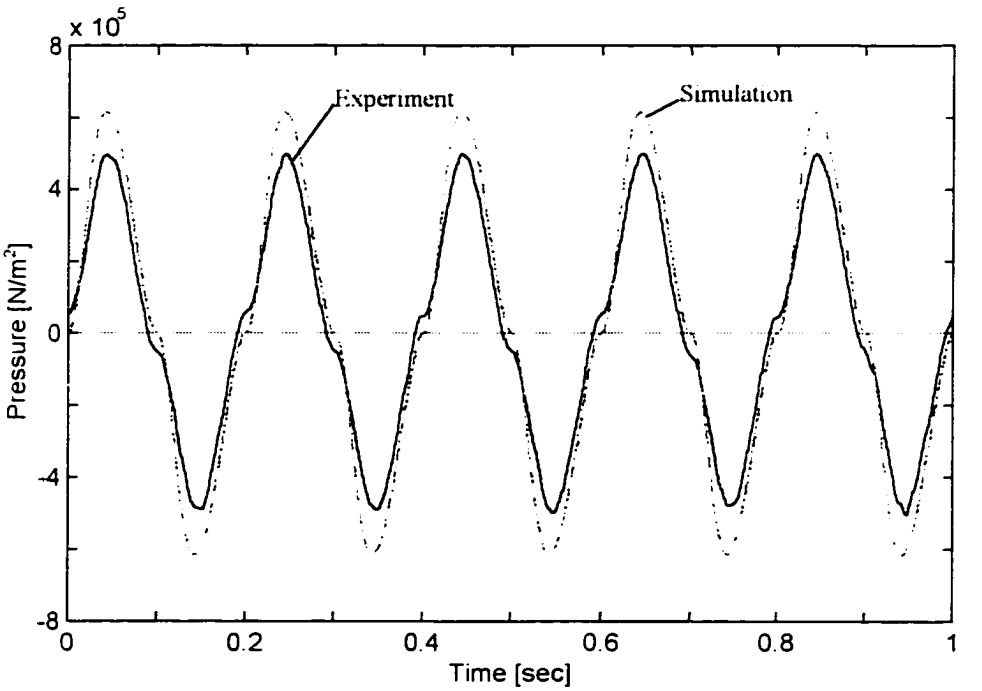

Figure 2.21 Comparison of the variation of differential pressure when the valve is partially open ($A_v = 4.0\times10^{-6}\ m^2$, $\theta = 30°$) with disturbance input, $x_d = 0.005\sin(10\pi t)$, $C_d = 0.842$.

2.4.2 Two-degree-of-freedom test fixture

Figure 2.3 depicts the schematic representation of TDOF experimental setup. For this setup, LVDTs and accelerometers were used to measure the relative displacements and absolute accelerations of the two moving masses, m_1 and m_2. One LVDT was used to measure $x_1(t) - x_2(t)$, while a second LVDT tracked coordinate $x_2(t) - x_4(t)$. Sinusoidal disturbance inputs were used to compare the exact solution with the experimental results. Two different valve positions were then used to determine response. Table 2.1 lists the specifications of the hydraulic cylinder of SAVA for the TDOF system, and the physical parameters of the TDOF test bed are listed in Table 2.3.

Table 2.3 Physical parameters of TDOF system

Description	Notation	Unit	Values
Mass # 1	m_1	Kg	245
Mass # 2	m_2	Kg	37
Spring stiffness # 1	k_1	N/m	28000
Spring stiffness # 2	k_2	N/m	125270
Damping coefficient # 1	c_1	N/m/sec	100
Damping coefficient # 2	c_2	N/m/sec	100

Case 1: Valve Fully Open ($\theta = 0°$)

In this case, the SAVA provides very little damping. Figures 2.22 through 2.25 depict the response of systems when the valve is in the fully open position. Next, Figures 2.22 and 2.23 represent the force-displacement and the force-velocity of SAVA, respectively, when the disturbance input is x_d $0.01\sin(6\pi t)$. Figures 2.24 and 2.25 show the responses of force-displacement and the force-velocity of SAVA when the disturbance input is x_d $0.005\sin(10\pi t)$. The discharge coefficient of the valve for these cases is $C_d = 0.65$.

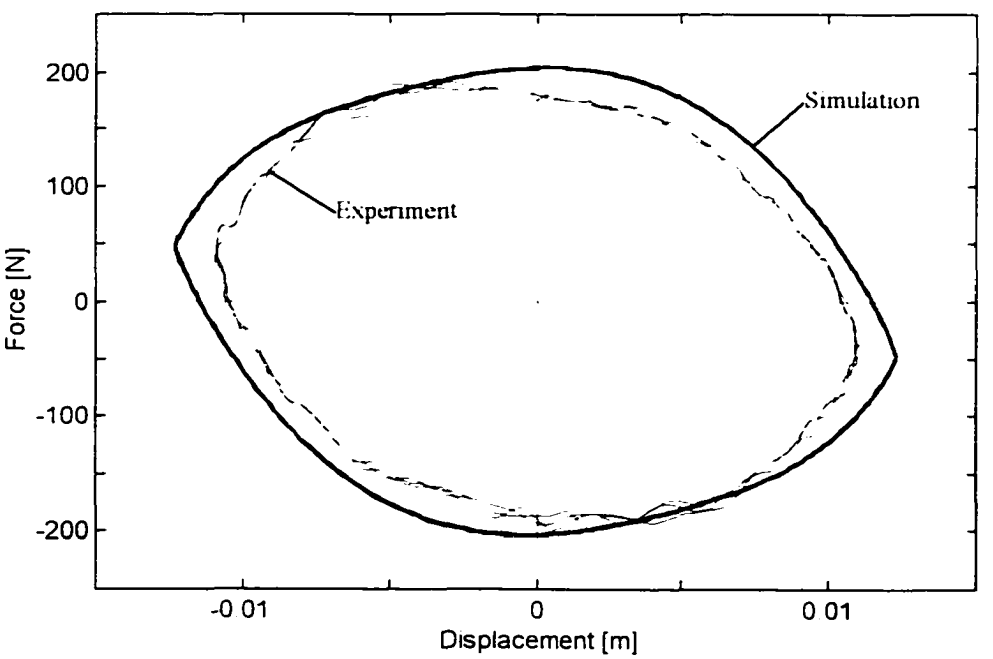

Figure 2.22 Force-displacement responses of SAVA when the valve is fully open with disturbance input $x_d = 0.01\sin(6\pi t)$, $C_d = 0.65$.

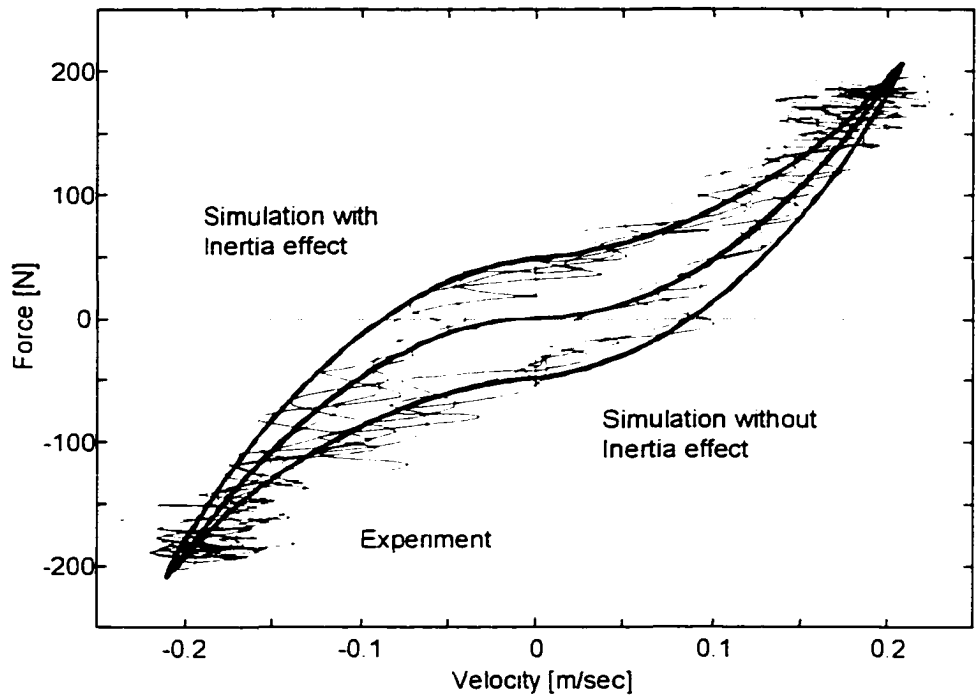

Figure 2.23 Force-velocity responses of SAVA when the valve is fully open with disturbance input, $x_d = 0.01\sin(6\pi t)$, $C_d = 0.65$.

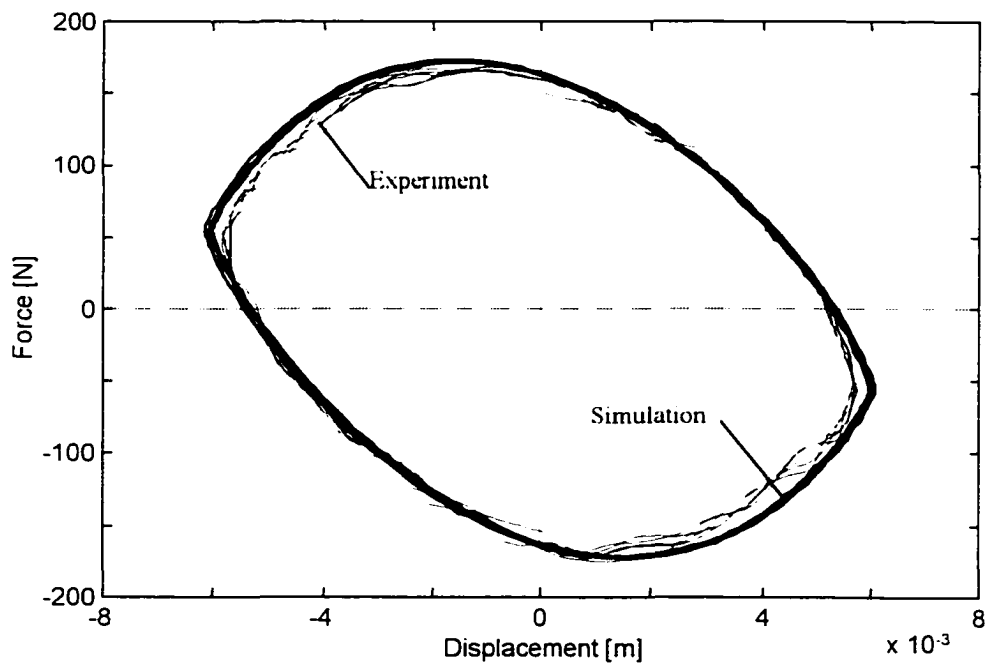

Figure 2.24 Force-displacement responses of SAVA when the valve is fully open with disturbance input, $x_d = 0.005\sin(10\pi t)$, $C_d = 0.65$.

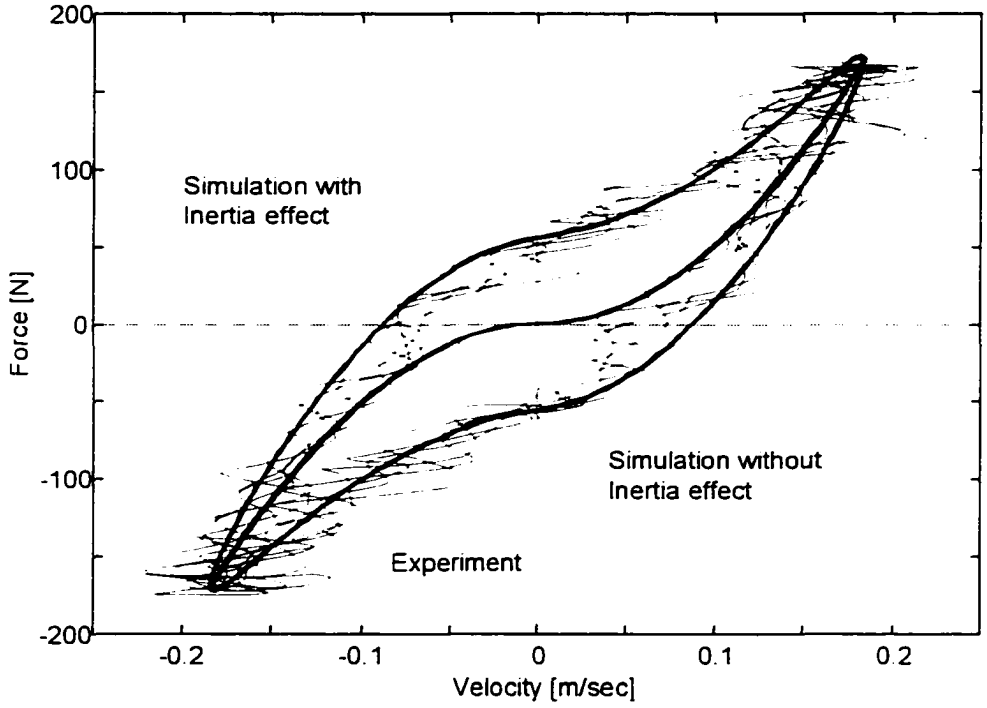

Figure 2.25 Force-velocity responses of SAVA when the valve is fully open with disturbance input, $x_d = 0.005\sin(10\pi t)$, $C_d = 0.65$.

Case 2: Valve Partially Open ($\theta = 30°$)

For this test, the valve angle is fixed at 30° relative to the fully open position. Sinusoidal disturbances with the amplitude set at 0.005m and frequency set at 3Hz, 4Hz and 5Hz were employed. Figures 2.26 and 2.27 represent the system responses of force-displacement and force-velocity, respectively, when $x_d = 0.005\sin(6\pi t)$. Figures 2.28 and 2.29 show the system responses of force-displacement and force-velocity when $x_d = 0.005\sin(8\pi t)$. Figures 2.30 and 2.31 depict the comparison between simulation and experiment when $x_d = 0.005\sin(10\pi t)$, which presents the responses of force-displacement and force-velocity, respectively. Here, the discharge coefficient of the valve is $C_d = 0.842$ for three different disturbance inputs.

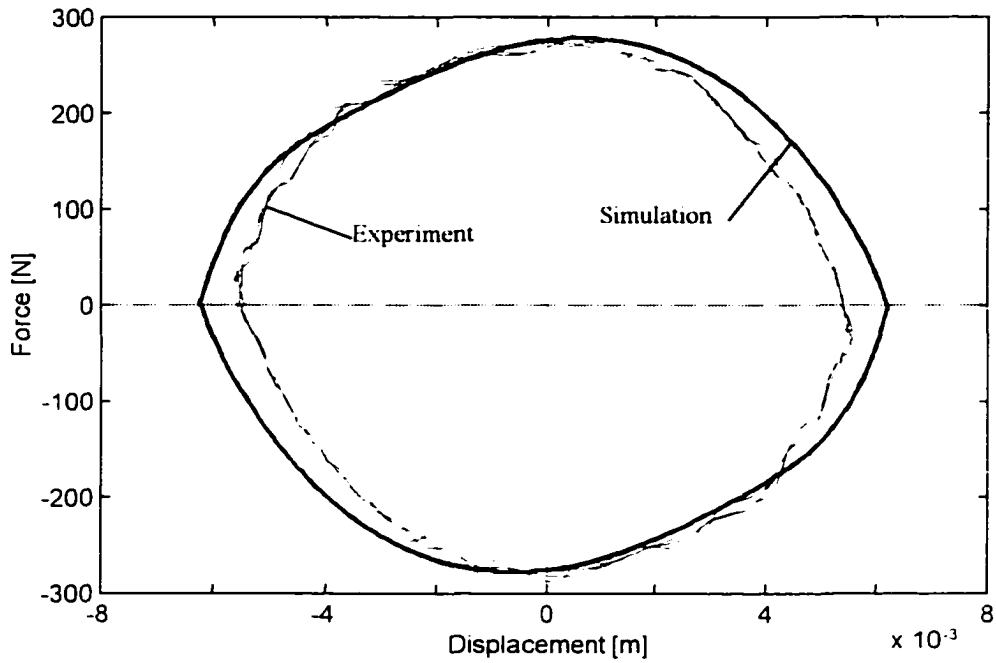

Figure 2.26 Force-displacement responses of SAVA when the valve is partially open ($A_v = 4.0\times10^{-6}\ m^2$, $\theta = 30°$) with disturbance input $x_d = 0.005\sin(6\pi t)$, $C_d = 0.842$.

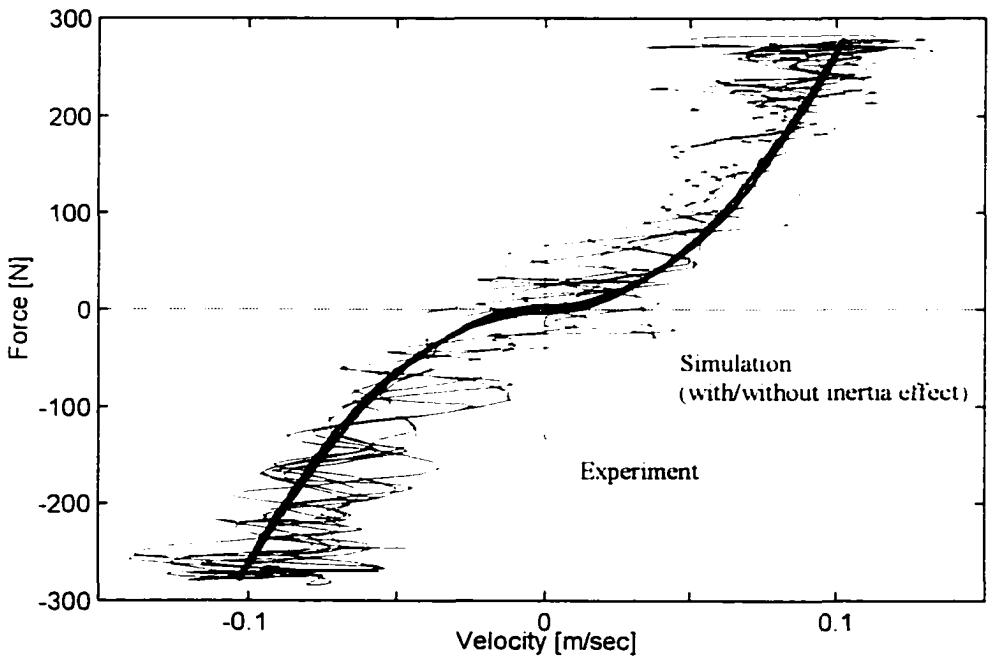

Figure 2.27 Force-velocity responses of SAVA when the valve is partially open ($A_v = 4.0\times10^{-6}\ m^2$, $\theta = 30°$) with disturbance input $x_d = 0.005\sin(6\pi t)$, $C_d = 0.842$.

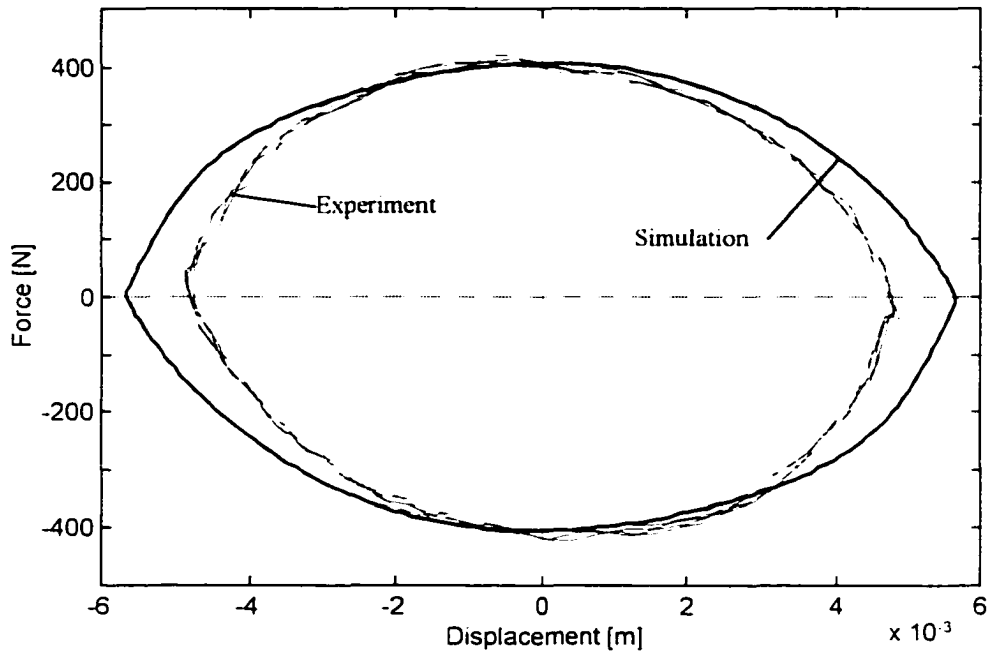

Figure 2.28 Force-displacement responses of SAVA when the valve is partially open ($A_v = 4.0\times10^{-6}\ m^2$, $\theta = 30°$) with disturbance input $x_d = 0.005\sin(8\pi t)$, $C_d = 0.842$.

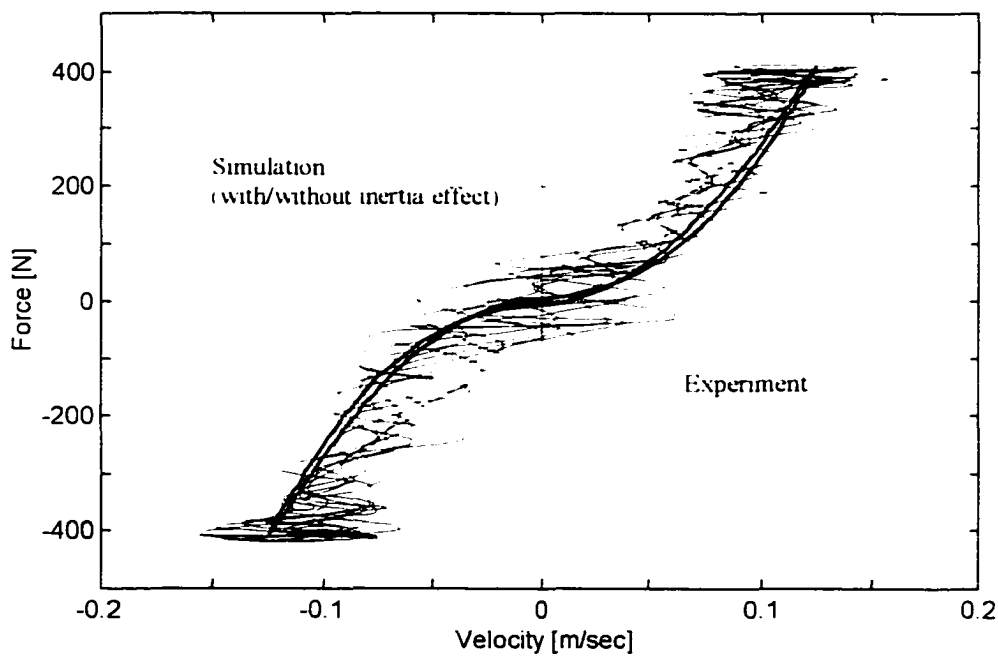

Figure 2.29 Force-velocity responses of SAVA when the valve is partially open ($A_v = 4.0\times10^{-6}\ m^2$, $\theta = 30°$) with disturbance input $x_d = 0.005\sin(8\pi t)$, $C_d = 0.842$.

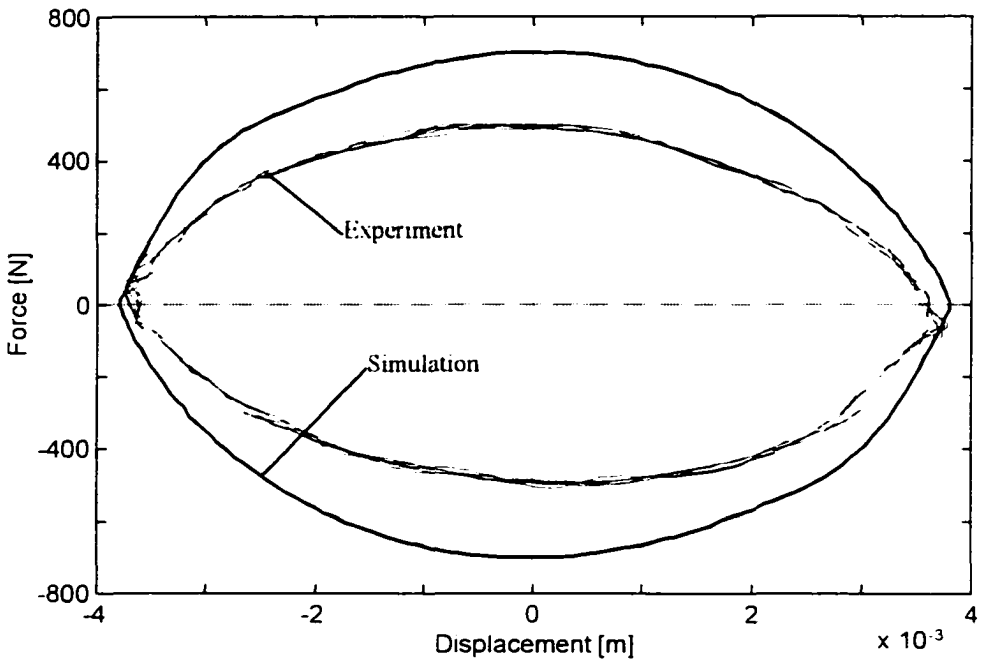

Figure 2.30 Force-displacement responses of SAVA when the valve is partially open (A_v = 4.0×10^{-6} m^2, θ = 30°) with disturbance input x_d = $0.005\sin(10\pi t)$, C_d = 0.842.

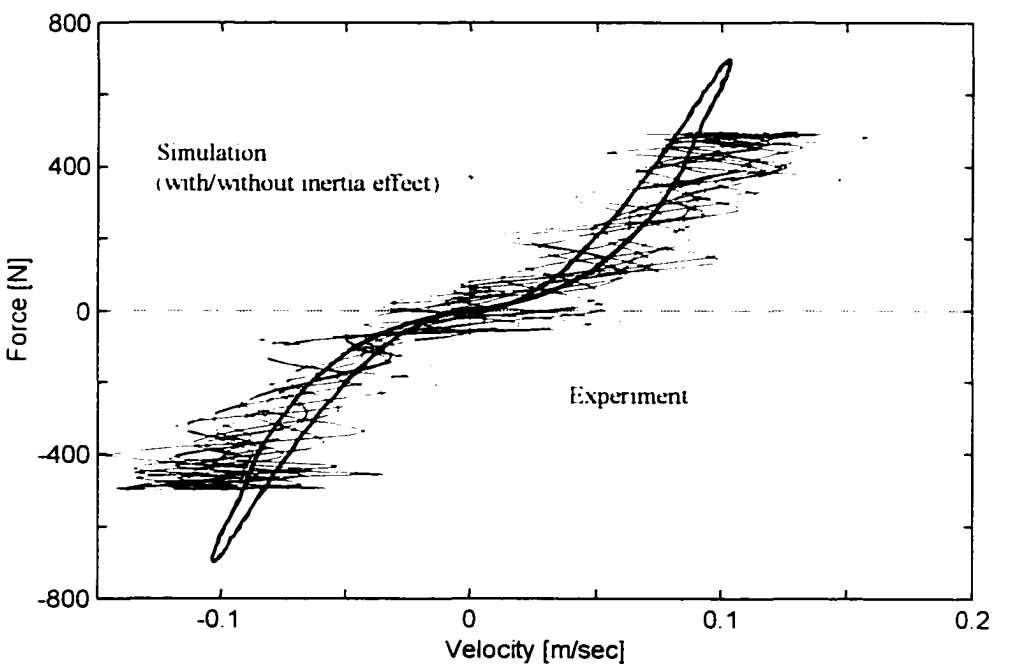

Figure 2.31 Force-velocity responses of SAVA when the valve is partially open (A_v = 4.0×10^{-6} m^2, θ = 30°) with disturbance input x_d = $0.005\sin(10\pi t)$, C_d = 0.842.

2.4.3 Fidelity of controlled response

The response of the SAVA system to step type inputs is examined here. That goal is achieved by imposing a bistate feedback law that produces a complete opening or closure of the valve based on a state feedback law. A widely used "local" semiactive law is used [Rakheja and Sankar, 1985];

$$A_v = \begin{cases} A_{v\max} & if\ x_{rel}\dot{x}_{rel} > 0 \\ A_{v\min} & if\ x_{rel}\dot{x}_{rel} \le 0 \end{cases} \tag{2.28}$$

where x_{rel} and $\dot{x}_{rel}$ are the relative displacement and velocity across the actuator.

A single-degree-of-freedom test stand was used to conduct the experiment (Figure 2.2). The equations of motion for the SDOF system were established previously (Equation 2.19). The system was subjected to a sinusoidal input. The following figures depict both the experimental and simulated for open loop operation (with the valve fully open ($\theta = 0°$) or partially closed ($\theta = 30°$)) and for a closed loop bistate control. The minimum valve angle was set to 30° to avoid large hydraulic shocks that accompany complete valve closure. Figure 2.32 depicts the product of $x_{rel}\dot{x}_{rel}$ when the product is positive, the valve angle is 0° (fully open) and when the product is negative, angle is set to 30°. Figures 2.33 and 2.34 depict a comparison of the open loop and controlled response displacement and acceleration for a sinusoidal input x_d $0.005\sin(6\pi t)$. The data shown in Figure 2.33 indicates a 12% reduction of displacement amplitude for the control performance. Figures 2.35 through 3.39 depict a

comparison of the simulated and experimentally measured controlled responses for a sinusoidal input $x_d = 0.005\sin(6\pi t)$.

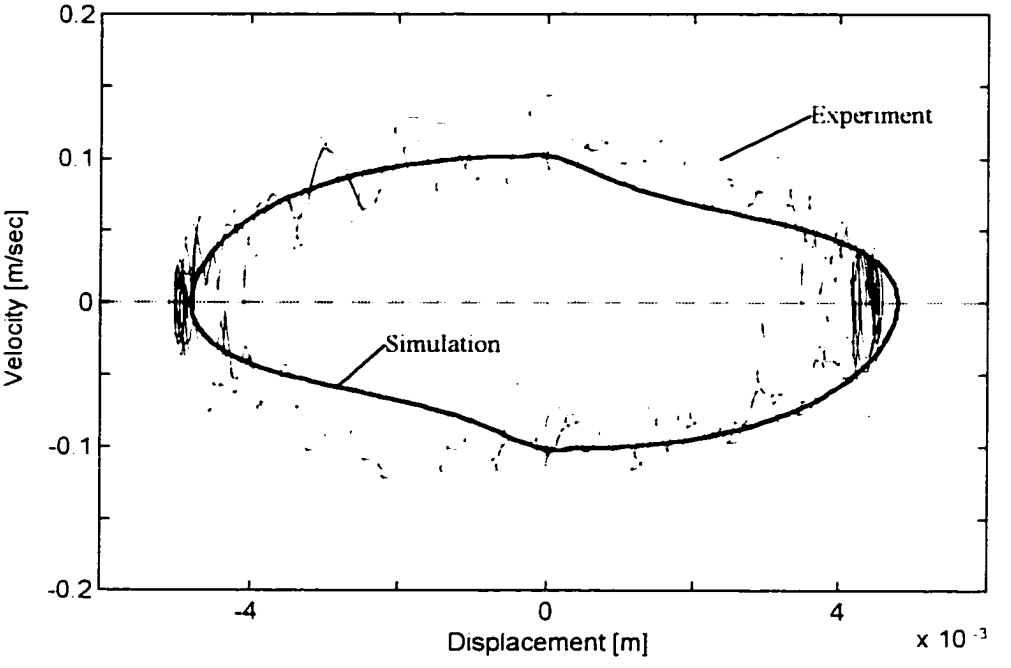

Figure 2.32 Comparison of experiment and simulation of displacement-velocity for controlled responses ($A_v = A_{vmin} = 4.0\times10^{-6}\ m^2$, $\theta = 30°$), $C_d = 0.842$.

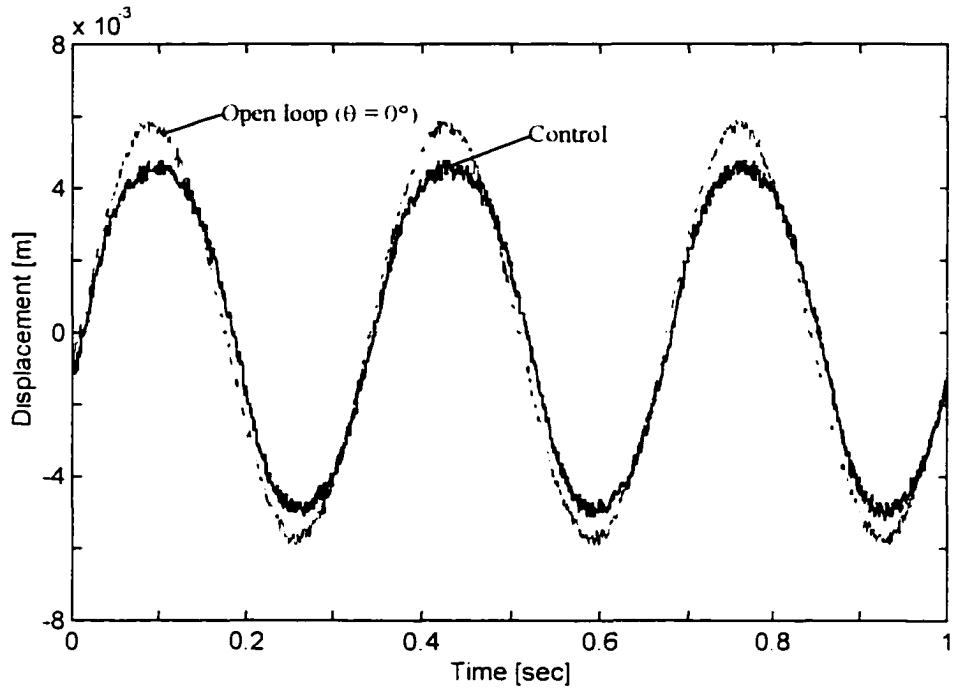

Figure 2.33 Comparison of displacement responses of experiments between open loop ($A_v = A_{vmax}$, $\theta = 0°$) and control ($A_v = A_{vmin} = 4.0\times10^{-6}\ m^2$, $\theta = 30°$) with disturbance input $x_d = 0.005\sin(6\pi t)$.

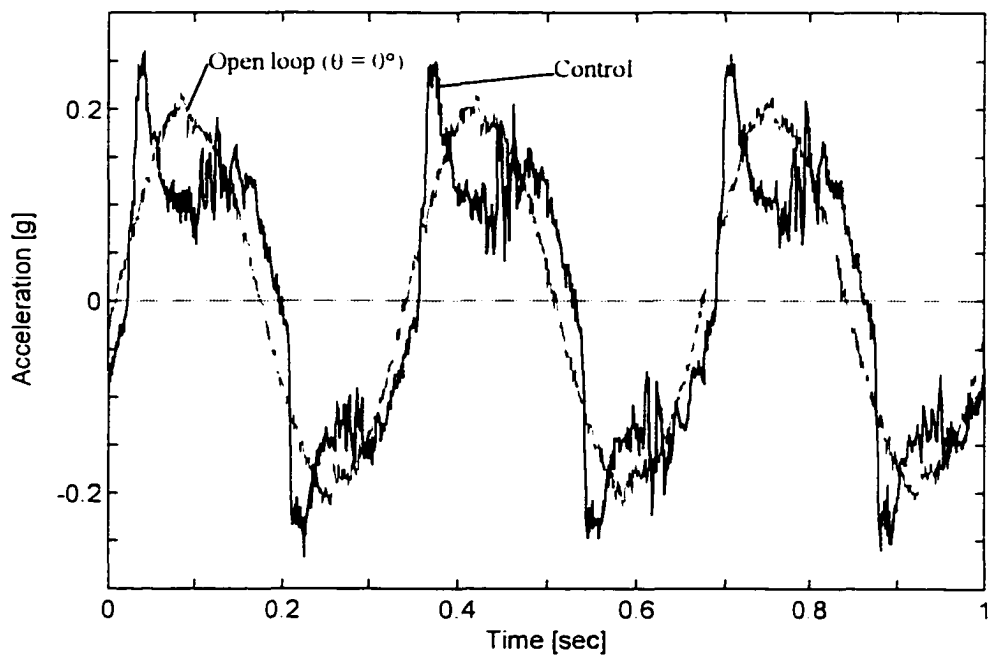

Figure 2.34 Comparison of acceleration responses of experiments between open loop ($A_v = A_{vmax}$, $\theta = 0°$) and control ($A_v = A_{vmin} = 4.0\times10^{-6}\ m^2$, $\theta = 30°$) with disturbance input $x_d = 0.005\sin(6\pi t)$.

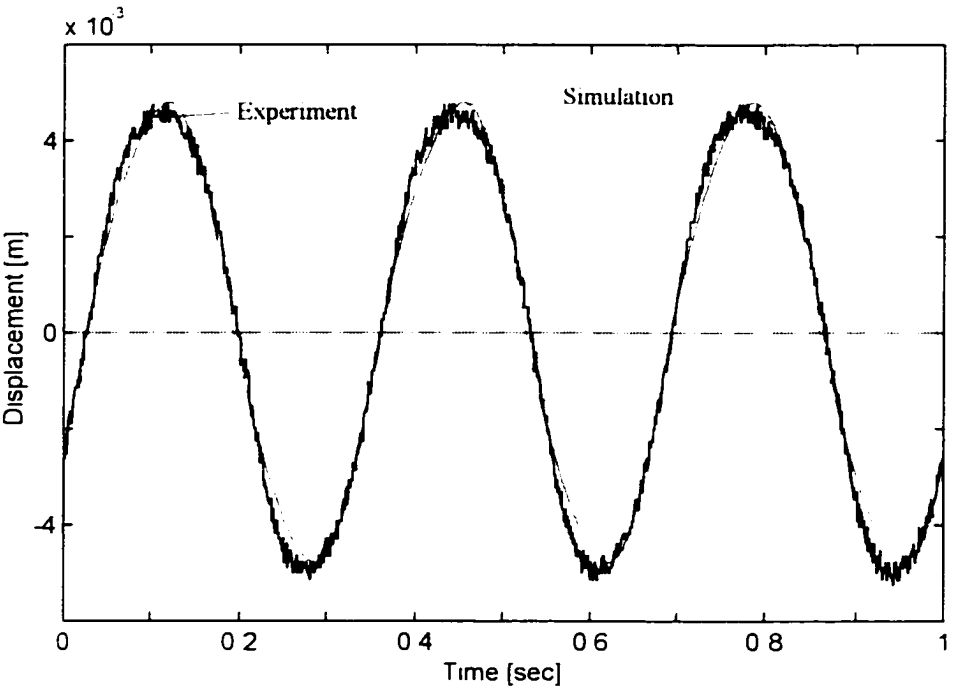

Figure 2.35 Comparison of controlled displacement responses (A_v A_{vmin} 4.0×10^{-6} m^2, θ $30°$) with disturbance input x_d $0.005\sin(6\pi t)$, C_d 0.842.

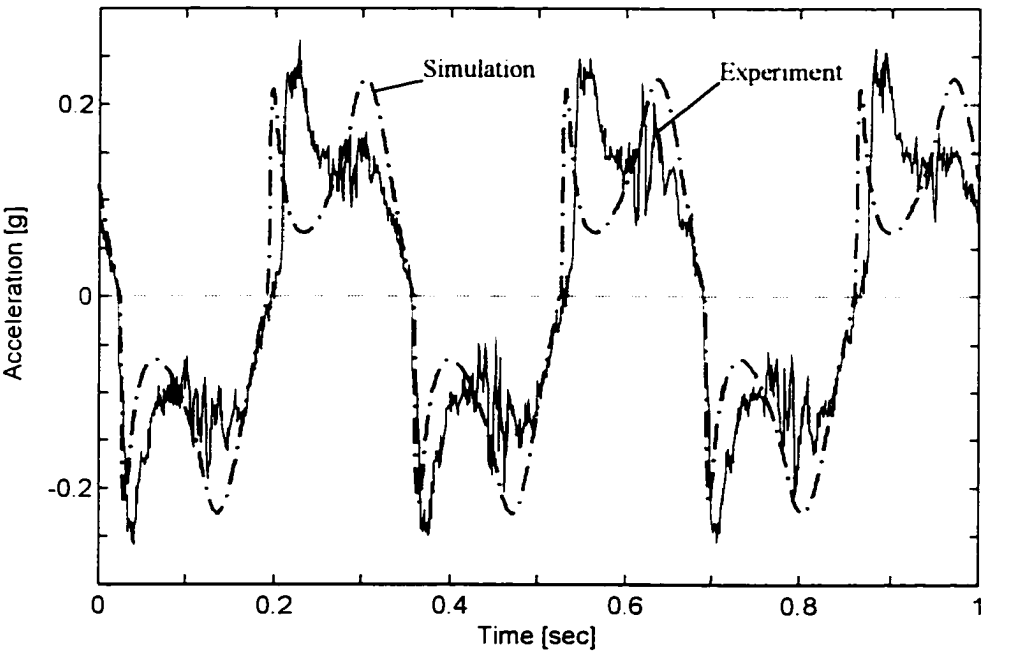

Figure 2.36 Comparison of controlled acceleration responses ($A_v = A_{vmin} = 4.0\times10^{-6}$ m^2, $\theta = 30°$) with disturbance input $x_d = 0.005\sin(6\pi t)$, $C_d = 0.842$.

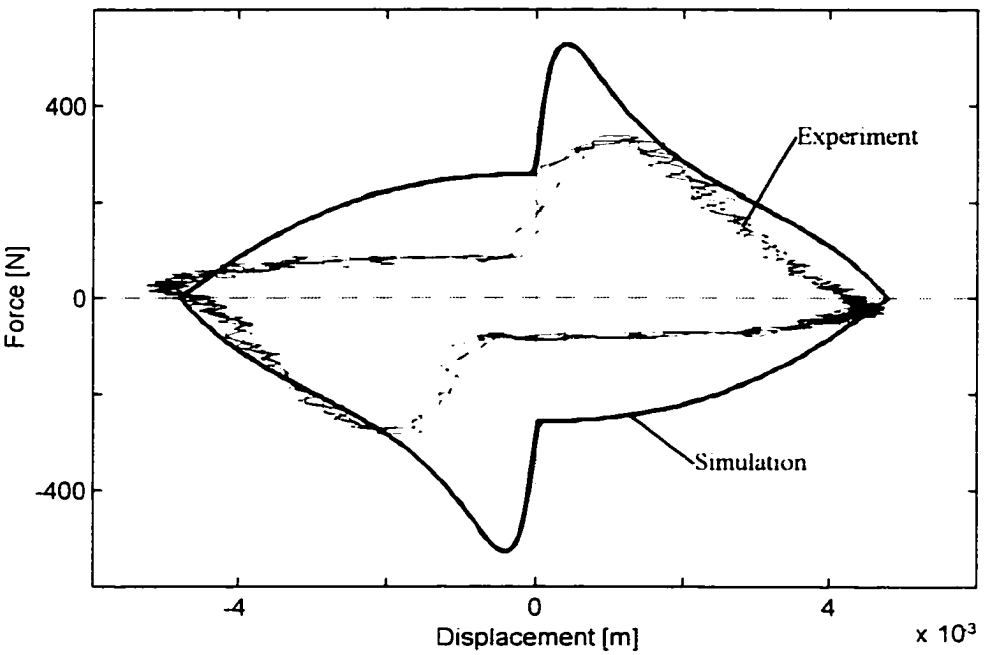

Figure 2.37 Force-displacement responses of SAVA when the valve is controlled ($A_v = A_{vmin} = 4.0\times10^{-6}\ m^2$, $\theta = 30°$) with disturbance input $x_d = 0.005\sin(6\pi t)$, $C_d = 0.842$.

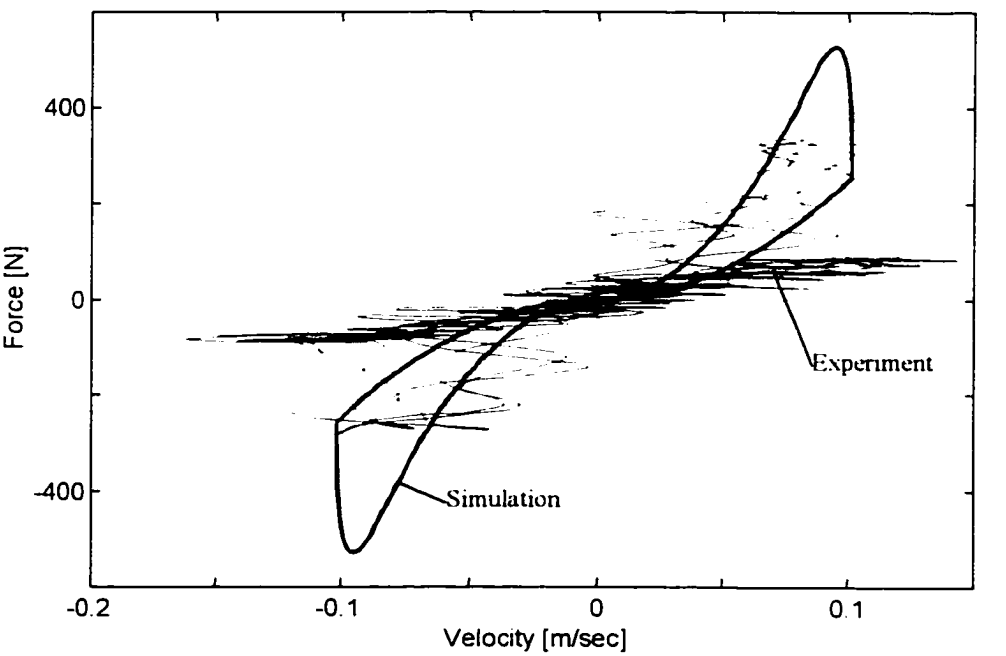

Figure 2.38 Force-velocity responses of SAVA when the valve is controlled ($A_v = A_{vmin} = 4.0\times10^{-6}\ m^2$, $\theta = 30°$) with disturbance input, $x_d = 0.005\sin(6\pi t)$, $C_d = 0.842$.

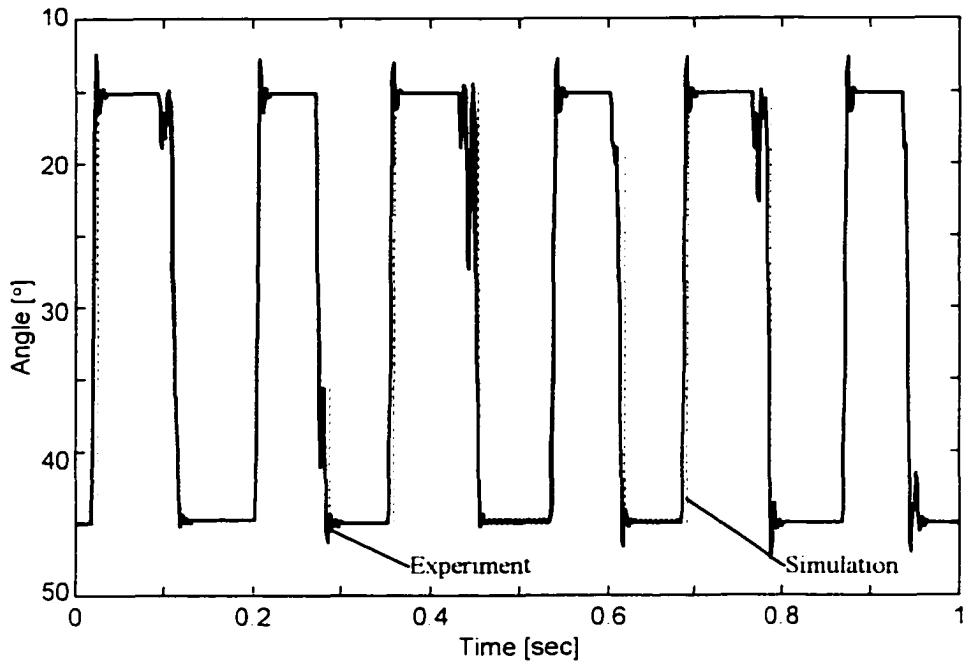

Figure 2.39 Time history of valve action between experiment and simulation.

2.5 Conclusion

The work reported in this chapter indicates that the model (Equations 2.15 through 2.19) of a SAVA actuator provides a reasonable means of characterizing it's dynamic performance. The work indicates that at low flow rate through valve, the device exhibits a linear characteristic, and at turbulent flow, a nonlinear (square root) characteristic.

The discharge coefficient of the valve directly relates to the Reynolds number and the opening area of the valve [Merritt, 1967]. The flow rate through the valve is restricted due to the size of SAVA and the relative motion of the system. The maximum computed Reynolds number of SAVA is not big different for each case, when the valve is fully open ($\theta = 0°$) and partially open ($\theta = 30°$). Therefore, the variation of Reynolds number is small and valve characteristic C_d is essentially constant. For the turbulent flow, the discharge coefficient of the valve is $C_d = 0.65$ when the valve is fully open ($\theta = 0°$) and $C_d = 0.842$ when the valve is partially open ($\theta = 30°$).

Finally, the experimental results suggest that inertia effects can be neglected at all but the lowest Reynolds numbers.

CHAPTER THREE

LYAPUNOV CONTROL

3.1 Introduction and Literature Review

The treatment of nonlinear control systems is a broad area of science that has been discussed in some detail in a number of texts. Section 3.1 of the chapter will provide a description of the material offered in those texts as it pertains to the control of the semiactive hydraulic systems being studied in this dissertation. A review of journal articles relevant to the work will also be offered. Section 3.2 of the chapter will describe the dynamics of a generic system that will be utilized in the control study here. The Section 3.2 will also provide a description of the dynamics of the generic (hydraulic) actuator that is used in the SA control design. The mechanical coupling between the dynamics of actuator and the system is also discussed.

The chapter will demonstrate that Lyapunov approach provides a rigorous technique for discovering the best possible control action at each point in time. Numerical and experimental verification of the effectiveness of the Lyapunov control approach for semiactive systems is presented in Sections 3.3 and 3.4 respectively. The chapter ends with a set observations and conclusions regarding the Lyapunov controller approach for semiactive systems. A review of the literature pertinent to the work presented in this chapter follows.

The objective of the chapter is to explore the utility and the flexibility of the Lyapunov control method and its application to semiactive systems. There are hundreds of papers in the open literatures that describe routinely test specific problems in the nonlinear control area. The technique applied in this chapter is not new. Certain texts that develop the Lyapunov approach are particularly readable. Examples include the work by Vidyasagar [1978] that provides a presentation of the general nonlinear problem with specific discussions of the Lyapunov method. Perhaps the most widely read and coincidentally the most recent text in the mechanical engineering field that treats nonlinear control is that by Slotine and Li [1991]. Those authors provide wide-ranging coverage of the Lyapunov method and include practical examples of the application. The text by Mohler [1991] affords the novice an introduction to Lyapunov control methods that emphasizes applications. The texts mentioned here are not all-inclusive and in fact there are many additional excellent texts that treat the subject; but are considered as intermediate or advanced presentations of the method. The text by Nijmeijer and Van der Schaft [1990] is a typical example.

Leitmann [1993, 1994] demonstrated semiactive control strategy for semiactive systems that is based on a Lyapunov approach. That control scheme has different switching conditions compared to a conventional "on-off" controller. Patten et al. [1996a] have also proposed the semiactive control algorithm based on a Lyapunov stability theorem in which the controller represents "on-off" control. The performance of that control scheme when applied to a SAVA system was verified in the areas of structure and auto suspension both analytically and experimentally [Patten et al., 1996a,

Mo et al., 1996b]. Hitada and Smith [1997] presented a nonlinear controller using variable damping devices for civil structure under earthquake excitations based on Lyapunov stability theorem. That proposed controller takes the form of filtered bang-bang control. The following section describes the semiactive hydraulic actuator control problem in a manner that will lead naturally to its treatment using a Lyapunov approach to synthesis of a controller.

3.2 Semiactive Control

The lexicon of control engineering has expanded during the past two decades to include various techniques and approaches to system control that do not fit classical definitions. One relatively recent modification is that systems, previously treated as either active or passive, are now examined in terms of an intermediate possibility: semiactive. The introduction of a new descriptor has been adopted to make clear the nature of the power needed to achieve the control objective. At one extreme, a passive control design is comprised of a collection of components with non-time varying characteristics. Properly selected passive components can very often achieve a best solution. This is especially true if the dynamics of disturbances are known apriori. Examples of passive control design include hydraulic shock absorbers on automobiles, and elastomeric bearing that are routinely used to mitigate a structures dynamic response to a seismic event. A purely passive design requires no external power source to achieve vibration mitigation.

Active control systems represent the other limiting control design. Active controllers typically rely on the availability of an external energy source to power an actuator, which is in turn regulated to achieve prescribed objectives. The power required to operate an active control system is (in general) assumed to be of the order of the power dissipated from a vibrating system. Active controllers are often plagued by features that make them less effective then might have been desired. Realities such as saturation, backlash friction, and actuator dynamics can severely compromise the sought for performance of an active control design.

The middle ground between a passive motion management design and active control designs for a system has emerged that presents today's control system engineer with a much-expanded family of control solutions. While no hard and fast definition can be pointed to, this middle ground is typically referred to as semiactive, or parameter adaptive control. The semiactive label was first introduced by control engineers in the automotive industry. The most common qualifier of a semiactive control system is a prescription for the extent of external power utilized by the actuator, relative to the energy (power) managed (or dissipated) by the actuator; it must be "small". Every SA system known to this author could also be thought of as a parameter adaptive passive control. In general, a SA actuator provides judiciously selected levels of compliance during a dynamic event. The varied compliance, in its simplest form, might be linear damping and/or linear stiffness. Indeed, almost all of the articles that treat semiactive control design that appear in the open literature prior to 1990 discuss the SA actuator as a linear damper with selectable levels of damping [Karnopp et al., 1974, Krasnicki, 1979, Rakheja and Sankar, 1985, Butsuen, 1989, Miller and Nobles, 1990]. Continuously variable linear stiffeners have also received attention [Kobori et al., 1993, Leitmann, 1994]. Those studies assumed an ideal actuator or component in which the supposed linear compliance characteristic could be designed into the hardware.

The nature of the SA device employed in an actual application governs the dynamics of the actuator. Those dynamics are typically complex and nonlinear, and are generally coupled to the dynamics of the system that is to be controlled. Those considerations must be addressed by the engineer before a system design can be

finalized. While a simplified analysis that assumes that the actuator can afford automatically selectable level of linear damping or stiffness, the actual hardware dynamics should be relied on at some point early in the design to confirm that the control does achieve desired levels of performance. The dynamics of a semiactive vibration absorber is discussed next.

3.2.1 SA hydraulic actuator dynamics

The mechanical elements that make up a SA actuator are shown in Figure 1.1. Nonlinear lumped parameter hydraulic model of the actuator has been previously reported [Patten, 1996a, b, 1988]. The general model takes the following form

$$\dot{\Delta P} = \frac{\beta(V_1 - V_2)}{V_1 V_2}\left(A_p \dot{s} - sgn(\Delta P)\lambda \Delta P^{N} \right) \tag{3.1}$$

where s is the displacement of the piston and $\dot{s}$ is the relative velocity of the piston. The flow through valve is linear when $N = 1$ $\left(\lambda = \frac{\pi d^4}{128 \rho v L}\right)$ and nonlinear when $N = 0.5$ $\left(\lambda = C_d A_v \sqrt{2/\rho}\right)$.

Equation 3.1 defines the state of the pressure in the actuator. Experimental evidence (see Chapter Two) indicates that fluid inertia, which is not accounted for in the above model, plays a minor roll for most physical applications. Equation 3.1 reflects an assumption that the fluid density in the fluid/air mix is uniform and non-time varying [Patten, 1996a, 1998]. The system is obviously nonlinear. The first term in the brackets

on the right hand side of the Equation 3.1 represents the stiffness effect. This is made more obvious if the valve is closed ($A_v = 0$) in that case, no flow takes place, and any change in pressure with time is a reflection of the displacement of the piston. That motion is possible if and only if the fluid (or fluid/air mix) is compressible, which it is. A study by Dulay et al. [1988] suggests that when air is entrained in the hydraulic fluid, then the following expression for the dependence of β on pressure holds

$$\beta = \beta_o \frac{\frac{V_f}{V_a} + 1}{\frac{V_f}{V_a} + \beta_o \frac{P_o}{P^2}} \tag{3.2}$$

where β_o represents bulk modulus of the pure fluid (free from dissolved air, β_o = 1.4 GN/m^2) and P_o represents atmospheric pressure. A plot of β versus P is shown in Figure 3.1. In any real application, air is always present in the system, and the effectiveness of the design can be significantly reduced if the design process neglects the variation of compressibility.

When the valve is opened, then the power term N on ΔP comes into play. When the flow is turbulent, the power term has a square root form, which corresponds to the Bernoulli loss term for flow through an orifice. The loss is manifestation of the damping, or dissipativeness of the system. When the flow is laminar, $N = 1$ (see Chapter Two). The model (Equation 3.1) suggests that the SA actuator can provide two phenomenological effects, damping and stiffness, and that those effects are combinative. It is worth noting that if the orifice area A_v is large, then the principal

effect is damping. The degree to which both damping and stiffness play a role in the dynamics is dependent on the orifice area (A_v) as well as on the kinematics of the stroke, which are reflected in the position dependent volumetric ratio in Equation 3.1 ($\frac{V_1 + V_2}{V_1 V_2}$). When the motion of the actuator is "small" then the ratio is often treated as a constant. If large strokes occur during the action, then the volumetric ratio can effect the expected results considerably. The preceding discussion makes it clear that the dynamics of a semiactive hydraulic actuator depart significantly from an ideal damper ($A_p \Delta P \quad c\dot{s}$).

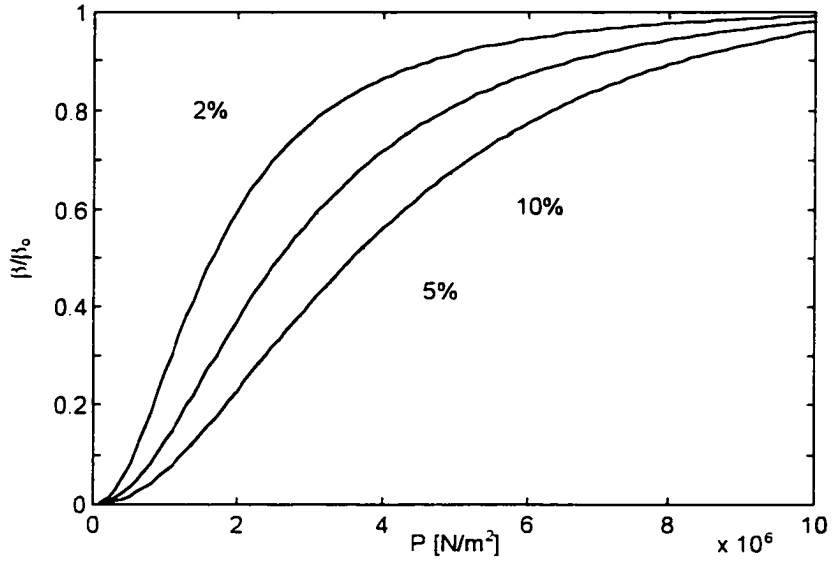

Figure 3.1 Effect of fluid/air ratio on bulk modulus

The following paragraphs describe the development of a closed loop control paradigm for the regulation of a hydraulic semiactive actuator. The variation of $\beta(P)$ with the

pressure is also assumed to be negligible for the purpose of the control design. On the other hand, when tuning the controller via simulation, the variation of β with pressure is included for each chamber. It is noted that the variation of β with the pressure can become a significant issue if there is an appreciable amount of air entrained in the hydraulic fluid (see Equation 3.2).

3.2.2 Lyapunov control

The general state equation (with the hydraulic SAVA and the external disturbance) can be expressed as

$$\dot{X} = AX + Bg(X) + D \tag{3.3}$$

where $g(X) = \Delta P$. The form of A, B and D are defined by the particular system being analyzed. The proceeding assumes a single actuator. The model also assumes turbulent flow through the valve. The extension of the functional forms to more actuators is straightforward.

A Lyapunov controller which is routinely applied to nonlinear systems with actuator saturation limits is used here [Mohler, 1991]. A quadratic Lyapunov function V is adopted

$$V = \frac{1}{2} X^T Q X . \tag{3.4}$$

V represents all forms of conservative energy stored in the system. The control goal is to dissipate any stored energy, which in turn suggest that the controller should be

crafted to move the system to its equilibrium position. Differentiating V with the respect to time and substitution of the state equation produces

$$\dot{V} = X^T(A^TQ + QA)X + X^TQBg(X) + X^TQD. \tag{3.5}$$

If $\dot{V}$ is negative, then we can conclude that the system is dissipative (stable). It is assumed that a Q exists and that $A^TQ + QA$ can be selected negative semi-definite. The last expression on the right hand side of equation (3.5) is disregarded, because there is nothing that can be done to effect the dissipativeness of that term. Here, Q represents the positive definite solution of the algebraic Lyapunov equation for a given symmetric positive definite P:

$$A^TQ \cdot QA = -P. \tag{3.6}$$

Several techniques have been proposed in the literature to solve the algebraic matrix Equation (3.6). One elementary way of solving Equation (3.6) includes direct application of the Kronecker matrix product. The Kronecker product was originally suggested by both Bellman [1959]. The algorithm is not unique, for example, both Chen and Shieh [1968] and Bingulac [1970] constructed their own algorithms. Nevertheless, this method remains both straightforward and simple for small matrices. The disadvantage of the method, however, is that it involves a great increase in calculation when the order of matrix A becomes large. The Bartels and Stewart algorithm [1972] continues to be widely used at present. The algorithm is based on

solving the generalized Sylvester's equation. The matrix A need not be asymptotically stable in order to use this algorithm.

At the present time, commercially available computer software (e.g., MATLAB®) can easily calculate the matrix Q of Equation (3.6). For any algorithm applied to this calculation, however, one should determine whether or not the calculated matrix Q is positive definite. One procedure that makes this determination involves confirming the eigenvalues of matrix Q -- according to this method, the real symmetric matrix Q is positive definite if, and only if, all eigenvalues are positive. Alternatively, Sylvester's criterion for positive definiteness of quadratic forms represents another method of calculating Q. Overall, these two methods provide a convenient (and efficient) way for checking the stability of given matrix.

The second term of Equation (3.5) can be controlled by changing the hydraulic damping force of SAVA. Here, let

$$f(X) = X^T Q B g(X). \tag{3.7}$$

For the multi-input control system, Equation (3.7) produces a scalar and can be rewritten in terms of state vectors and controller action as

$$S(X) = \sum_{k=1}^{m} \sum_{i=1}^{n} \rho_{ik} x_i g(X)_k \tag{3.8}$$

where n is the number of states of the system and m is the number of SAVA installed in the system. Equation (3.8) represents the generalized switching function with multiple

SAVA. The maximum dissipation is assured if A_v (the valve orifice area) is selected using the following bistate control law.

$$X^T \rho_i \operatorname{sgn}(\Delta P) \begin{cases} \geq 0, & A_v = A_{v\min} \\ < 0, & A_v = A_{v\max} \end{cases} . \tag{3.9}$$

The vector ρ_i provides a means of weighting the different states to emphasize a particular control objective.

The straightforward process outlined above produces, in essence, a feedback control. The notion that the control depends on all the states can appear to be problematic (This because a full state estimator will usually require some knowledge of the disturbance.). An inspection of the control rule makes it clear however that a judicious selection of ρ_i (some set to zero) can help to avoid the observer issue. A block diagram of the Lyapunov controller with full state feedback is shown in Figure 3.2. The implementation of the method is straightforward. The following section provides analytical and experimental evidence of the effectiveness of the control law, which is referred to as a bistate control law.

In summary, the more convenient procedures of the calculation of control gains of bi-state controller include the following steps:

1. defining a matrix P of Equation (3.6) as a positive definite matrix (For example, the unity matrix ($P = diag(1,1,...,1)$) is a simple positive definite matrix. The selection of the best diagonal elements in P ($diag(p_{11},p_{22},...,p_{nn})$) is accomplished using an

iterative tuning process with the comparison of system responses for a given input to the system.)

2. calculating matrix Q using convenient tools from the algebraic Lyapunov Equation (3.6) and

3. calculating the control gains from Equations (3.7) or (3.8).

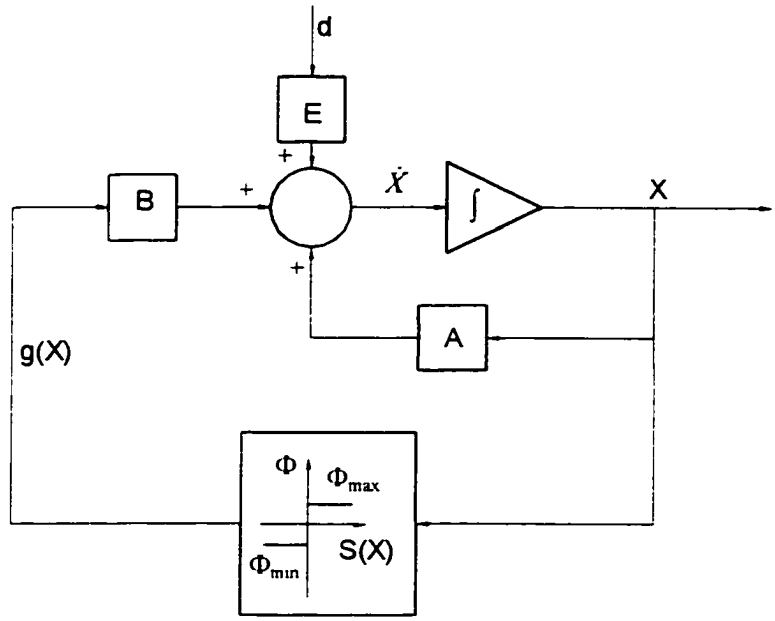

Figure 3.2 Block diagrams of a bistate controller.

3.2.3 Stability of SA systems

This subsection discusses the stability of time-invariant systems with both the stable-system matrix, A, along with nonlinear-controller action [Bellman, 1953,

Lefschetz, 1957]. The discussion, assumes the following form of dynamic control system with the initial conditions

$$\dot{X} \quad AX \cdot Bg(X) + GX_d, \quad X(t_i) \quad X_o \tag{3.10}$$

where $X \in R^{n\cdot 1}$, $X \in R^{r\cdot 1}$, the constant matrix $A \in R^{n\cdot n}$ and the constant matrix $B \in R^{n\cdot r}$. The controller action $g(X)$ represents the nonlinear damping force for SAVA system. The external disturbance $X_d \in R^n$ retains a bounded magnitude ($X_d \le X_{d\max}$). Consequently, the maximum magnitude of the disturbance should be restricted to the stable response of a system when the external input excites that system.

The solution of Equation (3.10) is then [Bellman, 1953]

$$X(t) \quad e^{At} X_o \cdot \int_{t_i}^{t_f} e^{A(t-\tau)} \{Bg(X,\tau) + GX_d\} d\tau \tag{3.11}$$

where Equation (3.11) indicates the response of the system for $t \ge t_i$.

Theorem: The linear state equation of the time-invariant system $\dot{X} \quad AX$ is stable if, and only if, all the eigenvalues of A have negative real parts. [Chen, 1970]

Here, the square matrix A can be expressed in Jordan canonical form, where the elements on the main diagonal represent the eigenvalues of A, and the elements just above the main diagonal are either 1 or 0, with all other elements being 0. Consequently, all elements of e^{At} exist in the form of $t^m e^{(\sigma_j \cdot i\omega_j)t}$, where $\sigma_j \cdot i\omega_j$

represents an eigenvalue of A. In addition, m represents the number of multiple eigenvalues $(m = 0, 1, 2, \ldots, m-1)$ with $t^m e^{(\sigma_j + i\omega_j)t}$ bounded for any m where σ_j is negative. The Jordan expression of the square matrix A thus signifies that $\| e^{At} \|$ is bounded because every entry of e^{At} is bounded. Thus,

$$\| e^{At} \| \leq \gamma e^{-\lambda t} \tag{3.12}$$

In addition, the controller action $g(X)$ and the external disturbance remain bounded (ψ, X_d):

$$\| Bg(X) + GX_d \| \leq \kappa \| X \| + \psi X_{d\max} \tag{3.13}$$

where κ and ψ are finite positive constants. Hence, from Equations (3.12) and (3.13)

$$\| X(t) \| \leq \gamma e^{-\lambda t} \| X_0 \| + \gamma e^{-\lambda t} \int_{t_i}^{t_f} e^{\lambda \tau} \{ \kappa \| X \| + \psi X_{d\max} \} d\tau \tag{3.14}$$

Multiplying both sides of Equation (3.14) by $e^{\lambda t}$ yields

$$e^{\lambda t} \| X(t) \| \leq \gamma \| X_0 \| + \int_{t_i}^{t_f} \gamma e^{\lambda \tau} \{ \kappa \| X \| + \psi X_{d\max} \} d\tau \tag{3.15}$$

Next, we recall Gronwall's Lemma [Lefschetz, 1957];

Gronwall's Lemma: Let K, ξ and ζ be positive constants and $f(t)$ be a scalar function such that

$$f(t) \le K + \int_{t_i}^{t_f} \{\xi f(\tau) + \varsigma\} d\tau \tag{3.16}$$

for $t_i \le t \le t_f$. If $t_f - t_i = M$, then

$$f(t) \le \{\varsigma M + K\} e^{\xi M} \qquad \text{for } t_i \le t \le t_f \tag{3.17}$$

Finally, by applying Gronwall's Lemma

$$\| X(t) \| \le \gamma \{ \| X_o \| + \psi X_{d\max} \} e^{-(\lambda - \gamma\kappa)(t_f - t_i)} \tag{3.18}$$

If we choose $\kappa < \dfrac{\lambda}{\gamma}$ small enough, then $0 < \kappa\gamma < \lambda$. In this case, $X(t) \to 0$ as $t \to \infty$ and the system is asymptotically stable. The analysis proves that for the conditions cited, the controlled system is BIBO (bounded input bounded output) stable and asymptotically stable.

3.3 Two DOF Structure with Base Isolation

In order to demonstrate the use of the techniques described above, we consider here a test rig that can be used to study the motion control of simple structure. The test rig is shown in Figure 3.3. The rig can be used to represent a two-story structure with base excitation for example. The actuation is provided via a powered hydraulic actuator. One possible location for a semiactive hydraulic actuator is shown in Figure 3.3

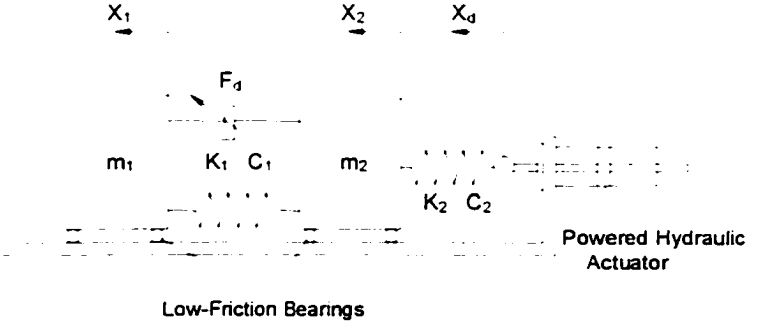

Figure 3.3 Configurations of TDOF test rigs (Case 1).

The equations of motion for the device are

$$\begin{aligned} m_1 \ddot{x}_1 &= -k_1(x_1 - x_2) - c_1(\dot{x}_1 - \dot{x}_2) - A_p \Delta P \\ m_2 \ddot{x}_2 &= k_1(x_1 - x_2) + c_1(\dot{x}_1 - \dot{x}_2) - k_2(x_2 - x_d) - c_2(\dot{x}_2 - \dot{x}_d) + A_p \Delta P \end{aligned} \tag{3.19}$$

Using the preceding definitions and introducing the state vector,

$$X = \{x_1 \quad x_2 \quad \dot{x}_1 \quad \dot{x}_2\}^T. \tag{3.20}$$

Then the matrix coefficients in Equation (3.20) can be shown to take the form

$$A \begin{bmatrix} 0 & 0 & 1 & 0 \\ 0 & 0 & 0 & 1 \\ -\frac{k_1}{m_1} & \frac{k_1}{m_1} & -\frac{c_1}{m_1} & \frac{c_1}{m_1} \\ \frac{k_1}{m_2} & -\frac{k_1+k_2}{m_2} & \frac{c_1}{m_2} & -\frac{c_1+c_2}{m_2} \end{bmatrix} \qquad (3.21\text{ a})$$

$$B \begin{bmatrix} 0 & 0 & -\frac{A_p}{m_1} & \frac{A_p}{m_2} \end{bmatrix}^T, \quad D \begin{bmatrix} 0 & 0 & 0 & \frac{k_2}{m_2} \\ 0 & 0 & 0 & \frac{c_2}{m_2} \end{bmatrix}^T \qquad (3.21\text{ b, c})$$

If the weighting matrix Ω is expressed as

$$\Omega = \{\rho_i\} \qquad i \quad 1, 2, \ldots, 4. \qquad (3.22)$$

Then the switching law for the system is

$$S(X) \quad \{\rho_1 x_1 + \rho_2 x_2 + \rho_3 \dot{x}_1 + \rho_4 \dot{x}_2\}\Delta P \qquad (3.23)$$

3.3.1 Case studies

The test rig discussed above provides a means of testing control laws as well as control realizations (control hardware layout possibilities). In buildings that may be subject to earthquakes, the engineer is faced with the responsibility of selecting an effective, least cost control configuration. The following section will examine the question of whether to mount the SA system between the top floor and the

intermediate floor (Case 1, Figure 3.3), or between the intermediate floor and the ground floor (Case 2, Figure 3.4).

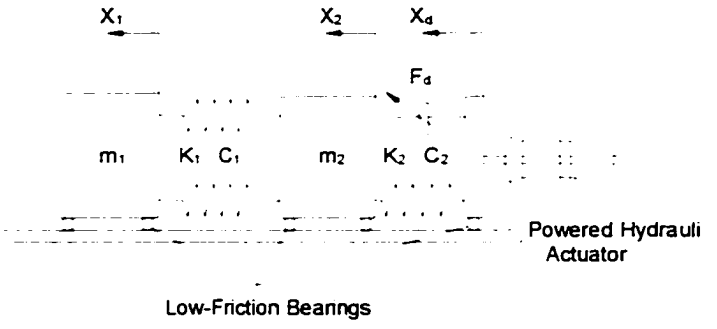

Figure 3.4 Configurations of TDOF test rigs (Case 2).

The amended system matrices for Case 2 are

$$A_2 = \begin{bmatrix} 0 & 0 & 1 & 0 \\ 0 & 0 & 0 & 1 \\ -\frac{k_1}{m_1} & \frac{k_1}{m_1} & -\frac{c_1}{m_1} & \frac{c_1}{m_1} \\ \frac{k_1}{m_1} & -\frac{k_1+k_2}{m_2} & \frac{c_1}{m_2} & -\frac{c_1+c_2}{m_2} \end{bmatrix} \qquad (3.24\text{ a})$$

$$B_2 = \begin{bmatrix} 0 & 0 & 0 & -\frac{A_p}{m_2} \end{bmatrix}^T, \quad D_2 = \begin{bmatrix} 0 & 0 & 0 & \frac{k_2}{m_2} \\ 0 & 0 & 0 & \frac{c_2}{m_2} \end{bmatrix}^T. \qquad (3.24\text{ b, c})$$

3.3.2 Test stand specifications

A test stand was constructed to test the effectiveness of a semiactive vibration absorber. The two masses were mounted on high precision, low friction ball bearings and attached to rails. The weights and spring rates were carefully measured and the system was assembled. Tests were conducted to determine the amount of apparent damping in the system prior to mounting the semiactive damper. The measured parameters for the test stand are given in Table 3.1.

Next, a semiactive damper was constructed. The parameters that characterize the damper are given in Table A.1 (see Appendix A). The valve orifice area is also given there. Testing was conducted to determine the dynamic response of the valve when operated with a DC servomotor. A simple PID control was utilized to regulate the commanded valve position. The closed loop bandwidth of the motor/valve pair was determined to be in excess of 80 Hz, with near perfect tracking at low to modest speeds. A standard high-pressure rated, low friction ball valve was used in conjunction with a high torque, pan/cake motor with low inherent inductance to actuate the valve.

The disturbance input (an earthquake time history) was provided by an active hydraulic actuator attached to the system through a spring. The characteristics of the double acting hydraulic actuator are given in Table A.3 (see Appendix A). A PID controller was used to accomplish command and tracking control of the base disturbance actuator. A two way, four port electrohydraulics spool valve manufactured by Moog Inc. was employed to provide regulation of the active fluid system. The measured bandwidth (closed loop) of the active disturbance system was in excess of

30Hz. The reader will note that the very light damping (less than 2% of critical damping ratio of the first mode of the system) made any testing without a damper problematic.

The instrumentation used in the experiment included two accelerometers mounted on each mass, an LVDT between mass #1 and #2, an LVDT between mass #2 and the inertial reference frame, and an LVDT to measure the position of the active hydraulic actuator. Velocities needed to determine a control action were computed via a numerical estimate based on the LVDT output.

Data acquisition was accomplished via a 16 channel, 200 kHz PC based I/O board. The sensors were sampled at 1 kHz. Each channel of analog input data was pre-filtered with a low pass hardware filter (second order) with a cut off frequency of 200 Hz.

3.3.3 Test results-open loop

Open loop tests were first conducted to determine the degree of damping that the SA actuator provided. In each case, the valve was fixed open and the system was subjected to simple random displacement input with an RMS amplitude of $0.0028m$. Transfer functions for Case 2 are shown in Figures 3.5 and 3.6. The added damping for the "passive" semiactive configuration is shown in Table 3.1. In order to determine the level of friction inherent in the SA dampers, stroke tests were executed on a separate head frame hydraulic testing unit. It was determined that the SA actuator exhibited approximately 545 N/sec of friction (see Equation 2.16), indicating that the

principal source of passive damping (when the valve is fixed open) is due primarily to the flow loss through the valve.

The time history of the earthquake (El Centro, 1940) that was used is shown in Figure 3.7 that time history is the twice integrated acceleration time history that was recorded during the actual event. The measured open loop time responses for Cases 1 and 2 are shown in Figures 3.8 and 3.14. Those results indicate that the model of the process provides an excellent means of determining the expected open loop response.

3.3.4 Test results-closed loop

Using the gain set ρ_1 (Table 3.2), then the closed loop response of the system was simulated, and experimentally measured for Case 1 and Case 2. Graphical comparisons are reproduced in Figure 3.9 (Case1) and in Figure 3.15 (Case 2). The data shown there confirms the accuracy of the model for the controlled system. The effectiveness of the closed loop versus passive response ($A_v = A_{vmax}$) for both cases is shown in Figures 3.12 and 3.19. Table 3.3 lists the peak and RMS (root mean square) values of the closed and open loop response for Case 1 and Case 2. For the accelerations and displacements (absolute and relative) in addition, the peak values of the pressures experienced in the actuator for Cases 1 and 2 are also listed.

Table 3.1 System parameters for experiments

Symbols	m_1	m_2	k_1	K_2	c_1	c_2	ω_1	ω_2
Unit	Kg	Kg	N/m	N/m	N/m/sec	N/m/sec	Hz	Hz
Case 1	131	136	45746	28420	100	645*	4.50	1.52
Case 2	144	193	28420	48470	645*	100	1.63	3.46

* includes 545 N/sec friction. ω_1, ω_2 = damped natural frequencies.

Table 3.2 Control gains for experiments (obtained via the Lyapunov Equation (3.7))

	ρ_1	ρ_2	ρ_3	ρ_4
Case 1	-1.306×10^{-6}	1.497×10^{-3}	1.466×10^{-3}	-3.296×10^{-3}
Case 2	-2.032×10^{-6}	1.448×10^{-5}	1.495×10^{-3}	-3.297×10^{-3}

Table 3.3 Response reductions of control compared to passive [%]

	Peak		RMS	
	1st floor	2nd floor	1st floor	2nd floor
Case 1	49.3 [1]	24.4 [2]	47.7 [5]	9.3 [6]
Case 2	6.5 [3]	14.7 [4]	3.9 [7]	15.9 [8]

[1, 5]: see Figure 3.12 [2, 6]: see Figure 3.13.
[3, 7]: see Figure 3.18 [4, 8]: see Figure 3.19.

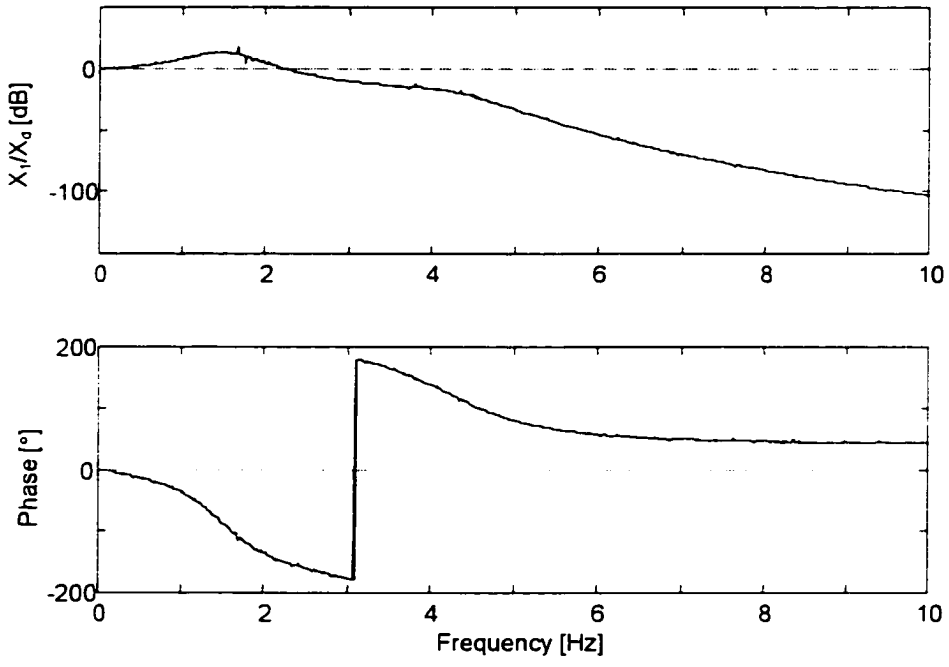

Figure 3.5a Open loop transfer function and phase between the second floor and random excitation: Case 2.

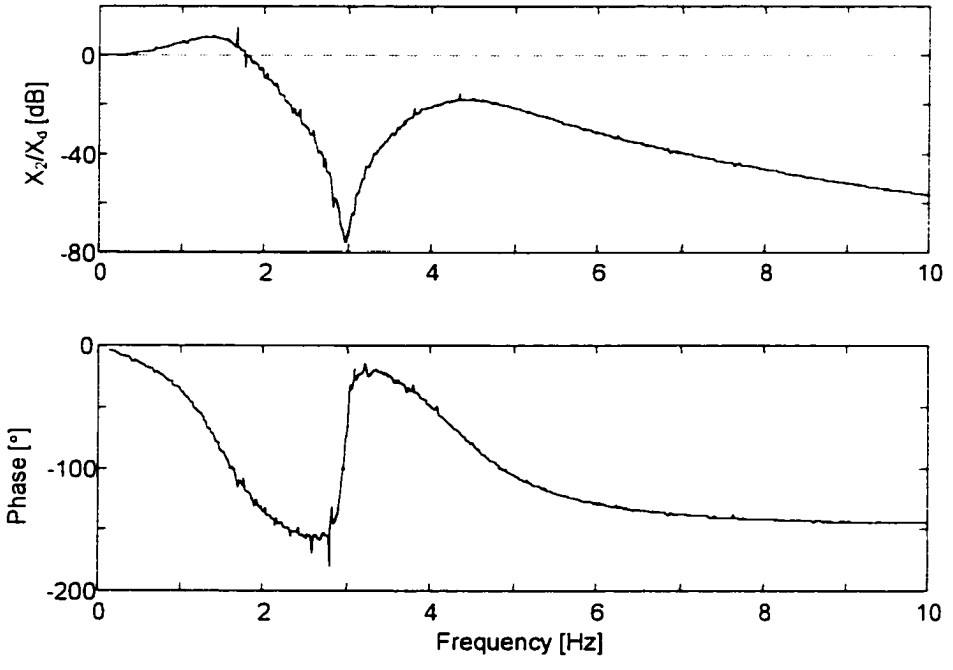

Figure 3.5b Open loop transfer function and phase between the first floor and random excitation: Case 2.

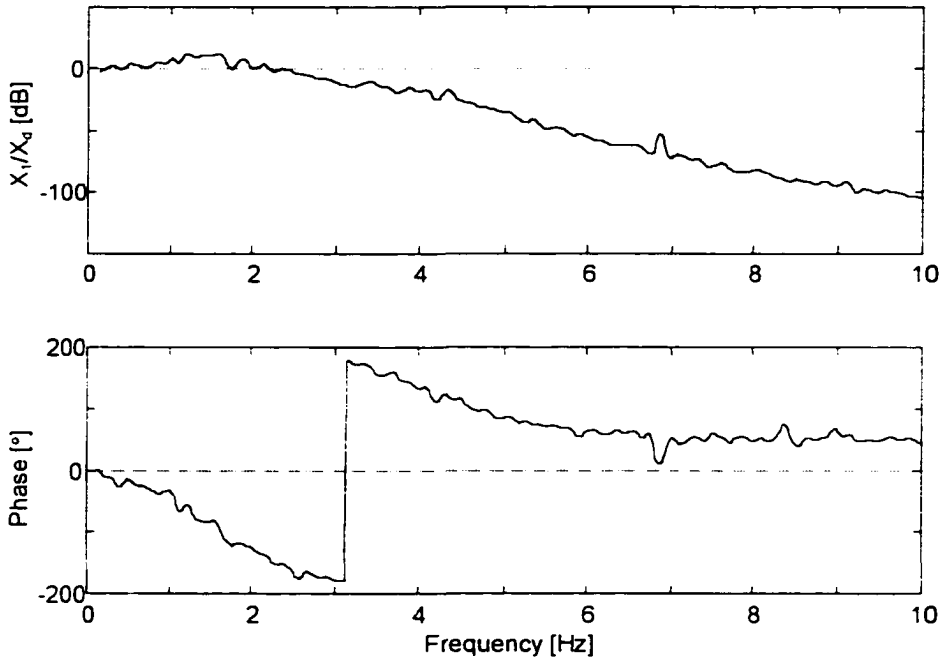

Figure 3.6a Closed loop (bistate control) transfer function and phase between the second floor and random excitation: Case 2.

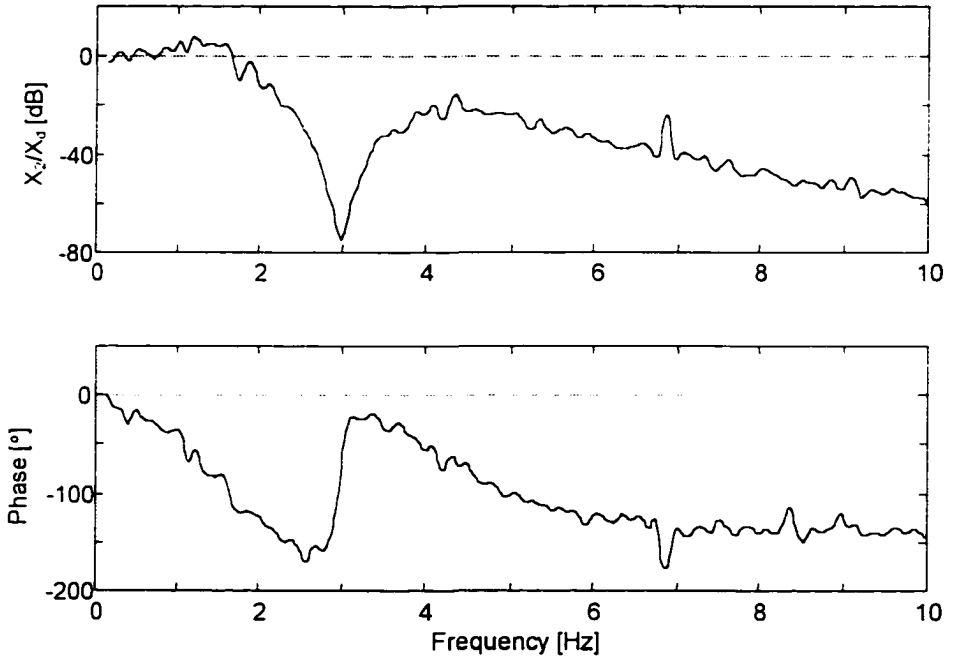

Figure 3.6b Closed loop (bistate control) transfer function and phase between the first floor and random excitation: Case 2.

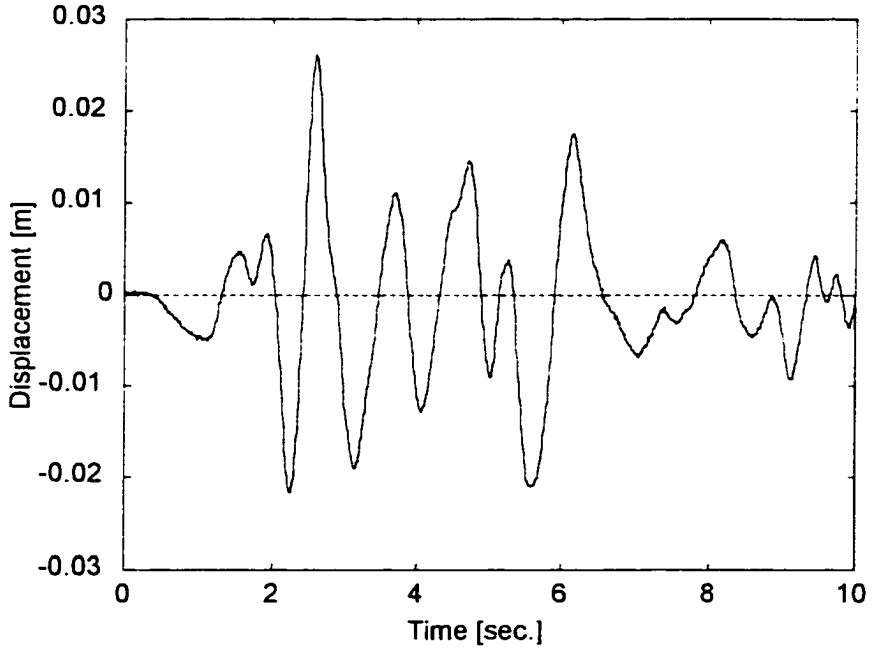

Figure 3.7 Time history of input disturbance

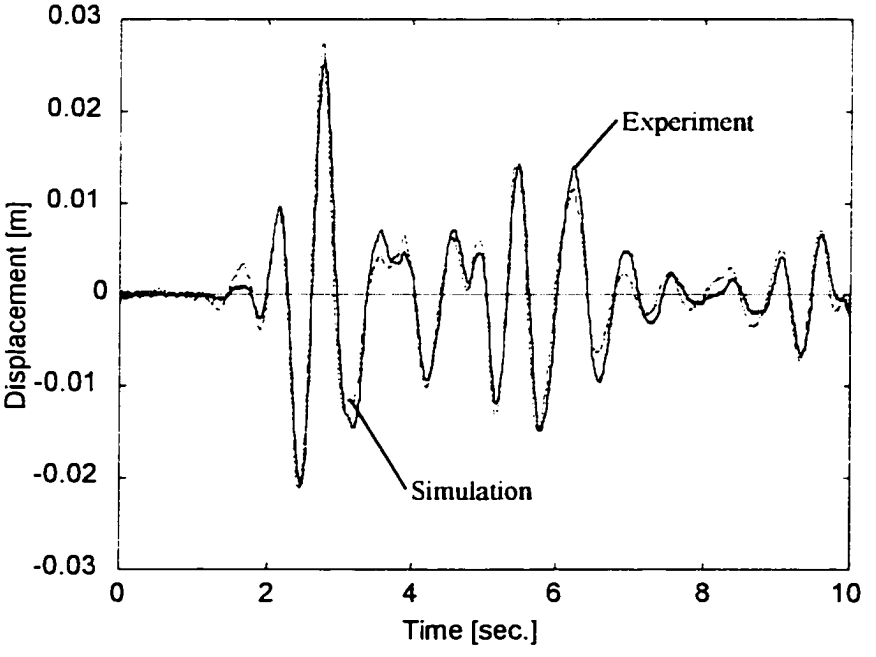

Figure 3.8 Comparison of simulation and experiment of the relative displacement of the first floor with the passive SAVA (valve fixed open, $A_v = A_{vmax}$): Case 1.

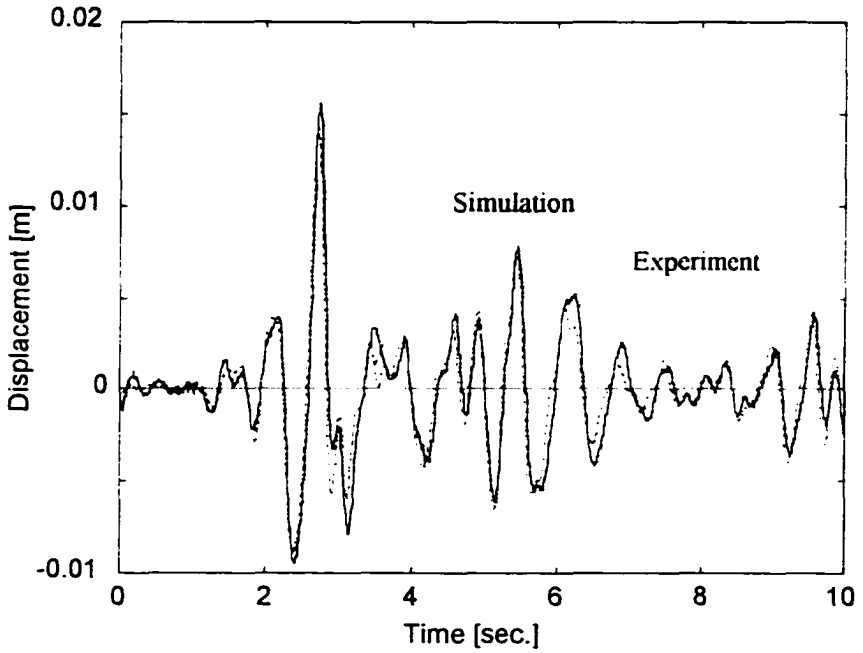

Figure 3.9 Comparison of simulation and experiment of the relative displacement of the second floor with the passive SAVA (valve fixed open, $A_v = A_{vmax}$): Case 1.

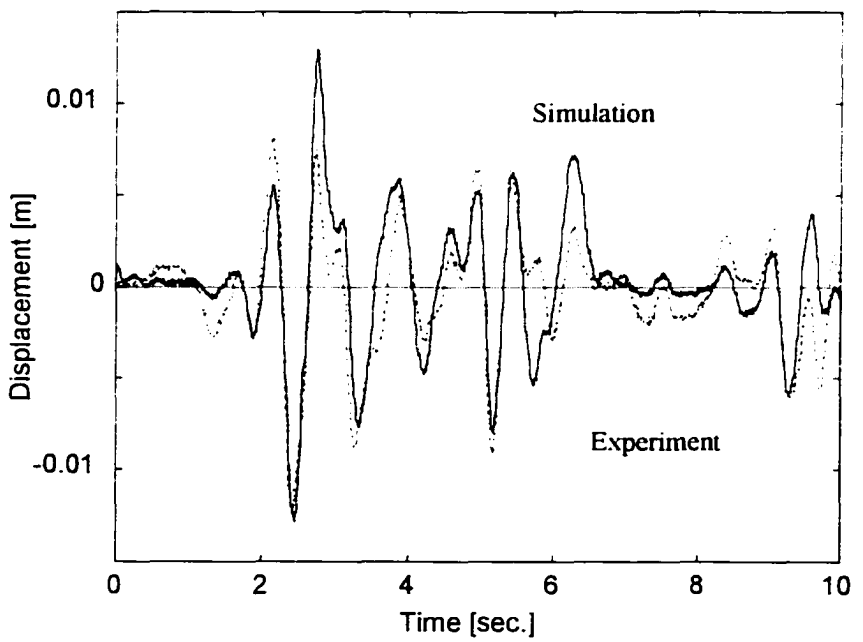

Figure 3.10 Comparison of simulation and experiment of the relative displacement of the first floor with the controlled SAVA ($A_v = A_{vmin} = 1.0 \times 10^{-6}\ m^2$, $\theta = 40°$): Case 1.

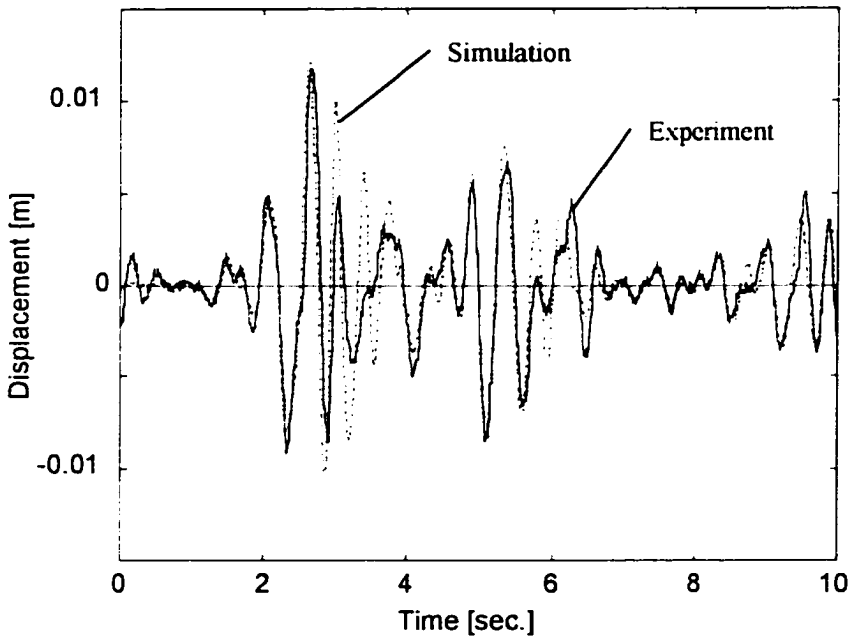

Figure 3.11 Comparison of simulation and experiment of the relative displacement of the second floor with the controlled SAVA (A_v A_{vmin} 1.0×10^{-6} m^2, θ 40°): Case 1.

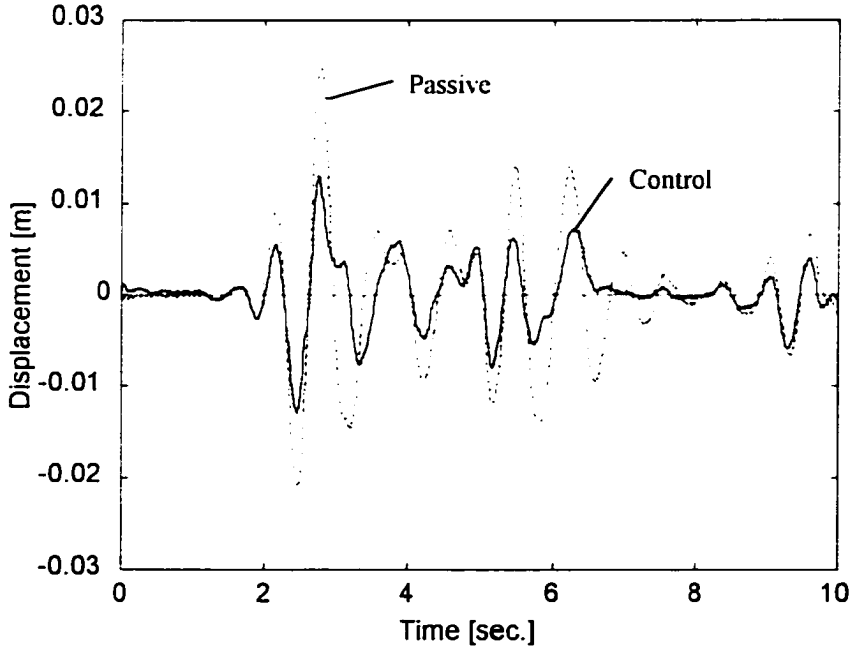

Figure 3.12 Comparison of experimental results of the relative displacement of the first floor with control ($A_v = A_{vmin} = 1.0\times10^{-6}$ m^2, $\theta = 40°$) and passive (with SAVA, valve fixed open, $A_v = A_{vmax}$): Case 1.

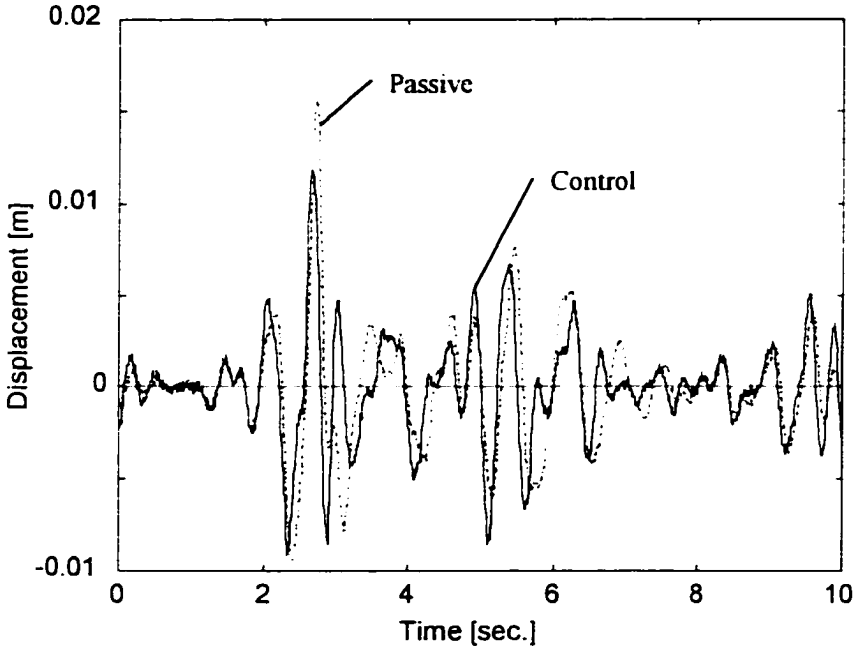

Figure 3.13 Comparison of experimental results of the relative displacement of the second floor with control (A_v A_{vmin} 1.0×10^{-6} m^2, θ $40°$) and passive (with SAVA, valve fixed open, A_v A_{vmax}): Case 1

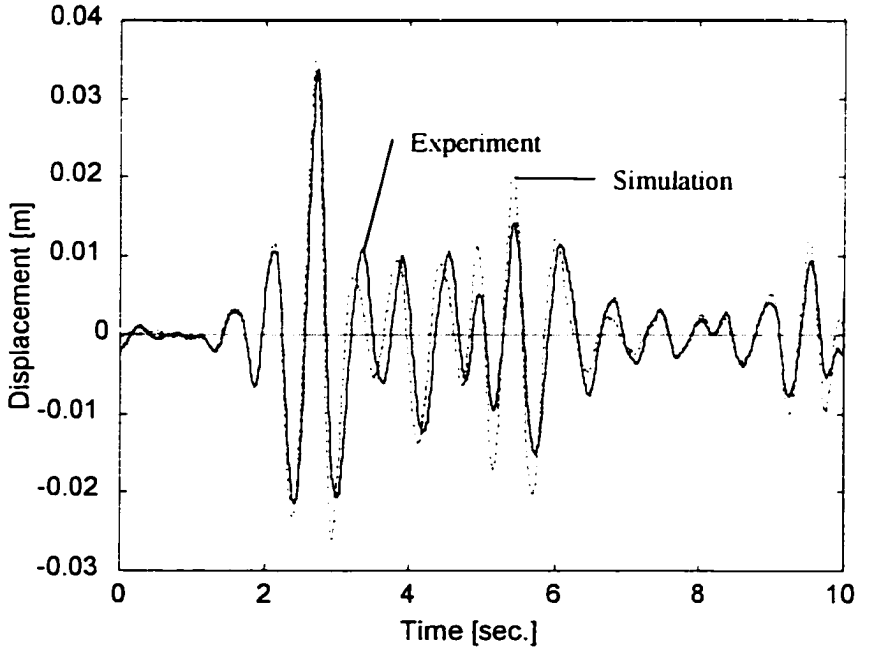

Figure 3.14 Comparison of simulation and experiment of the relative displacement of the first floor with the passive SAVA (valve fixed open, $A_v = A_{vmax}$): Case 2.

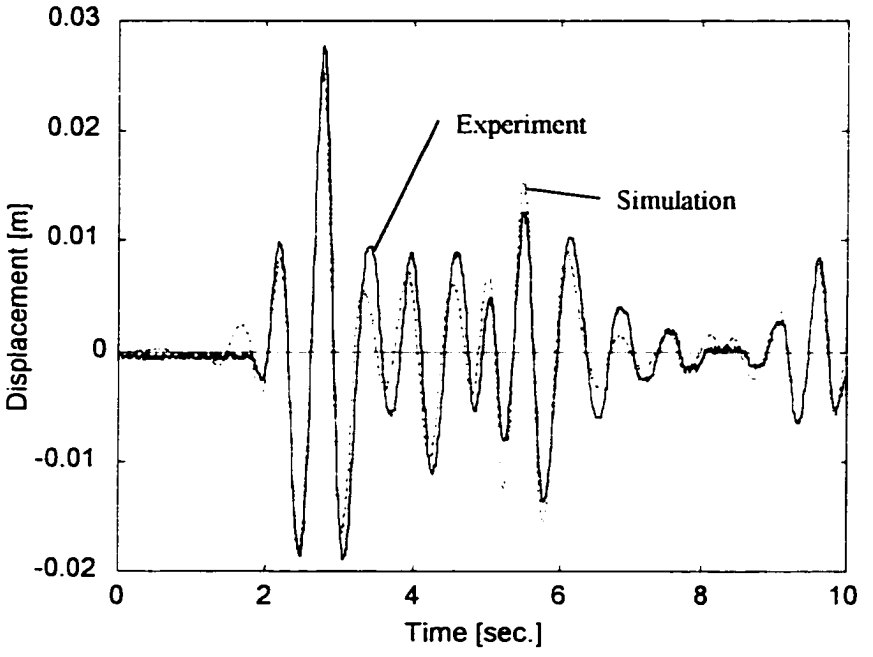

Figure 3.15 Comparison of simulation and experiment of the relative displacement of the second floor with the passive SAVA (valve fixed open, A_v A_{vmax}): Case 2.

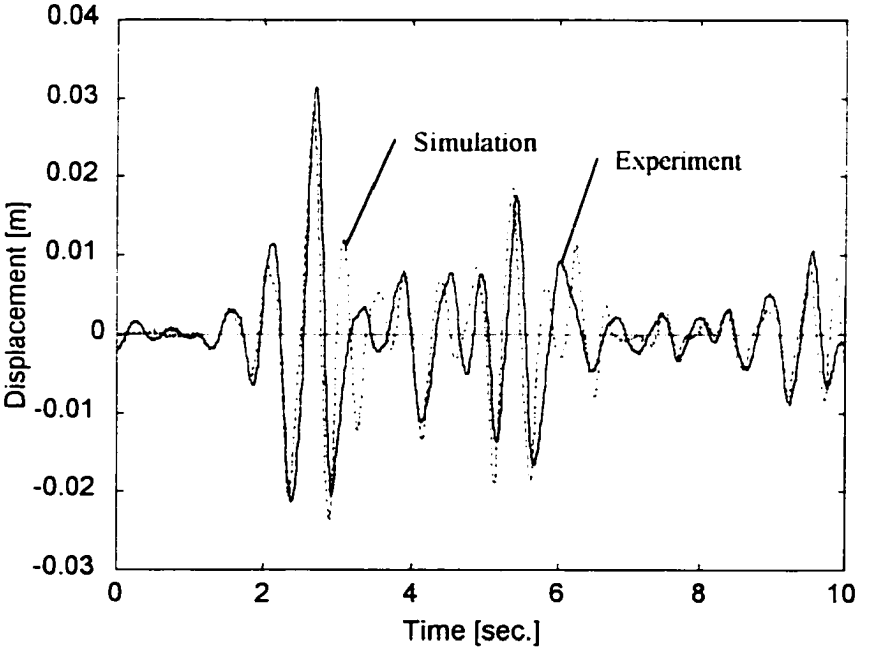

Figure 3.16 Comparison of simulation and experiment of the relative displacement of the first floor with the controlled SAVA ($A_v = A_{vmin} = 1.0\times10^{-6}\ m^2$, $\theta = 40°$): Case 2.

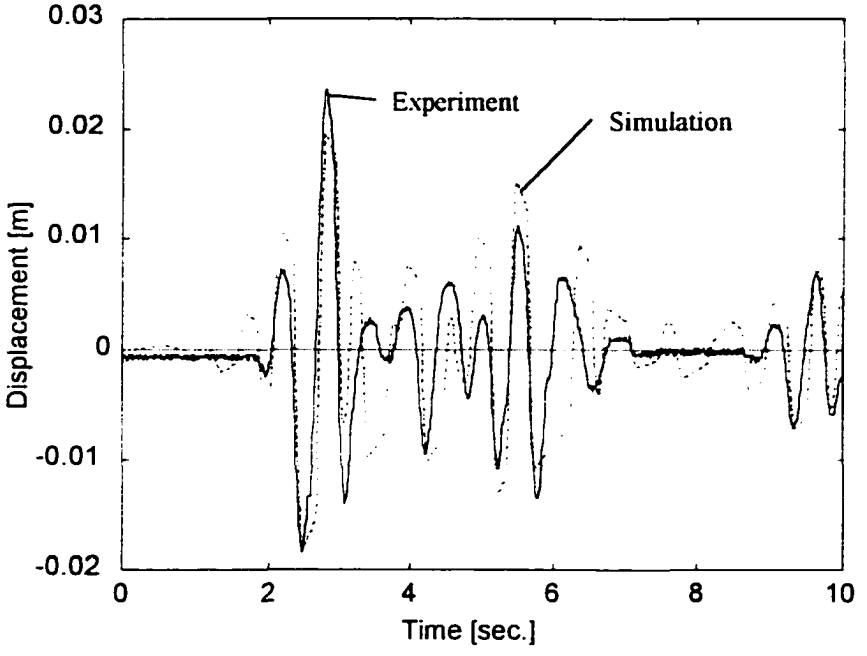

Figure 3.17 Comparison of simulation and experiment of the relative displacement of the second floor with the controlled SAVA ($A_v = A_{vmin} = 1.0\times10^{-6}\ m^2$, $\theta = 40°$): Case 2.

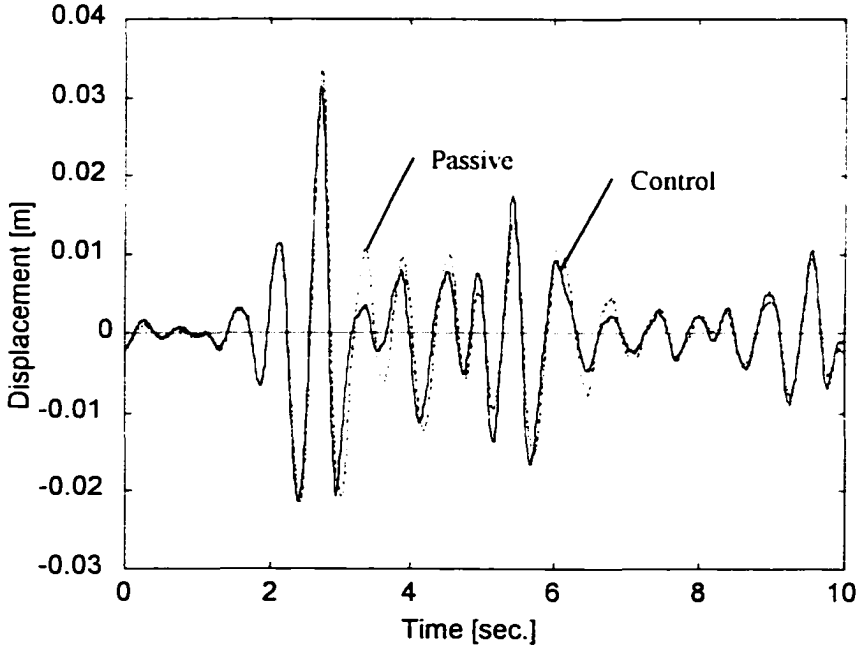

Figure 3.18 Comparison of experimental results of the relative displacement of the first floor with control ($A_v = A_{vmin} = 1.0\times10^{-6}\ m^2$, $\theta = 5°$) and passive (with SAVA, valve fixed open, $A_v = A_{vmax}$): Case 2.

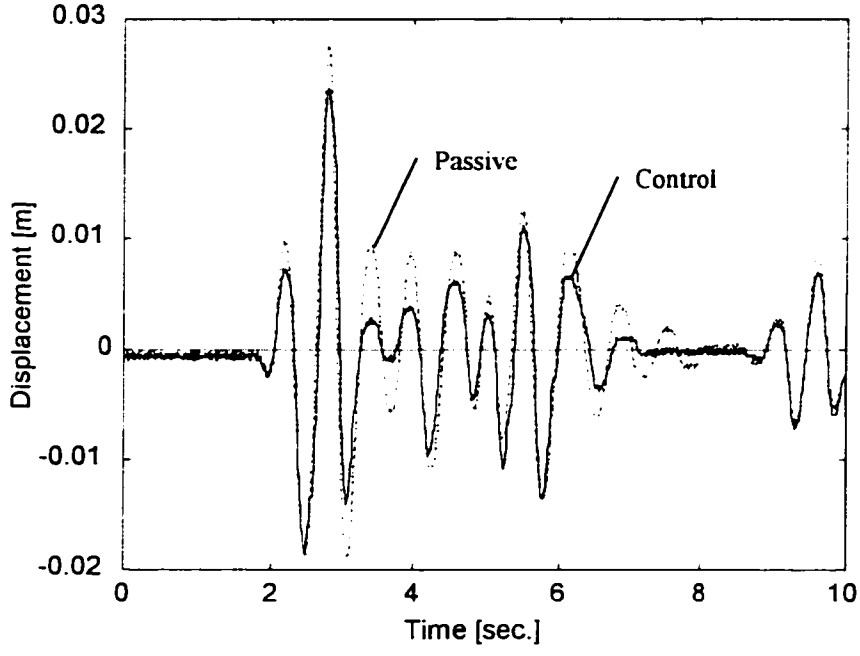

Figure 3.19 Comparison of experimental results of the relative displacement of the second floor with control (A_v A_{vmin} 1.0×10^{-6} m^2, θ 5°) and passive (with SAVA, valve fixed open, A_v A_{vmax}): Case 2.

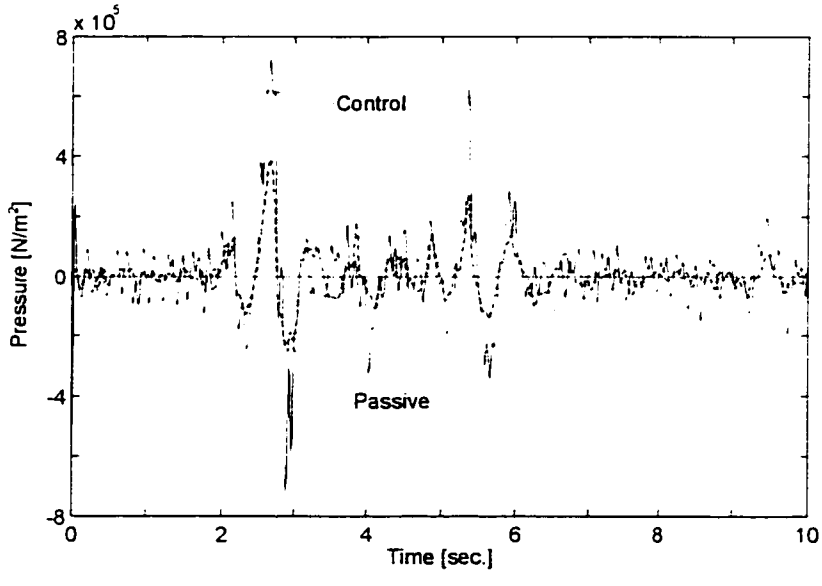

Figure 3.20 Comparison of experimental results of the pressure difference between control ($A_v = A_{vmin} = 1.0\times10^{-6}$ m^2, $\theta = 40°$) and passive (with SAVA, valve fixed open, $A_v = A_{vmax}$): Case 1.

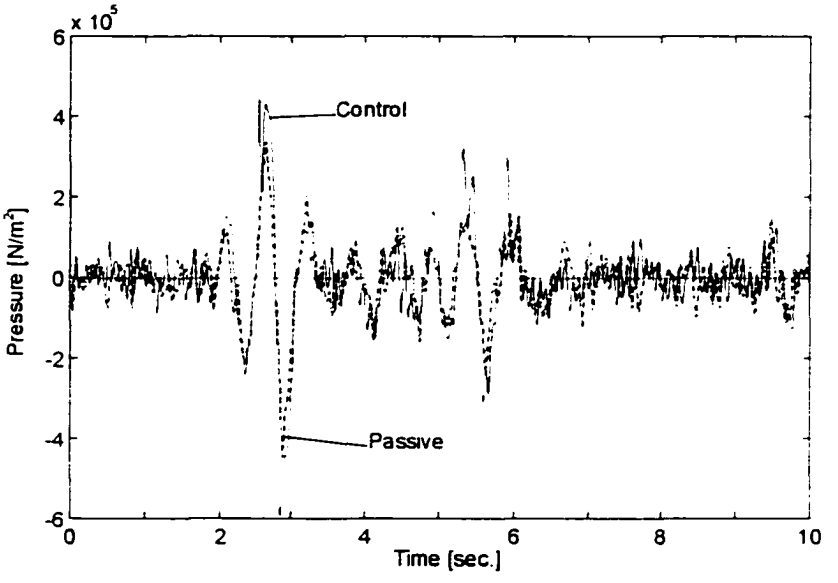

Figure 3.21 Comparison of experimental results of the pressure difference between control ($A_v = A_{vmin} = 1.0\times10^{-6}\ m^2$, $\theta = 40°$) and passive (with SAVA, valve fixed open, $A_v = A_{vmax}$): Case 2.

3.4 Discussion and Conclusion

The results confirm that a single actuator mounted between two of the floors in the structure does provide significant mitigation. The reductions of the maximum relative peak are 49.3% (first floor) and 22.4% (second floor) for Case 1, and 6.5% (first floor) and 14.7% (second floor) for Case 2, for the first and second floors, respectively. Using the Lyapunov bistate control, the experiment for each case is accomplished with respectively accomplishment for case 1 of 47.7% (first floor) and 9.3% (second floor), and for case 2 of 3.9% (first floor) and 15.9% (second floor) reductions in RMS for the relative displacement.

The data suggests that the semiactive hardware provide only marginal reductions of motion of those floors to which the actuator is not attached. The results leave unanswered the question of whether the SA hardware design might not effect the performance. That question is addressed in part in the next chapter.

CHAPTER FOUR

COMPARATIVE PERFORMANCE OF COMPETING SA CONTROLLERS

The Lyapunov control law developed in the previous chapter provides a rational and analytic basis for the regulation of a SA hydraulic actuator. Much of the past literature that reports control design for SA systems has relied on heuristic control laws. In some cases those alternative controllers have been demonstrated to provide an effective approach to control. The majority of those works do not include a consideration of the dynamics of the actuator. The common approach used is to assume that the SA actuator acts like an adjustable (linear) damper with the following constraint

$$c_{\min} \le c \le c_{\max} . \tag{4.1}$$

The desired level of damping (c) is determined via a control law (The selection of c is sometimes restricted to discrete levels of c.). A common approach to the establishment of a control rule is to impose a realistic constraint on the operability of the device, that is accomplished by restricting the work performed by a SA actuator. To be dissipative,

$$0 \le F_d v_{rel} \tag{4.2}$$

where $F_d = A_p \Delta P$ is the force delivered by the device, A_p is the piston area, ΔP is the difference of pressure across the piston and v_{rel} is the relative velocity across the actuator.

Recalling the hydraulic analysis given in the preceding chapter, it is clear then that the

constraint (Equation 4.1) fails to recognize the energy storage that is possible because of the compressibility (see Equation 3.2). Various strategies can be used to establish a desired value of damping at any instant. Hrovat et al. [1988] and Patten et al. [1994b] have for example employed a "clipped" optimal control policy that appears to work well in simulations. The "clipped" optimal approach presumes a linear system with a standard LQR feedback controller. Patten et al. [1994b] does include the nonlinear dynamics of the actuator when developing a "clipped" optimal control, but he linearizes the hydraulics with nonlinear feedback (feedback linearization). The controller produces a desired actuator force at each moment. Next, Equation 4.2 was checked to assure dissipativeness of the desired control force. If the dissipativeness condition is satisfied (Equation 4.2), then the required force is achieved by adjust the damping. Noting that the force output of the adjustable damper is linearly related to the relative velocity across the actuator

$$F_d = cv_{rel} \tag{4.3}$$

then the desired damping is

$$c = \frac{A_p \Delta P}{v_{rel}}. \tag{4.4}$$

In addition to the "clipped" optimal algorithm, other control laws have been proposed in the past to regulate adjustable dampers. The purpose of this chapter is to compare the performance of various control rules for semiactive dampers.

4.1 Comparison between Different Control Algorithms

4.1.1 Case (a)

The performance comparison will be made in terms of a specific application. Consider first the two-degree-of-freedom structure introduced previously (Figure 4.1) with two alternative configurations. The first (Case (a)) assumes the placement of a SA actuator between m_1 and m_2.

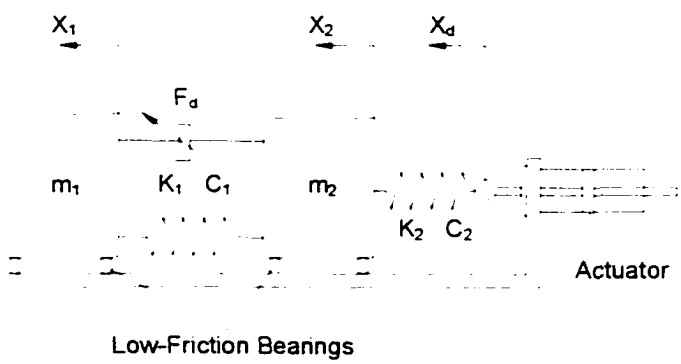

Figure 4.1 Configurations of TDOF system for Case (a).

Simulations of the systems response to a seismic disturbance with different controllers will be determined. In addition to the Lyapunov and "clipped" optimal algorithms, the following four algorithms will be employed

Algorithm 1 [Karnopp et al., 1974];

$$\begin{cases} c = c_{min} & if\ \dot{x}_1(\dot{x}_1 - \dot{x}_2) \le 0 \\ c = c_{max} & if\ \dot{x}_1(\dot{x}_1 - \dot{x}_2) > 0 \end{cases} \tag{4.5}$$

Algorithm 2 [Rakheja and Sankar, 1985];

$$\begin{cases} c = c_{min} & if\ (x_1 - x_2)(\dot{x}_1 - \dot{x}_2) \le 0 \\ c = c_{max} & if\ (x_1 - x_2)(\dot{x}_1 - \dot{x}_2) > 0 \end{cases} \tag{4.6}$$

Algorithm 3;

$$\begin{cases} c = c_{min} & if\ (x_1 - x_2)\,\Delta P \le 0 \\ c = c_{max} & if\ (x_1 - x_2)\,\Delta P > 0 \end{cases} \tag{4.7}$$

Algorithm 4;

$$\begin{cases} c = c_{min} & if\ (\dot{x}_1 - \dot{x}_2)\,\Delta P \le 0 \\ c = c_{max} & if\ (\dot{x}_1 - \dot{x}_2)\,\Delta P > 0 \end{cases} \tag{4.8}$$

Algorithm 1 was proposed by Karnopp et al. [1974] as a means of adjusting a variable automotive shock absorber. The logic is referred to as a sky hook damper. Algorithm 2 was proposed by Rakheja and Sankar [1985] as an alternative to the sky hook damper to avoid the need to estimate (or measure) the absolute velocity $\dot{x}_1$. The proposed algorithm can for example be realized by a single sensor (an LVDT to measure relative displacement) and a software filter to establish the relative velocity. Algorithm 3 is a variant of algorithm of Algorithm 2. The two are equivalent if the actuator force is assumed to be linearly related to the relative velocity across the actuator. Algorithm 4 is in essence a bistate control logic that enforces the dissipativeness rule discussed above. While the origin of the rule is not clear, a review of SA control laws by Ivers and Miller [1991] indicate that this algorithm is in routine use by investigators. It is also noted that Algorithms 3 and 4 are in

fact variants of the Lyapunov law (Equation 3.26) with certain weight (ρ_i) set either to 1 or 0.

Simulations were carried out using each of the six controllers. In each case, the dynamics of the actuator are included in the simulation. The effectiveness of the controls is established by comparing the RMS and maximum amplitude of the displacements and accelerations that result. The parameters used in the simulation are given in Tables 3.1 and 3.4.

Table 4.1 Control gains of the bistate controller for Case (a)

Gains	ρ_1	ρ_2	ρ_3	ρ_4
Values	-1.2823×10^{9}	8.2237×10^{8}	-4.3998×10^{5}	-5.8969×10^{5}

Clipped Optimal [Hac, 1992]

Consider the linear system described by

$$\dot{X} = AX + Bf + EX_d \tag{4.9}$$

and a performance index for the system

$$J = \lim_{T \to \infty} \frac{1}{2}\int_0^T \{\rho_1 \ddot{x}_1^2 + \rho_2 (x_1 - x_2)^2 + \rho_3 \ddot{x}_2^2 + \rho_4 (x_2 - x_d)^2\} dt . \tag{4.10}$$

where ρ_1 and ρ_3 are weighting factors for the absolute accelerations of the second ($\ddot{x}_1$) and first ($\ddot{x}_2$) floors, and ρ_2, and ρ_4 for the relative displacements of the second ($x_1 - x_2$) and

first ($x_2 - x_d$) floors. The performance index given by Equation (4.9) can be rewritten as

$$J = \lim_{T \to \infty} \frac{1}{2} \int_0^T \{X^T QX + 2X^T Nf + f^T Rf + 2X^T Q_2 X_d + X_d^T Q_1 X_d\} dt \qquad (4.11)$$

Assuming that x_d can be suppressed, then, the control law that minimizes J for the system (Equation (4.9)) is given by

$$f_o = -R^{-1}(N^T + B^T P)X \qquad (4.12)$$

where P is a positive definite solution of the following algebraic Riccati equation:

$$P(A - BR^{-1}N^T) + (A - BR^{-1}N^T)P - PBR^{-1}B^T P + (Q - NR^{-1}N^T) = 0 \qquad (4.13)$$

The "on-off" control law based on the clipped optimal (CO) is given as follow:

$$\begin{cases} A_v = A_{v\min} & if \quad c^* > 0 \\ A_v = A_{v\max} & if \quad c^* \le 0 \end{cases} \qquad (4.14)$$

where c^* is the damping rate modulated using Equation (4.4) and

$$c^* = \frac{f_o}{\dot{s}}. \qquad (4.15)$$

Table 4.2 lists the control gains of clipped optimal controller for simulation of Cases (a) and (b), relative coordinates and two SAVAs. The minimum valve area of semiactive actuator is fixed for the simulation of Cases (a) and (b) and relative coordinates (A_{vmin} $2.5\times10^{-6}\ m^2$, θ = 10°).

Table 4.2 Control gains of clipped optimal controller for each case

Gains	ρ_1	ρ_2	ρ_3	ρ_4
Cases (a)	1.0	1.0×10^9	0.0	1.0×10^9
Cases (b)	1.0	3.0×10^9	1.0	3.0×10^9
System (4.16)	1.0	1.0×10^9	1.0	1.0×10^9
Two SAVAs	1.0	1.0×10^8	1.0	1.0×10^8

Table 4.3 lists the RMS and maximum peak values of the response of the relative displacements and absolute accelerations. The comparisons are offered relative to the performance of the Lyapunov control. Negative values in Table 4.3 indicate that the value is larger relative to the Lyapunov result. Larger relative displacements and accelerations are less desirable. The results in Table 4.3 indicate that there is no one "best" controller. The RMS relative displacement of Algorithm 1 is 30.8% better at the first floor than the Lyapunov control, yet the relative displacement between the first and second floor is -35.9% (larger). The acceleration responses (RMS) using Algorithm 1 (the sky hook damper) are reduced (22.2% and 34.4%) from those that result from the Lyapunov law. The RMS values obtained using Algorithms 3 and 4 are less effective than the Lyapunov law because both the relative displacement and absolute acceleration of the upper stories are larger than those obtained using the Lyapunov control.

In order to make a decision on which algorithm is best the following reasoning was employed. The increase (or decrease) of motion (displacement or acceleration) for each floor was added (e.g. for Algorithm 1, Table 4.3 then the sum of relative response indices

is –4.1% = 30.8% – 34.9%). Those sums are shown in Tables 4.3 and 4.4. The nature of the problem (seismic protection) indicates that the maximum peak measurements are the most important criteria (Table 4.4) and that peak displacements are more critical than peak accelerations. Given that prioritization, then one can conclude that Algorithm 4 provides slightly better performance than the Lyapunov control, and that both Algorithm 4 and Lyapunov control provide significantly greater seismic protection than do Algorithms 1 through 3 and the clipped optimal controller.

Table 4.3 RMS reduction compared with the bistate controller for Case (a)

Control Algorithms	Relative displacement [m]			Absolute acceleration [m/s^2]		
	1st floor ($x_2 - x_d$)	2nd floor ($x_1 - x_2$)	1st +2nd	1st floor ($\ddot{x}_2$)	2nd floor ($\ddot{x}_1$)	1st +2nd
Algorithm 1	30.9%	-34.8%	-3.9%	22.1%	33.5%	55.6%
Algorithm 2	1.2%	-22.5%	-21.3%	-3.3%	-12.5%	-13.8%
Algorithm 3	1.2%	-22.3%	-21.1%	-3.6%	-12.4%	-16.0%
Algorithm 4	-0.3%	8.7%	8.4%	2.3%	8.1%	10.4%
Clipped optimal	11.8%	-9.4%	2.4%	14.8%	17.0%	31.8%
Lyapunov control	0.0067	0.9683		0.00217	1.11	

Negative values indicate larger values relative to Lyapunov control result.
Positive values indicate smaller values relative to Lyapunov control result.
$A_{vmin} = 2.5\times10^{-6}\ m^2$, $\theta = 35°$.

Table 4.4 Maximum-peak reduction compared with the bistate controller for Case (a)

Control Algorithms	Relative displacement [m]			Absolute acceleration [m/s^2]		
	1st floor ($x_2 - x_d$)	2nd floor ($x_1 - x_2$)	1st +2nd	1st floor ($\ddot{x}_2$)	2nd floor ($\ddot{x}_1$)	1st +2nd
Algorithm 1	18.8%	-124.1%	-105.3%	-47.8%	57.6%	9.8%
Algorithm 2	-2.0%	-38.3%	-40.3%	-21.4%	-38.0%	-59.4%
Algorithm 3	-2.0%	-38.3%	-40.3%	-32.6%	-38.0%	-70.6%
Algorithm 4	0.4%	1.1%	1.5%	0.4%	46.8%	47.2%
Clipped optimal	7.3%	-71.0%	-63.7%	8.7%	48.1%	56.8%
Lyapunov control	0.0473	0.0108		6.656	13.1	

Negative values indicate larger values relative to Lyapunov control result.
Positive values indicate smaller values relative to Lyapunov control result.
$A_{vmin} = 2.5\times10^{-6}\ m^2$, $\theta = 35°$.

4.1.2 Case (b)

The work next examines the performance of each of the six control algorithms (see above) when the actuator is used to provide base isolation for a seismic structure.

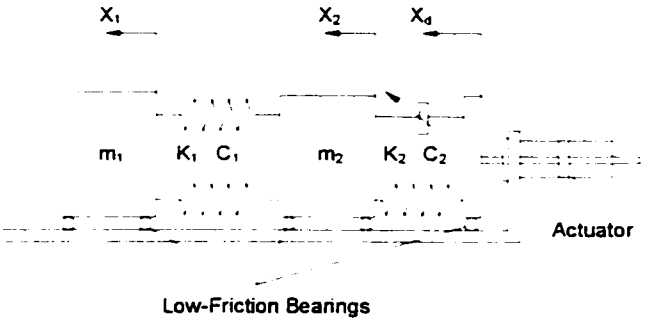

Figure 4.2 Configurations of TDOF system for Case (b).

The simulations assume the same disturbance used in the previous section (El Centro, 1940). The Lyapunov gains were established using the method described in Section 3.2. Those gains are given in Table 4.5. The parameters that define the system are given in Table 3.1. The results of the simulations are listed in Table 4.6 (RMS) and Table 4.7 (maximum peak values) using the same criteria described in the previous section. The data suggests that Algorithm 4 provide the best performance, with the Lyapunov controller again placing a close second. In particular, Algorithm 4 provides significant peak displacement reduction at the first floor (17%) and a 32% reduction of acceleration there. Algorithm 4 realizes a small increase of both displacement and acceleration at the second floor relative to the Lyapunov control when base isolation is employed.

Table 4.5 Control gains for the bistate controller for Case (b)

Gains	ρ_1	ρ_2	ρ_3	ρ_4
Values	1.3828×10^{8}	-4.0094×10^{13}	3.3630×10^{5}	-1.4214×10^{1}

Table 4.6 RMS reduction compared with the bistate controller for Case (b)

Control Algorithms	Relative displacement [m]			Absolute acceleration [m/s^2]		
	1st floor ($x_2 - x_d$)	2nd floor ($x_1 - x_2$)	1st +2nd	1st floor ($\ddot{x}_2$)	2nd floor ($\ddot{x}_1$)	1st +2nd
Algorithm 1	-24.0%	11.1%	-12.9%	16.1%	11.1%	27.2%
Algorithm 2	-22.1%	-22.4%	-44.5%	-38.8%	-22.4%	-61.2%
Algorithm 3	-21.9%	-22.5%	-44.4%	-38.7%	-22.5%	-61.2%
Algorithm 4	10.2%	-4.1%	6.3%	-7.2%	-4.1%	-11.3%
Clipped optimal	16.4%	-17.6%	-1.2%	-33.5%	-17.6%	-51.1%
Bistate control	0.00169	0.00147		0.537	0.512	

Negative values indicate larger values relative to Lyapunov control result.
Positive values indicate smaller values relative to Lyapunov control result.
A_{vmin} 2.5×10^{-6} m^2, θ 35°.

Table 4.7 Maximum-peak reduction compared with the bistate controller for Case (b)

Control Algorithms	Relative displacement [m]			Absolute acceleration [m/s^2]		
	1st floor ($x_2 - x_d$)	2nd floor ($x_1 - x_2$)	1st +2nd	1st floor ($\ddot{x}_2$)	2nd floor ($\ddot{x}_1$)	1st +2nd
Algorithm 1	-54.0%	-20.0%	-74.0%	35.6%	-20.2%	15.8%
Algorithm 2	-31.2%	-46.4%	-77.6%	-95.3%	-46.4%	-141.7%
Algorithm 3	-31.2%	-46.4%	-77.6%	-95.3%	-46.4%	-141.7%
Algorithm 4	17.1%	-10.2%	6.9%	31.4%	-10.0%	21.4%
Clipped optimal	27.2%	-24.0%	3.2%	-1.5%	-23.9%	-25.4%
Bistate control	0.00971	0.00971		8.059	3.389	

Negative values indicate larger values relative to Lyapunov control result.
Positive values indicate smaller values relative to Lyapunov control result.
A_{vmin} 2.5×10^{-6} m^2, θ = 35°.

4.1.3 Relative coordinates for Case (b)

An open question at this point is whether the performance of the control scheme is affected if relative coordinates are used to define the system. There is a clear reason to relay on relative coordinates; the size (magnitude) of the relative displacement between floors in a seismic structure is a direct indication of the potential for damage. We rely again on the base isolation system to make a determination (Figure 4.2, Case (b)).

Selecting the relative state coordinates as $z_1 = x_1 - x_2$ and $z_2 = x_2 - x_d$ then the equations of motion of the system in state space have the form

$$\dot{Z} = AZ + Bg(Z) + E\ddot{X}_d \tag{4.16}$$

where

$$A = \begin{bmatrix} 0 & 0 & 1 & 0 \\ 0 & 0 & 0 & 1 \\ -\frac{k_1}{m_1} - \frac{k_1}{m_2} & \frac{k_2}{m_2} & -\frac{c_1}{m_1} - \frac{c_1}{m_2} & \frac{c_2}{m_2} \\ \frac{k_1}{m_2} & -\frac{k_2}{m_2} & \frac{c_1}{m_2} & -\frac{c_2}{m_2} \end{bmatrix}, \quad B = \begin{bmatrix} 0 \\ 0 \\ \frac{A_p}{m_2} \\ -\frac{A_p}{m_2} \end{bmatrix} \tag{4.17 a, b}$$

$$E = [0 \quad 0 \quad 0 \quad -1]^T, \quad Z = [z_1 \quad z_2 \quad \dot{z}_1 \quad \dot{z}_2]^T. \tag{4.17 c, d}$$

The switching functions for the four test algorithms in terms of the relative coordinates are shown in Table 4.8.

Table 4.8 Switching functions of the four control algorithms

Algorithm 1	Algorithm 2	Algorithm 3	Algorithm 4
$\dot{x}_2, \dot{z}_2$	$z_2, \dot{z}_2$	$z_2, \Delta P$	$\dot{z}_2, \Delta P$

The gains used in the Lyapunov controller were recomputed using the same information given in Section 3.2 above. The P matrix used was (the diagonal elements are obtained by tuning for the best performance of system responses with a given acceleration earthquake (El Centro, 1940, horizontal direction) input to the system, see Section 3.2.)

$$P = \begin{bmatrix} 1 & 0 & 0 & 0 \\ 0 & 10^5 & 0 & 0 \\ 0 & 0 & 1 & 0 \\ 0 & 0 & 0 & 10^5 \end{bmatrix}. \tag{4.18}$$

The gains obtained are listed in Table 4.9. The weighting factors used in the LQR/clipped optimal algorithm are given in Table 4.2.

Simulations of the controlled response were conducted using each of the candidate controllers. The El Centro 1940 earthquake was used as the disturbance (Figure 4.3). The RMS and maximum peak reduction relative to the Lyapunov controller are listed in Tables 4.9 and 4.10. The results reinforce the observation that Algorithm 4 provides isolation that is essentially identical to the isolation afforded by the Lyapunov controller. Tables 4.10 and 4.11 also list the response norms when the semiactive actuator valve is fixed open ($A_v = A_{vmax} = 5.0\times10^{-6}\ m^2$). Plots of the response of the structure when the Lyapunov controller is used, and the actuator operates with an open valve (passive mode) are shown in Figures

4.4 and 4.5. The results of the simulations indicate;

a) There is essentially no difference in performance when the coordinate system is changed from absolute to relative coordinates.

b) The Lyapunov controller and the local pressure/velocity (LPV) controller (Algorithm 4) provide virtually identical levels of seismic isolation.

c) Should the SA actuator fail in a valve open mode, some damping (which is desirable) is achieved.

Table 4.9 Control gains for the bistate controller

Gains	ρ_1	ρ_2	ρ_3	ρ_4
Values	-4.4445×10^{-2}	-1.8355×10^{-3}	-1.2110×10^{-2}	-7.6073×10^{-2}

Table 4.10 RMS reduction compared with the bistate controller

Control Algorithms	Relative displacement [m]			Absolute acceleration [m/s^2]		
	1st floor ($x_2 - x_d$)	2nd floor ($x_1 - x_2$)	1st +2nd	1st floor ($\ddot{x}_2$)	2nd floor ($\ddot{x}_1$)	1st +2nd
Algorithm 1	0.1%	4.2%	4.3%	-11.4%	4.2%	-7.2%
Algorithm 2	-11.6%	-1.9%	-13.5%	-43.0%	-1.9%	-44.9%
Algorithm 3	-48.0%	10.7%	-37.3%	-11.4%	10.7%	-1.3%
Algorithm 4	0.0%	0.1%	0.1%	0.3%	0.1%	0.4%
Clipped optimal	-29.2%	14.0%	-15.2%	1.7%	14.0%	15.7%
Passive*	-63.2%	10.7%	-52.5%	-4.3%	10.7%	6.4%
Bistate control	0.0109	0.00928		2.109	3.244	

* Passive represents that SAVA is installed in the system and valve is fully open.
Negative values indicate larger values relative to Lyapunov control result.
Positive values indicate smaller values relative to Lyapunov control result.
A_{vmin} 5.0×10^{-6} m^2, θ 28°.

Table 4.11 Maximum-peak reduction compared with the bistate controller

Control Algorithms	Relative displacement [m]			Absolute acceleration [m/s^2]		
	1st floor ($x_2 - x_d$)	2nd floor ($x_1 - x_2$)	1st +2nd	1st floor ($\ddot{x}_2$)	2nd floor ($\ddot{x}_1$)	1st +2nd
Algorithm 1	-2.2%	2.1%	-0.1%	-54.0%	2.1%	-51.9%
Algorithm 2	-3.8%	-9.5%	-13.3%	-244.5%	-9.5%	-254.0%
Algorithm 3	-86.0%	3.6%	-82.4%	-10.3%	3.2%	-7.1%
Algorithm 4	0.0%	0.1%	0.1%	0.0%	0.1%	0.1%
Clipped optimal	-38.5%	16.4%	-22.1%	-1.6%	16.4%	14.8%
Passive*	-72.3%	13.1%	-59.2%	14.5%	13.1%	27.6%
Bistate control	0.0449	0.0550		12.7	19.2	

* Passive represents that SAVA is installed in the system and valve is fully open.
Negative values indicate larger values relative to Lyapunov control result.
Positive values indicate smaller values relative to Lyapunov control result.
A_{vmin} = 5.0×10^{-6} m^2, θ = 28°.

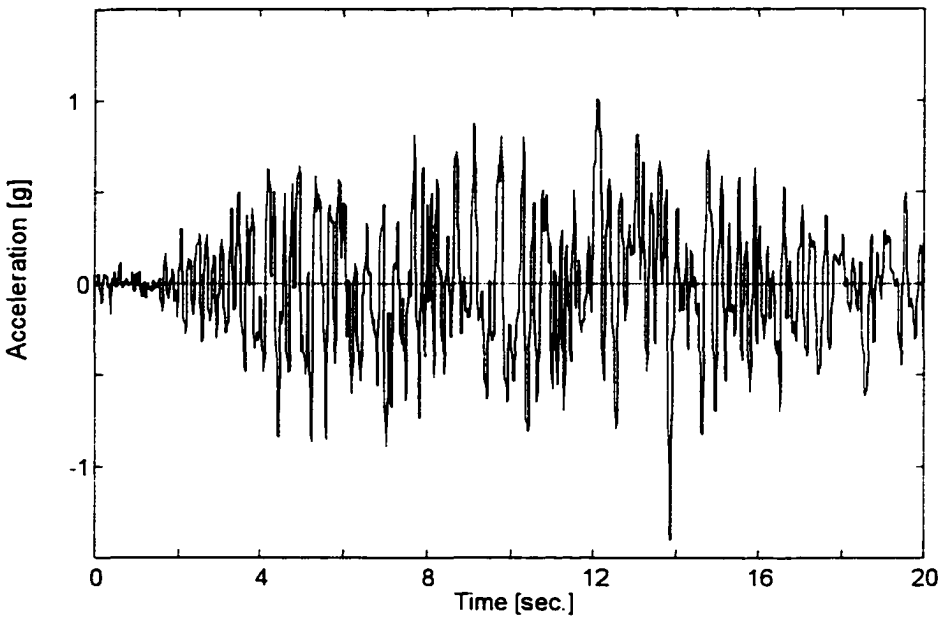

Figure 4.3 Time history of acceleration earthquake disturbance

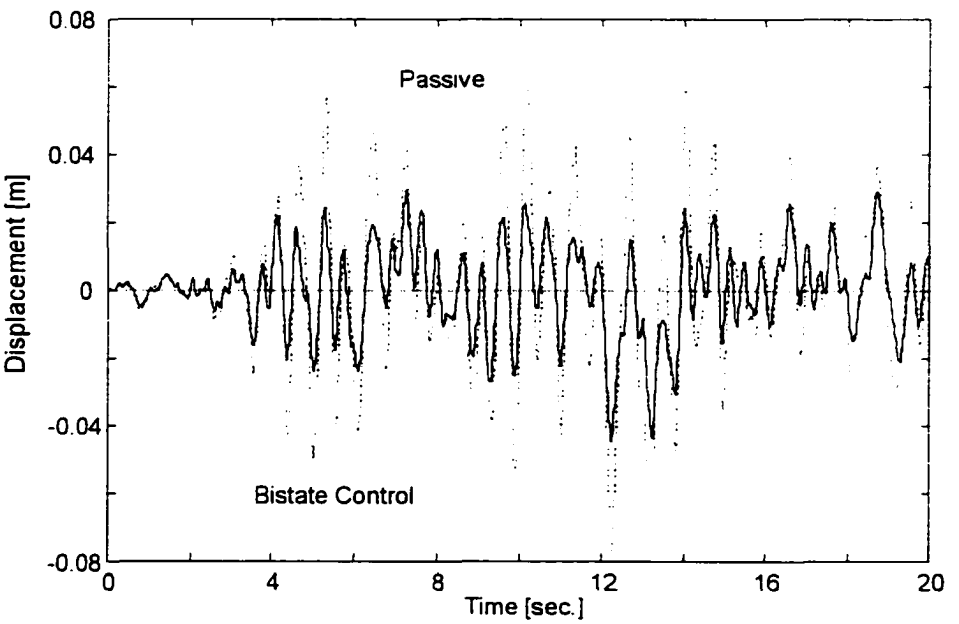

Figure 4.4 Comparison of the relative displacement of the first floor between the bistate controller ($A_{vmin} = 5.0 \times 10^{-6}\ m^2$, $\theta = 28°$) and passive (with SAVA, valve fully open, $A_v = A_{vmax}$)

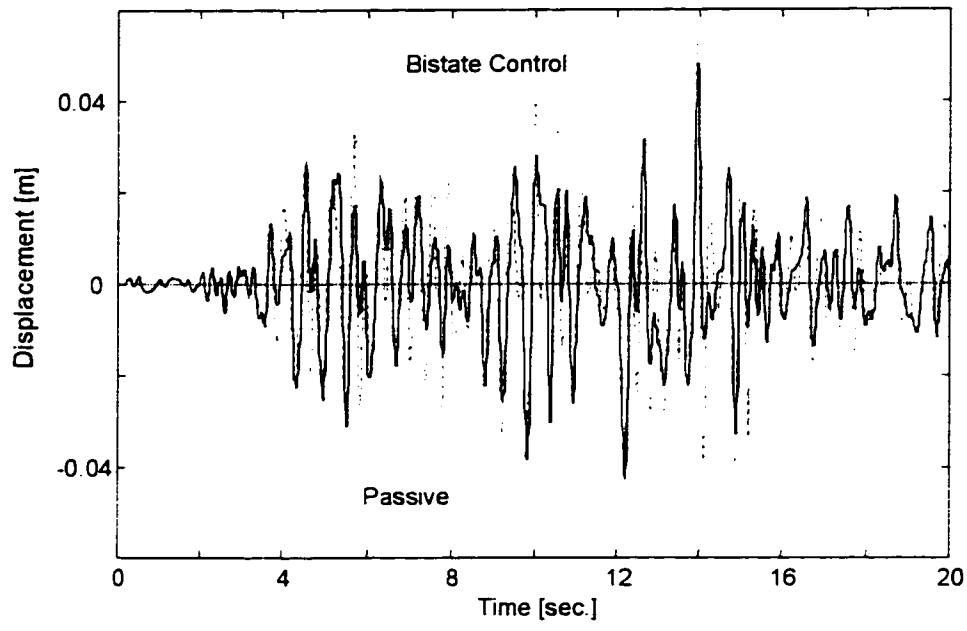

Figure 4.5 Comparison of the relative displacement of the second floor between the bistate controller ($A_{vmin} = 5.0\times10^{-6}\ m^2$, $\theta = 28°$) and passive (with SAVA, valve fully open, $A_v = A_{vmax}$)

4.2 TDOF Seismic Control with Two SAVAs

4.2.1 Mathematical models

The preceding results would appear to indicate that the Lyapunov and LPV control provide the same performance. A final test of that observation is offered here. In this case, the seismic structure is assumed to be outfitted with an actuator at each story. The kinematic arrangement is shown in Figure 4.6.

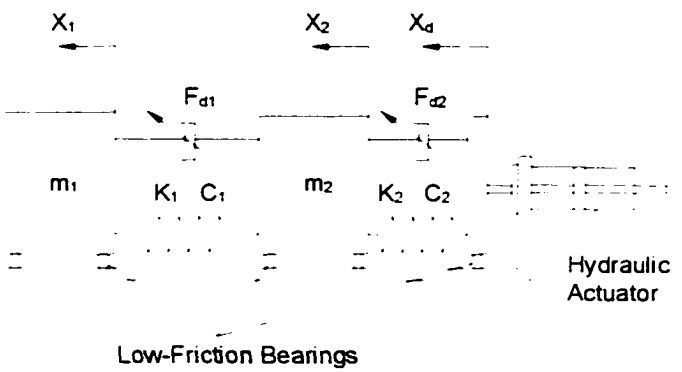

Figure 4.6 Schematic representation of TDOF system with two SAVAs.

The equations of motion in absolute coordinates are given in Equation (4.19) and relative coordinates in Equation (4.20), where $y_1 = x_1 - x_2$ and $y_2 = x_2 - x_d$.

$$\begin{aligned} m_1\ddot{x}_1 &= -k_1(x_1 - x_2) - c_1(\dot{x}_1 - \dot{x}_2) - F_{d1} \\ m_2\ddot{x}_2 &= k_1(x_1 - x_2) + c_1(\dot{x}_1 - \dot{x}_2) - k_2(x_2 - x_d) - c_2(\dot{x}_2 - \dot{x}_d) + F_{d1} - F_{d2} \end{aligned} \tag{4.19}$$

or,

$$\ddot{y}_1 = -\left(\frac{k_1}{m_1} + \frac{k_1}{m_2}\right) y_1 + \frac{k_2}{m_2} y_2 - \left(\frac{c_1}{m_1} + \frac{c_1}{m_2}\right) \dot{y}_1 + \frac{c_2}{m_2} \dot{y}_2 - \left(\frac{1}{m_1} + \frac{1}{m_2}\right) F_{d1} - \frac{F_{d2}}{m_2}$$
$$\ddot{y}_2 = \frac{k_1}{m_2} y_1 - \frac{k_2}{m_2} y_2 - \frac{c_1}{m_2} \dot{y}_1 - \frac{c_2}{m_2} \dot{y}_2 - \frac{F_{d1}}{m_2} - \frac{F_{d2}}{m_2} - \ddot{x}_d \quad (4.20)$$

The dynamics of each SA actuator is defined in Equations (4.21 a, b) and (4.22 a, b)

$$\Delta \dot{P}_1 = \alpha_1 \left(A_{p1} \dot{y}_1 - sgn(\Delta P_1) C_{d1} A_{v1} \sqrt{\frac{2 \Delta P_1}{\rho}} \right) \quad (4.21 a)$$

$$\Delta \dot{P}_2 = \alpha_2 \left(A_{p2} \dot{y}_2 - sgn(\Delta P_2) C_{d2} A_{v2} \sqrt{\frac{2 \Delta P_2}{\rho}} \right) \quad (4.21 b)$$

where

$$\alpha_1 = \frac{\beta_1 (V_1 + V_2)}{V_1 V_2}, \quad \alpha_2 = \frac{\beta_2 (V_3 + V_4)}{V_3 V_4} \quad (4.22 a, b)$$

The forces provided by each of the actuators are

$$F_{d1} = A_{p1} \Delta P_1, \quad F_{d2} = A_{p2} \Delta P_2 \quad (4.23 a, b)$$

where $\Delta P_1 = P_1 - P_2$ and $\Delta P_2 = P_3 - P_4$. Defining state space vector,

$$Y = \{y_1 \quad y_2 \quad \dot{y}_1 \quad \dot{y}_1\}^T \quad (4.24)$$

The preceding model can be cast in state space form as

$$\dot{Y} = AY + Bg(Y) + E\ddot{X}_d \quad (4.25)$$

where

$$A = \begin{bmatrix} 0 & 0 & 1 & 0 \\ 0 & 0 & 0 & 1 \\ -\left(\frac{k_1}{m_1}+\frac{k_1}{m_2}\right) & \frac{k_2}{m_2} & -\left(\frac{c_1}{m_1}+\frac{c_1}{m_2}\right) & \frac{c_2}{m_2} \\ \frac{k_1}{m_2} & -\frac{k_2}{m_2} & \frac{c_1}{m_2} & -\frac{c_2}{m_2} \end{bmatrix} \quad (4.26\text{ a})$$

$$B = \begin{bmatrix} 0 & 0 \\ 0 & 0 \\ -\left(\frac{1}{m_1}+\frac{1}{m_2}\right)A_{p1} & \frac{A_{p2}}{m_2} \\ \frac{A_{p1}}{m_2} & -\frac{A_{p2}}{m_2} \end{bmatrix}, \quad E = \begin{bmatrix} 0 \\ 0 \\ 0 \\ -1 \end{bmatrix}, \quad g(Y) = \begin{bmatrix} \Delta P_1 \\ \Delta P_2 \end{bmatrix}. \quad (4.26\text{ b, c, d})$$

4.2.2 Controllers

The general form of the controller for multiple SA actuator can be rewritten from Equation (3.7).

$$f(Y) = Y^T QBg(Y). \quad (4.27)$$

Expanding the terms of Equation (4.27) out then the bistate rule for each actuator is

$$S_1(Y) = \{\rho_{11} y_1 + \rho_{21} y_2 + \rho_{31} \dot{y}_1 + \rho_{41} \dot{y}_2\} \Delta P_1 \quad (4.28\text{ a})$$

$$S_2(Y) = \{\rho_{12} y_1 + \rho_{22} y_2 + \rho_{32} \dot{y}_1 + \rho_{42} \dot{y}_2\} \Delta P_2. \quad (4.28\text{ b})$$

In addition to the Lyapunov controller, we also examine variations of the heuristic controllers when applied to two actuators. Those control laws are listed in Table 4.12.

Table 4.12 Switching functions of four control algorithms with two SAVAs

	Algorithm 1	Algorithm 2	Algorithm 3	Algorithm 4
SAVA #1	$\dot{x}_1\dot{y}_1$	$y_1\dot{y}_1$	$y_1\Delta P_1$	$\dot{y}_1\Delta P_1$
SAVA #2	$\dot{x}_2\dot{y}_2$	$y_2\dot{y}_2$	$y_2\Delta P_2$	$\dot{y}_2\Delta P_2$

4.3 Numerical Simulations

The passive parameters used in the simulation are listed in Table 4.13 included in that table are passive dampers which were employed to obtain the passive response of the system assuming a forced and wear ideal level of damping;

(1) Damping ratio of the first floor -- $\zeta_1 \quad \frac{c_1}{2\sqrt{k_1 m_1}} = 0.13.$ (4.29)

(2) Damping ratio of the second floor -- $\zeta_2 \quad \frac{c_2}{2\sqrt{k_2 m_2}} = 0.16.$ (4.30)

Those two hypothetical dampers were not included when the SA control simulations were conducted.

Table 4.13 System parameters for simulations

Symbols	m_1	m_2	k_1	k_2	c_1	c_2
Unit	Kg	Kg	N/m	N/m	N/m/sec.	N/m/sec.
Values	131	136	45746	28420	645	645

Using the Lyapunov control gains listed in Table 4.14 and the control laws listed above, the RMS and maximum motion norms of the responses are listed in Tables 4.15 and 4.16. Next, Figures 4.7 and 4.8 compare the relative displacement of each floor between the passive (when the SA actuator valve is fixed at fully open ($A_v = A_{vmax}$) and bistate controller. As seen in Figures 4.7 and 4.8, one should naturally expect that the system with two SAVAs proves superior to the system with one SAVA in the reduction of relative

displacement. The minimum valve area of semiactive actuator is fixed for this simulation ($A_{vmin1} = 1.0\times10^{-6}\ m^2\ (\theta_1 = 40°)$, $A_{vmin2} = 5.0\times10^{-6}\ m^2\ (\theta_2 = 28°)$).

Table 4.14 Control gains for bistate control (j = 1 or 2)

	ρ_{1j}	ρ_{2j}	ρ_{3j}	ρ_{4j}
SAVA #1	-1.1456	-0.0001	-0.2323	-0.2318
SAVA #2	0.0028	-1.8371	-0.3731	-0.7610

Table 4.15 RMS reduction compared with the bistate controller

Control Algorithms	Relative displacement [m]			Absolute acceleration [m/s^2]		
	1st floor ($x_2 - x_d$)	2nd floor ($x_1 - x_2$)	1st +2nd	1st floor ($\ddot{x}_2$)	2nd floor ($\ddot{x}_1$)	1st +2nd
Algorithm 1	2.6%	10.0%	12.6%	-7.3%	-10.3%	-17.6%
Algorithm 2	-4.9%	-6.1%	-11.0%	-28.1%	-45.3%	-73.4%
Algorithm 3	-4.6%	-1.3%	-5.9%	-30.0%	-46.4%	-76.4%
Algorithm 4	-0.4%	2.6%	2.2%	0.8%	-0.3%	0.5%
Clipped optimal	0.1%	-6.0%	-5.9%	1.0%	0.4%	1.4%
Passive*	-62.6%	-176.0%	-238.6%	1.9%	-22.6%	-20.7%
Bistate control	0.0105	0.00244		2.008	2.024	

* Passive represents that SAVA is installed in the system and valve is fully open.
Negative values indicate larger values relative to Lyapunov control result.
Positive values indicate smaller values relative to Lyapunov control result.
(A_{vmin1} 1.0×10^{-6} m^2 (θ_1 = 40°), A_{vmin2} = 5.0×10^{-6} m^2 (θ_2 = 28°)).

Table 4.16 Maximum-peak reduction compared with the bistate controller

Control Algorithms	Relative displacement [m]			Absolute acceleration [m/s^2]		
	1st floor ($x_2 - x_d$)	2nd floor ($x_1 - x_2$)	1st +2nd	1st floor ($\ddot{x}_2$)	2nd floor ($\ddot{x}_1$)	1st +2nd
Algorithm 1	-3.9%	0.3%	-3.6%	-48.2%	-95.3%	-143.5%
Algorithm 2	-3.3%	-2.4%	-5.7%	-160.6%	-303.4%	-464.0%
Algorithm 3	-3.5%	-0.3%	-3.8%	-198.0%	-301.9%	-499.9%
Algorithm 4	0.0%	0.8%	0.8%	0.0%	-0.1%	-0.1%
Clipped optimal	0.7%	-5.0%	-4.3%	1.7%	18.1%	19.8%
Passive*	-75.0%	-242.0%	-317.0%	33.3%	17.9%	51.2%
Bistate control	0.0424	0.00948		14.04	14.43	

* Passive represents that SAVA is installed in the system and valve is fully open.
Negative values indicate larger values relative to Lyapunov control result.
Positive values indicate smaller values relative to Lyapunov control result.
(A_{vmin1} = 1.0×10^{-6} m^2 (θ_1 = 40°), A_{vmin2} = 5.0×10^{-6} m^2 (θ_2 = 28°)).

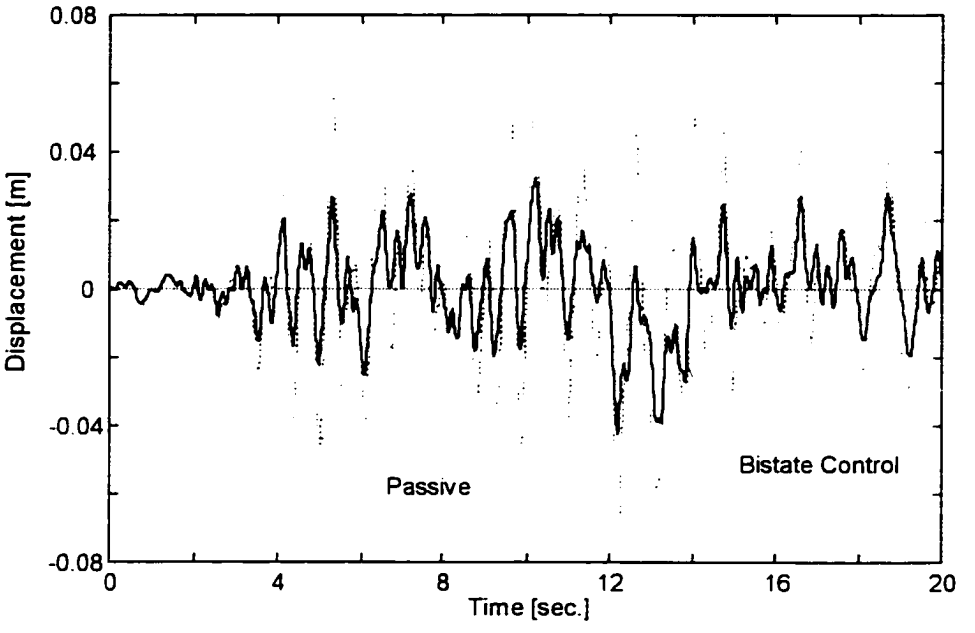

Figure 4.7 Comparison of the relative displacement of the first floor between bistate control (A_{vmin1} 1.0×10^{-6} m^2 (θ_1 = 40°), A_{vmin2} 5.0×10^{-6} m^2 (θ_2 = 28°)) and passive (with SAVA, valve fully open, $A_{v1} = A_{vmax1}$, $A_{v2} = A_{vmax2}$) for two SAVAs.

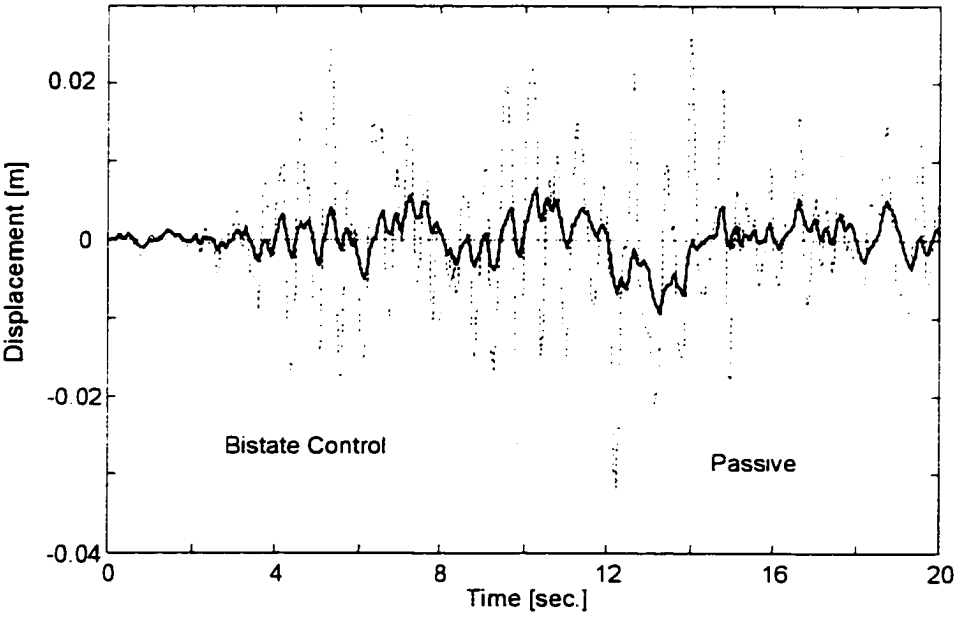

Figure 4.8 Comparison of the relative displacement of the second floor between bistate control (A_{vmin1} = 1.0×10^{-6} m^2 (θ_1 = 40°), A_{vmin2} = 5.0×10^{-6} m^2 (θ_2 = 28°)) and passive (with SAVA, valve fully open, $A_{v1} = A_{vmax1}$, $A_{v2} = A_{vmax2}$) for two SAVAs.

4.4 Conclusion

The purpose of the chapter was to provide a comparison of the performance of various control laws that are often suggest for the regulation of semiactive hydraulic actuators. The comparison included four heuristic rules, the clipped optimal control, the Lyapunov control, and the passive system (SAVA attached and valve fully open). The comparisons were made relative to the Lyapunov control performance. A two story seismic structure was employed in the simulations, and three possibilities for the installation of the SA actuator were considered. A comparative analysis using relative rather than absolute coordinates was also included. Comparisons of the RMS displacement and acceleration and the maximum displacement and acceleration were provided. Using the maximum displacement results from the simulations, it is clear that the Lyapunov controller and the pressure/velocity algorithm (LPV, Algorithm 4) provide the best performance. An open question is whether that finding would hold for different application of the SAVA system. That question is addressed in the next chapter where a similar comparative analysis is conducted in terms of an automotive suspension application.

CHAPTER FIVE

COMPARATIVE ANALYSIS OF SA CONTROL ALGORITHMS FOR VEHICLE SUSPENSION APPLICATIONS

5.1 Introduction

The previous chapter reported on the comparative performance of various control strategies that provide bistate control commands for the regulation of the orifice valve of a semiactive hydraulic damper (actuator). That study was conducted via simulations of a seismic structure, where the principal objective was to reduce the maximum relative displacement between floors of the structure. The results there indicated that the Lyapunov control and the LPV (Algorithm 4) provided similar levels of performance.

The question that remains to be addressed is; do the results of the seismic structure analysis hold for other dynamic system, where the objective of the control is different? In order to address that question this chapter reports on the comparative performance of various semiactive bistate controllers when applied to vehicle suspensions. The nature of the vehicle suspension design objective is established below in terms of simplified (but standard) chassis suspension models. Comparisons of the performance of the candidate controllers for application to a heavy tractor-trailer type suspension with linearized stiffness and non-linear leaf spring is considered. A review of the literature pertinent to

semiactive automotive suspension design is discussed in the following paragraphs.

As noted previously, the semiactive suspension has been the object of considerable previous research; both analytical and experimental. The reason is that the automotive industry took an interest in the development of adaptable suspensions to improve ride and handling qualities of vehicles, while costing less than a fully powered (active) suspension design. Many of the seminal papers on SA control were published by a handful of investigators in the 1970's and 1980's (see for example Hrovat [1981, 1983, 1988], Karnopp [1974, 1987, 1988], Margolis [1975, 1982, 1983, 1984]). A review of the development of SA suspensions for vehicles appears in Karnopp [1995].

The effort by automotive manufacturers never matured to the platform product release stage; though trials were conducted for large numbers of various vehicles. Many problems were encountered with the new technology. The cost and reliability of the SA hardware components that were developed was less than acceptable, but the most significant draw back was the lack of apparent improvement that that a SA suspension provides relative to a passive suspension design. The human's inability to distinguish between small differences in dynamic levels of vibration made it impossible to convince the buyer to invest in the proposed systems. Another serious problem encountered in the application of SA suspensions to automobiles was the harshness that was experienced, which was caused by a host of different factors including friction in the actuators, valve lockup at large loads, and by hydraulic hammer effects caused by instantaneously closing the hydraulic valve under load. The added cost of the SA systems for automobiles and the perceived harshness combined to end any real interest by manufacturers in SA systems for

automobiles.

While the application of SA suspensions to automobiles is not considered practical, there is an open possibility that the addition of a semiactive shock absorber to a truck suspension may have utility. The following text treats the SA truck suspension problem, and examines the performance of the various competing controller designs.

5.2 Truck Suspension Dynamics

The standard practice among suspension engineers is to use a simplified model to assess the dominant features of the system design. A so-called one-quarter vehicle model is used here to characterize the features of a typical tandem axle suspension (Figure 5.1). The model assumes that the tire compliance is essentially linear elastic.

There are several suspension options available for trucks. A most common feature is a compliant spring mechanism mounded between the axle and the sprung mass. Options include leaf springs, coil springs, air springs and combinations of these and other devices. Leaf springs [Fancher et al., 1980] and air spring [Klinger and Galzade, 1977] are typically nonlinear devices, which can be treated as linear components for small amplitude vibration. In the case of a leaf spring, the sliding of the steel leaf spring produces a (hysteric) damping effect in addition to an essentially linear elastic effect. Air springs provide much less damping, and tend to be "softer" than leaf springs.

The work here examines the effectiveness of a semiactive hydraulic suspension when installed on a generic ¼ truck model. Measurements of the dynamic characteristics of a full size truck were used [Patten et al., 1997, Kang, 1998] to obtain a set of parameters that are desirable to the truck suspension (see Table 5.1). The truck was outfitted with steel leaf springs.

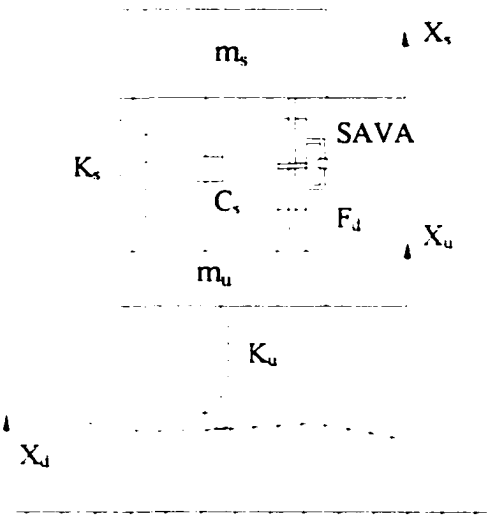

Figure 5.1 Schematic representation of quarter-car model with linear spring and SAVA.

The equations of motion of the system are

$$\begin{aligned} m_s \ddot{x}_s &= -k_s(x_s - x_u) - c_s(\dot{x}_s - \dot{x}_u) - A_p \Delta P \\ m_u \ddot{x}_u &= k_s(x_s - x_u) + c_s(\dot{x}_s - \dot{x}_u) - k_u(x_u - x_d) + A_p \Delta P \end{aligned} \tag{5.1}$$

The dynamics of the semiactive actuator (see Section 2.2) are

$$\Delta \dot{P} = \frac{\beta(V_1 + V_2)}{V_1 V_2}\left(A_p(\dot{x}_s - \dot{x}_u) - sgn(\Delta P) C_d A_v \sqrt{\frac{2\ \Delta P}{\rho}} \right). \tag{5.2}$$

Defining the state space vector as

$$X = [x_s \quad x_u \quad \dot{x}_s \quad \dot{x}_u]^T \tag{5.3}$$

then the system equations for the ¼ truck are

$$\dot{X} = A X + B g(X) + E X_1 \tag{5.4}$$

where

$$A = \begin{bmatrix} 0 & 0 & 1 & 0 \\ 0 & 0 & 0 & 1 \\ -\frac{k_s}{m_s} & \frac{k_u}{m_s} & -\frac{c_s}{m_s} & \frac{c_s}{m_s} \\ \frac{k_s}{m_u} & -\frac{k_s + k_u}{m_u} & \frac{c_s}{m_u} & -\frac{c_s}{m_u} \end{bmatrix} \tag{5.5 a}$$

$$B = \begin{bmatrix} 0 & 0 & -\frac{A_p}{m_s} & \frac{A_p}{m_u} \end{bmatrix}^T, \quad E = \begin{bmatrix} 0 & 0 & 0 & \frac{k_u}{m_u} \end{bmatrix}^T, \quad g(X) = \Delta P \tag{5.5 b, c}$$

The physical parameters that characterize the system components are given in Table 5.1. It is emphasized that the system is assumed to behave in a linear fashion for small displacement if large displacements are to be examined, then the nonlinearity of the spring components (leaf or air) would have to be included in the analysis.

Table 5.1 System parameters of a quarter-car for a heavy truck

Symbols	m_s	m_u	k_c	k_u	c_s	ω_s	ω_u
Unit	Kg	Kg	KN/m	KN/m	kN/m/sec	Hz	Hz
Values	6840	794	236	3150	10.0	0.93	10.0

5.3 Control

The control objective for a vehicle suspension is more complex then that for a seismic structure. Like the seismic control, one objective is to limit the relative displacement between the sprung and unsprung masses. This is the least important criterion. The comfort of the passenger in the vehicle is a strong consideration. A vibration comfort metric that has been adopted by the International Standards Organization (ISO) suggests that the RMS acceleration level of the sprung mass be highly correlated with a human's perception of vibration comfort [ISO, 1991]. In addition, the control should enhance the handling characteristics of the vehicle. In terms of the quarter truck model, desirable handling is reflected in the variation of the tire force from static conditions.

The controllers that are examined here will be shown to affect those three goals in varying degrees. Four local controllers which are based on popular usage are included, as is the clipped optimal control and Lyapunov control. The performance of each control is measured relative to the Lyapunov control. The controller performance is also compared to the valve open passive operation of the system. Recalling the previous description of the four local algorithms (see Section 4.1) then those algorithms expressed in terms of the vehicle models are given in Table 5.2.

Table 5.2 Switching functions of the four control algorithms for a quarter-car model

Algorithm 1	Algorithm 2	Algorithm 3	Algorithm 4
$\dot{x}_s(\dot{x}_s - \dot{x}_u)$	$(x_s - x_u)(\dot{x}_s - \dot{x}_u)$	$(x_s - x_u)\Delta P$	$(\dot{x}_s - \dot{x}_u)\Delta P$

The development of "on-off" controller based on the clipped optimal (CO) was discussed in Section 4.1. The CO control, restated in terms of the vehicle suspension problem, is requires a two step procedure;

(1) Find an optimal control, which minimizes

$$J = \frac{1}{2}\int_0^T \{\rho_1 \ddot{x}_1^2 + \rho_2 (x_1 - x_2)^2 + \rho_3 (x_2 - x_d)^2\} dt \tag{5.6}$$

subjected to

$$\dot{X} = AX + Bf + EX_d. \tag{5.7}$$

(Note that the plant model does not include the nonlinear dynamics of the actuator.)

(2) Control law for a SA system is

$$\begin{cases} A_v = A_{v\min} & \text{if } c^* \le c_{\max} \\ A_v = A_{v\max} & \text{if } c^* \le c_{\min} \end{cases} \tag{5.8}$$

where c^* is the damping rate derived from

$$c^* = \frac{f_o}{\dot{s}}. \tag{5.9}$$

The penalty terms ρ_i used were $\rho_1 = 1.0$, $\rho_2 = 10^9$, $\rho_3 = 0.0$ and $\rho_4 = 1.0^9$.

Finally, the Lyapunov control was established using the methods described in Section 3.2. The Lyapunov equation was

$$A^T Q \cdot QA = -P, \quad Q \cdot 0 \text{ and } P \cdot 0 \tag{5.10}$$

where P was selected as (the diagonal elements are obtained by tuning for the best performance of system responses with a given white noise input to the system, see Section 3.2.):

$$P = \begin{bmatrix} 1 & 0 & 0 & 0 \\ 0 & 1 & 0 & 0 \\ 0 & 0 & 1 & 0 \\ 0 & 0 & 0 & 1 \end{bmatrix}. \tag{5.11}$$

The switching function of Lyapunov control for Equation (5.4) is

$$S(X) = -\alpha\sqrt{\frac{2}{\rho}}\left\{ q_{15}x_s + q_{25}x_u + q_{35}\dot{x}_s + q_{45}\dot{x}_u + q_{55}\Delta P \right\} g(X). \tag{5.12}$$

The selection of the elements in P was accomplished using an iterative tuning process, with a given white noise input to the system assumed. The Lyapunov control gains obtained via that tuning process are listed in Table 5.3. The minimum valve area of semiactive actuator is fixed for this simulation ($A_{vmin} = 4.0\times10^{-6}\ m^2$, $\theta = 30°$).

Table 5.3 Control gains of the bistate controller for a heavy truck

Gains	ρ_1	ρ_2	ρ_3	ρ_4
Values	-3.8647×10^{-9}	2.7120×10^{-7}	-6.1684×10^{-8}	5.1210×10^{-8}

In order to make legitimate comparisons, an excitation input were assumed; a random face characterized by a random displacement and a small road bump. A portion of the

random road surface profile is shown in Figure 5.2. The road bump is shown in Figure 5.3. Next, Figures 5.4 through 5.6 represent the simulation results of bistate controller as compared with passive suspensions with (SA actuator valve is fixed at fully open (A_v A_{vmax})) and without SAVA. Figure 5.4 depicts the transfer function between the tire deflection and road excitation. Figure 5.5 represents the transfer function between the acceleration of sprung mass and road excitation × ω_{nu}^2 (natural frequency of unsprung mass). The transfer function between the suspension deflection and road excitation is compared in Figure 5.6. The corresponding differential pressures in each chamber of the actuator are shown in Figure 5.7. The simulation results of the open and closed loop performance for the "bump" excitation are shown in Figures 5.8 through 5.10. Figure 5.11 shows the differential pressure versus time. Figure 5.12 depicts the comparisons of the valve actions.

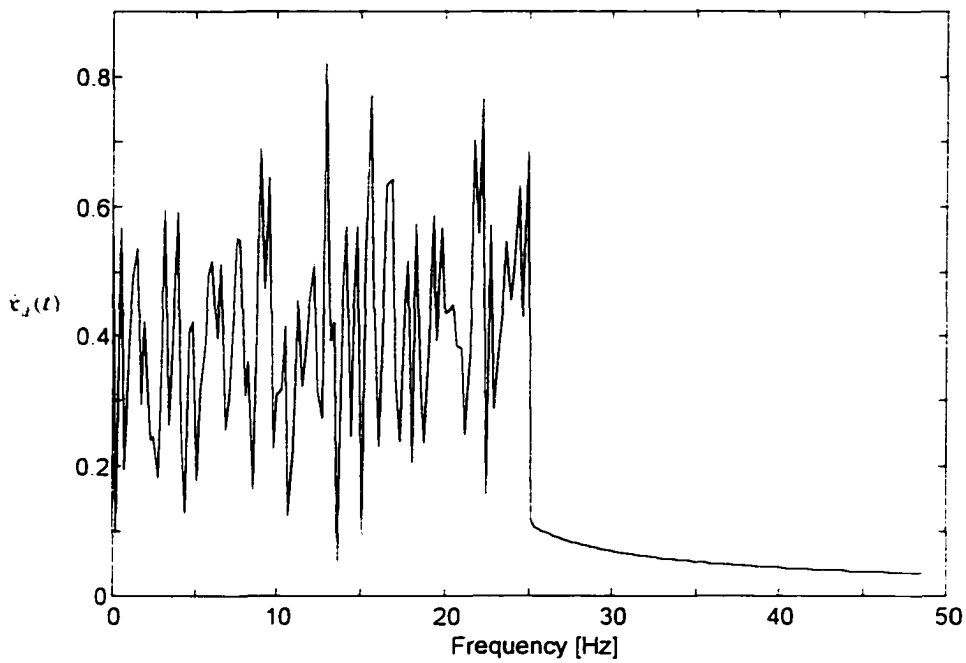

Figure 5.2 FFT of the random displacement input.

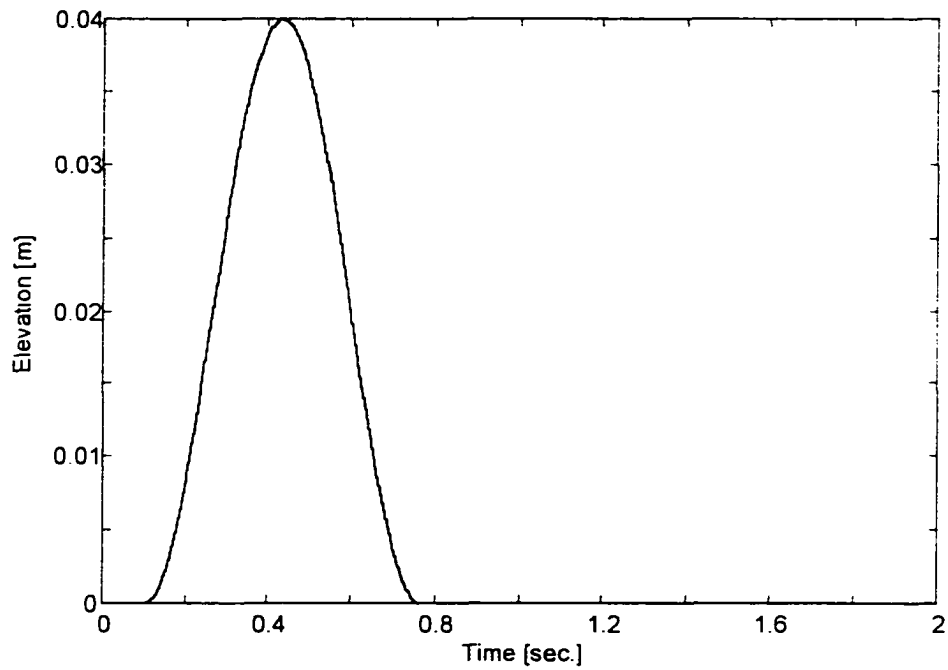

Figure 5.3 Road profiles for a swell bump used for simulation, $x_d = 0.02(1-\sin(3\pi t - t_i - t_f))$.

Table 5.4 Maximum-peak reduction for a bump roadway with linearized spring

Control Algorithms	Acceleration of Sprung Mass	Tire Deflection	Suspension Deflection
Algorithm 1	-29.6%	-32.7%	22.8%
Algorithm 2	0.4%	1.2%	-0.2%
Algorithm 3	0.4%	1.2%	-0.2%
Algorithm 4	-3.4%	6.9%	-3.8%
Clipped Optimal	-33.3%	-33.6%	34.8%
Passive (no SA)	7.9%	-4.5%	-6.7%
Passive (with SA)*	5.8%	-3.1%	-2.0%
Lyapunov Control	1.28	0.0029	0.034

Negative: worse than Lyapunov control. Positive: better than Lyapunov control.
*: with valve fully open ($A_{vmin} = 4.0\times10^{-6}\ m^2$, $\theta = 30°$).

Table 5.5 RMS reduction for a bump roadway with linearized spring

Control Algorithms	Acceleration of Sprung Mass	Tire Deflection	Suspension Deflection
Algorithm 1	0.8%	-1.2%	20.7%
Algorithm 2	0.2%	0.4%	-0.5%
Algorithm 3	0.2%	0.4%	-0.5%
Algorithm 4	-34.7%	-30.3%	-44.3%
Clipped Optimal	-15.8%	-16.4%	27.2%
Passive (no SA)	-42.5%	-37.8%	-55.3%
Passive (with SA)*	-30.7%	-26.5%	-38.1%
Lyapunov Control	0.34	0.00077	0.0087

Negative: worse than Lyapunov control. Positive: better than Lyapunov control.
*: with valve fully open ($A_{vmin} = 4.0\times10^{-6}\ m^2$, $\theta = 30°$).

Table 5.6 RMS reduction for a random displacement excitation with linearized spring

Control Algorithms	Acceleration of Sprung Mass	Tire Deflection	Suspension Deflection
Algorithm 1	16.1%	-11.1%	-5.0%
Algorithm 2	17.9%	-8.4%	-28.9%
Algorithm 3	15.8%	-8.0%	-33.0%
Algorithm 4	-0.1%	0.5%	12.5%
Clipped Optimal	8.0%	-7.0%	21.1%
Passive (no SA)	31.5%	-72.7%	-72.5%
Passive (with SA)*	26.8%	-29.7%	-31.0%
Lyapunov Control	1.27	0.0035	0.011

Negative: worse than Lyapunov control. Positive: better than Lyapunov control.
*: with valve fully open ($A_{vmin} = 4.0\times10^{-6}\ m^2$, $\theta = 30°$).

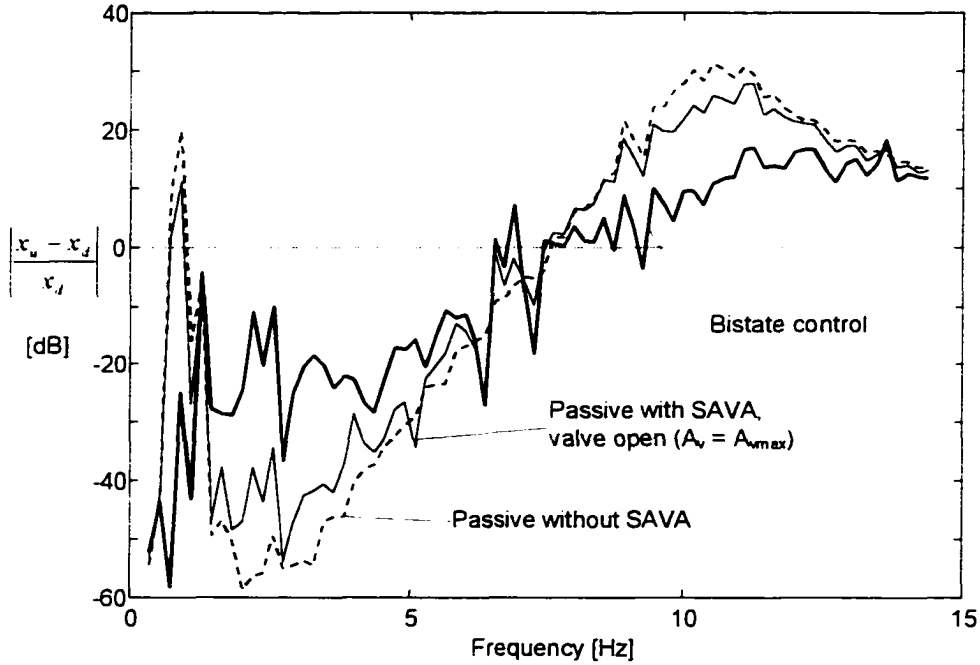

Figure 5.4 Comparison of transfer function of tire deflection for bistate controller and passive with linearized spring for a random displacement roadway ($A_{vmin} = 4.0 \times 10^{-6}\ m^2$, $\theta = 30°$).

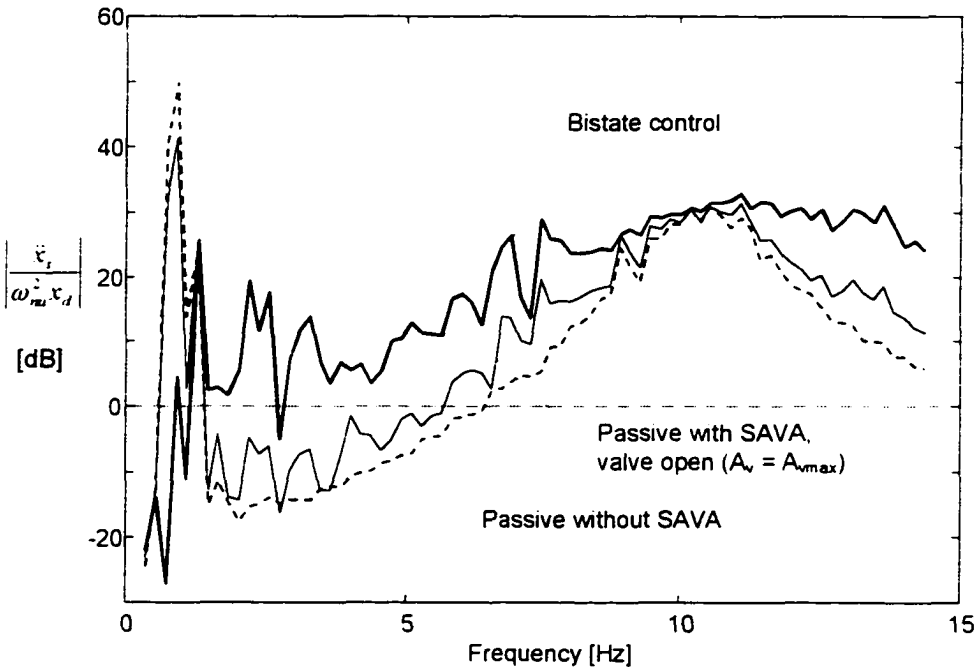

Figure 5.5 Comparison of transfer function of acceleration of sprung mass for bistate controller and passive with linearized spring for a random displacement roadway ($A_{vmin} = 4.0 \times 10^{-6}\ m^2$, $\theta = 30°$).

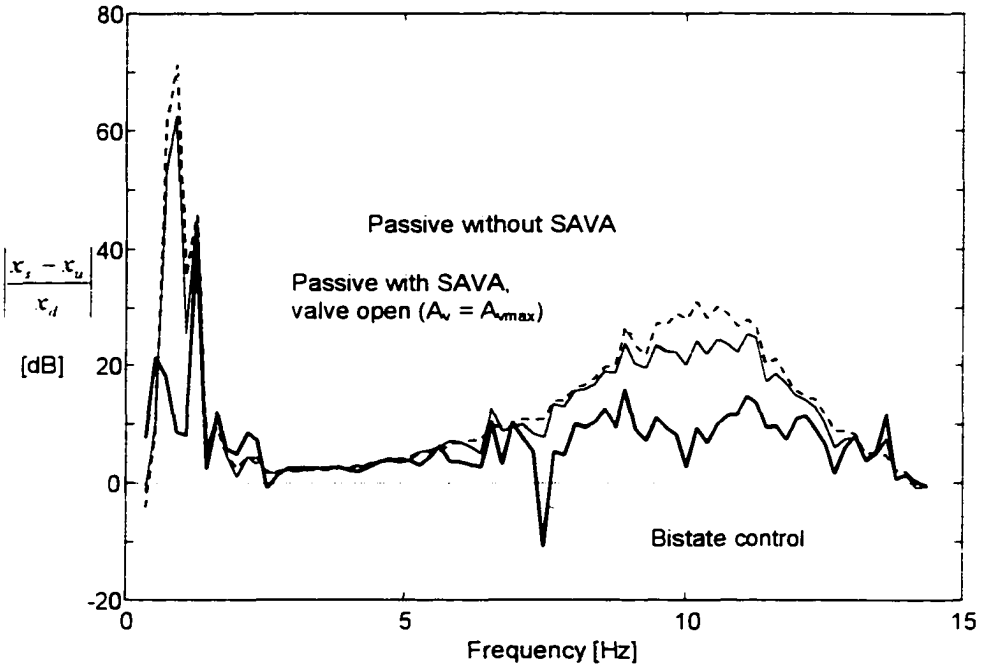

Figure 5.6 Comparison of transfer function of suspension deflection for bistate controller and passive with linearized spring for a random displacement roadway ($A_{vmin} = 4.0 \times 10^{-6}\ m^2$, $\theta = 30°$).

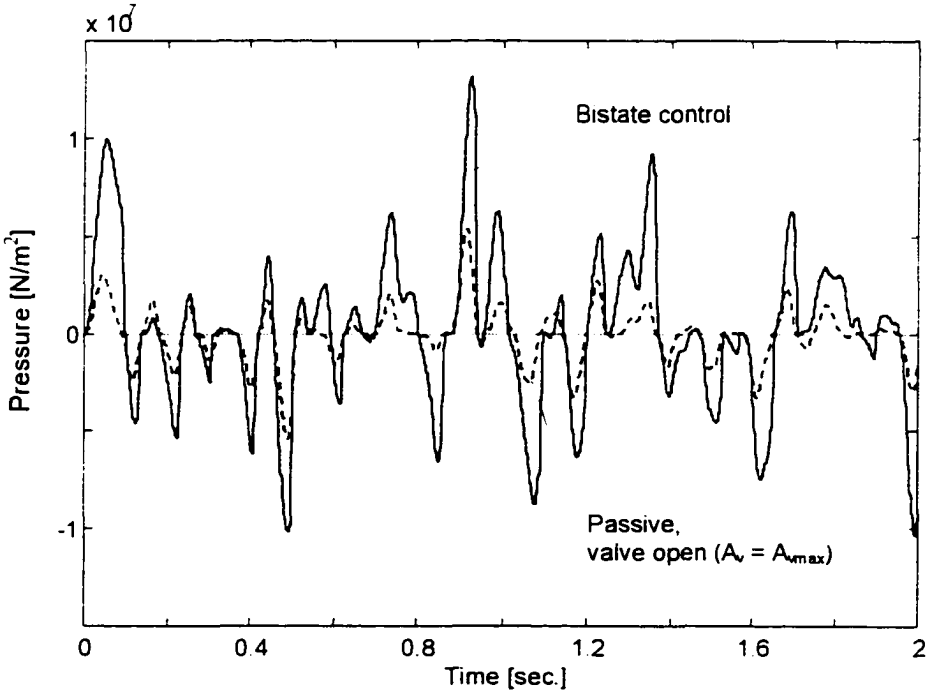

Figure 5.7 Comparison of pressure difference between bistate controller and passive (SAVA valve fully open) with linearized spring for a random displacement roadway ($A_{vmin} = 4.0 \times 10^{-6}\ m^2$, $\theta = 30°$).

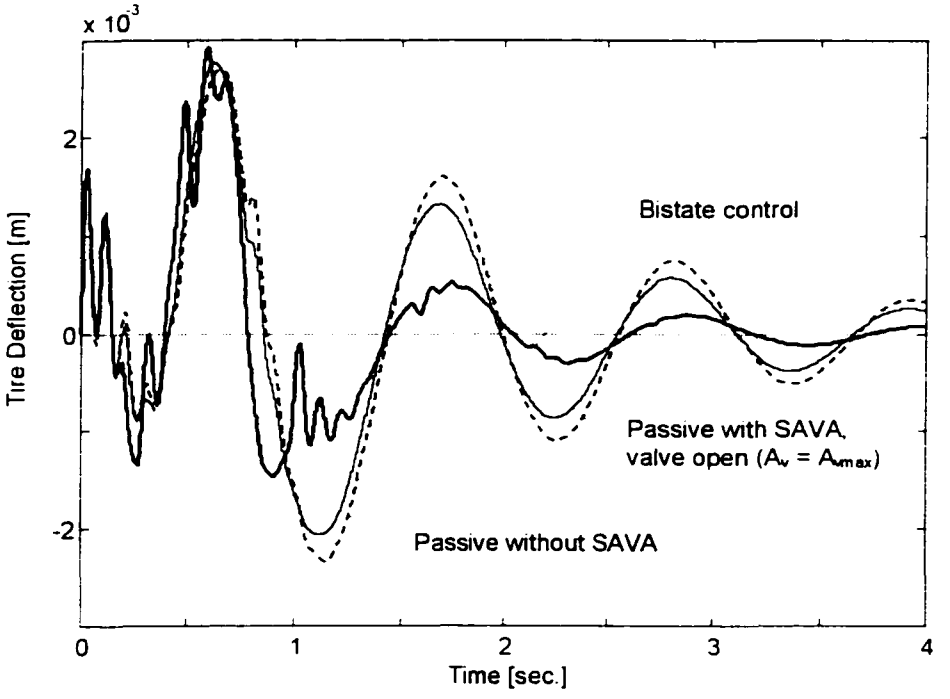

Figure 5.8 Comparison of tire deflection between bistate controller and passive with linearized spring for a bump roadway (A_{vmin} 4.0×10^{-6} m^2, θ $30°$).

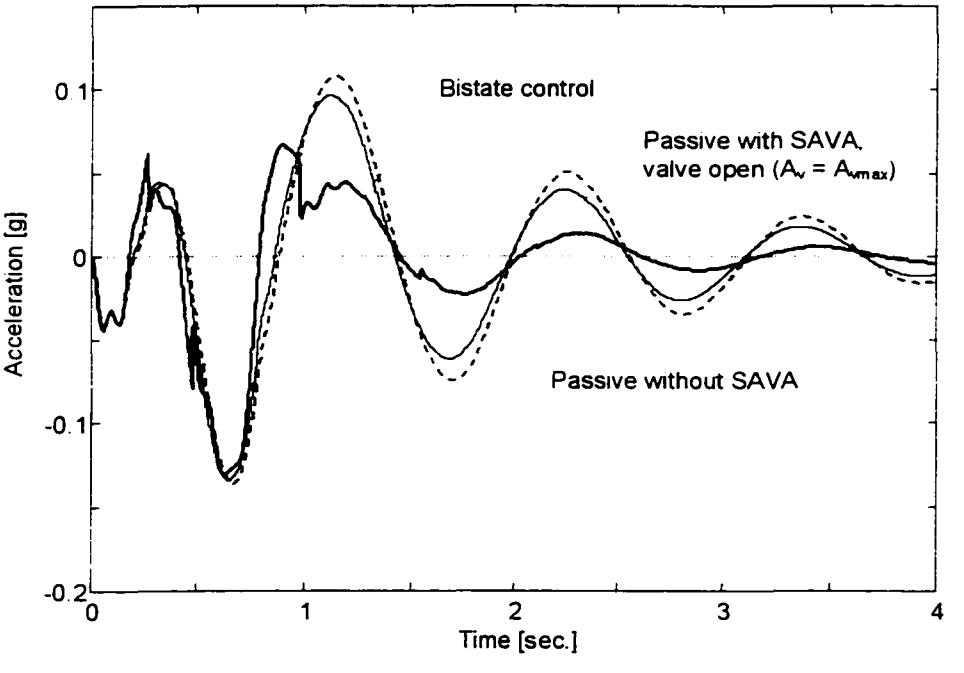

Figure 5.9 Comparison of acceleration of sprung mass between bistate controller and passive with linearized spring for a bump roadway (A_{vmin} = 4.0×10^{-6} m^2, θ = $30°$).

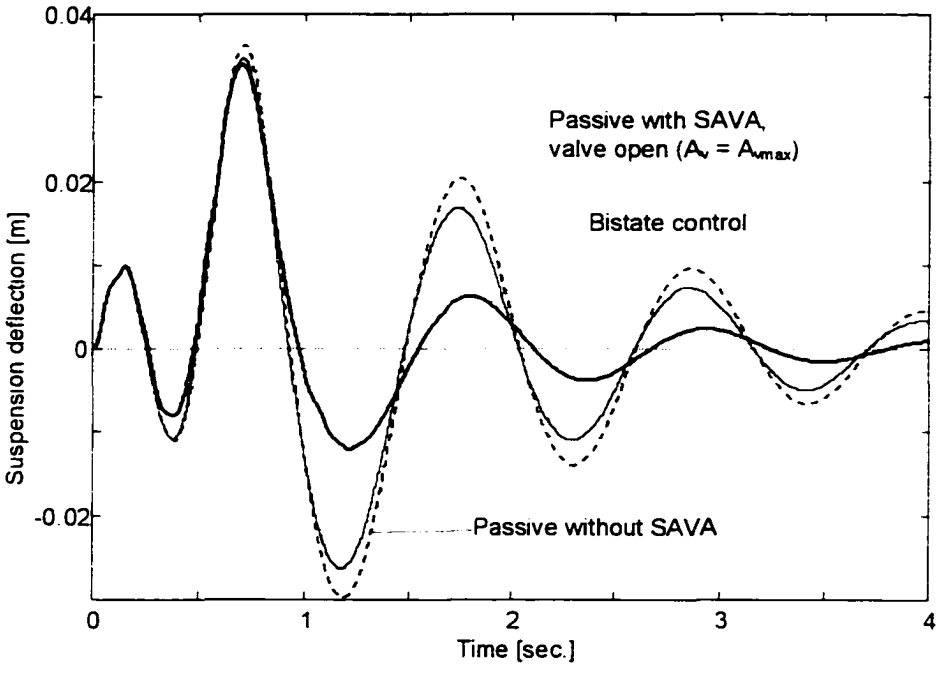

Figure 5.10 Comparison of suspension deflection between bistate controller and passive with linearized spring for a bump roadway ($A_{vmin} = 4.0 \times 10^{-6}\ m^2$, $\theta = 30°$).

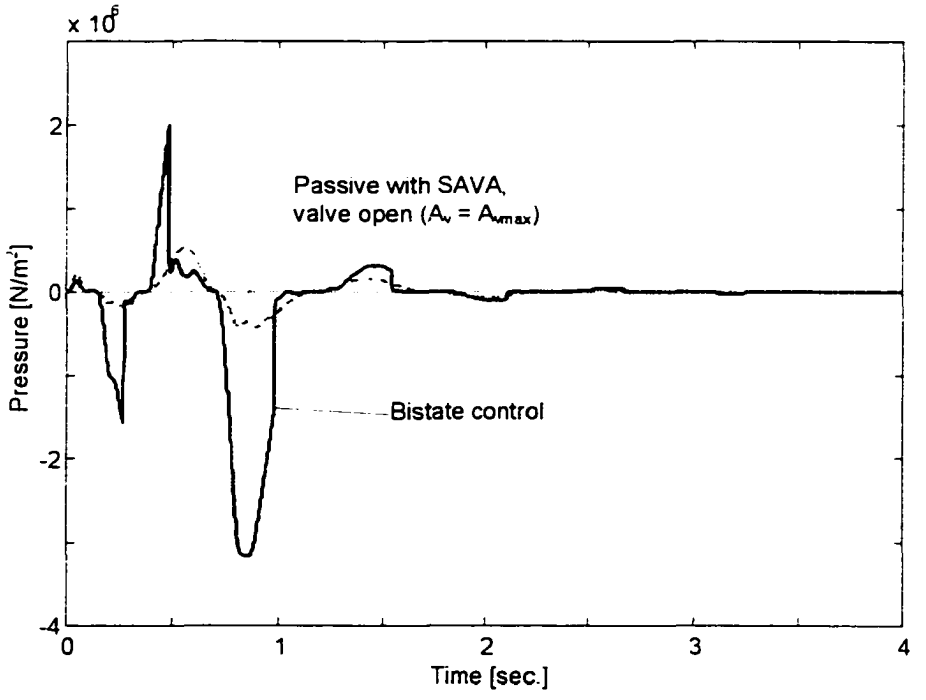

Figure 5.11 Comparison of pressure difference between bistate controller and Algorithm 4 with linearized spring for a bump roadway ($A_{vmin} = 4.0 \times 10^{-6}\ m^2$, $\theta = 30°$).

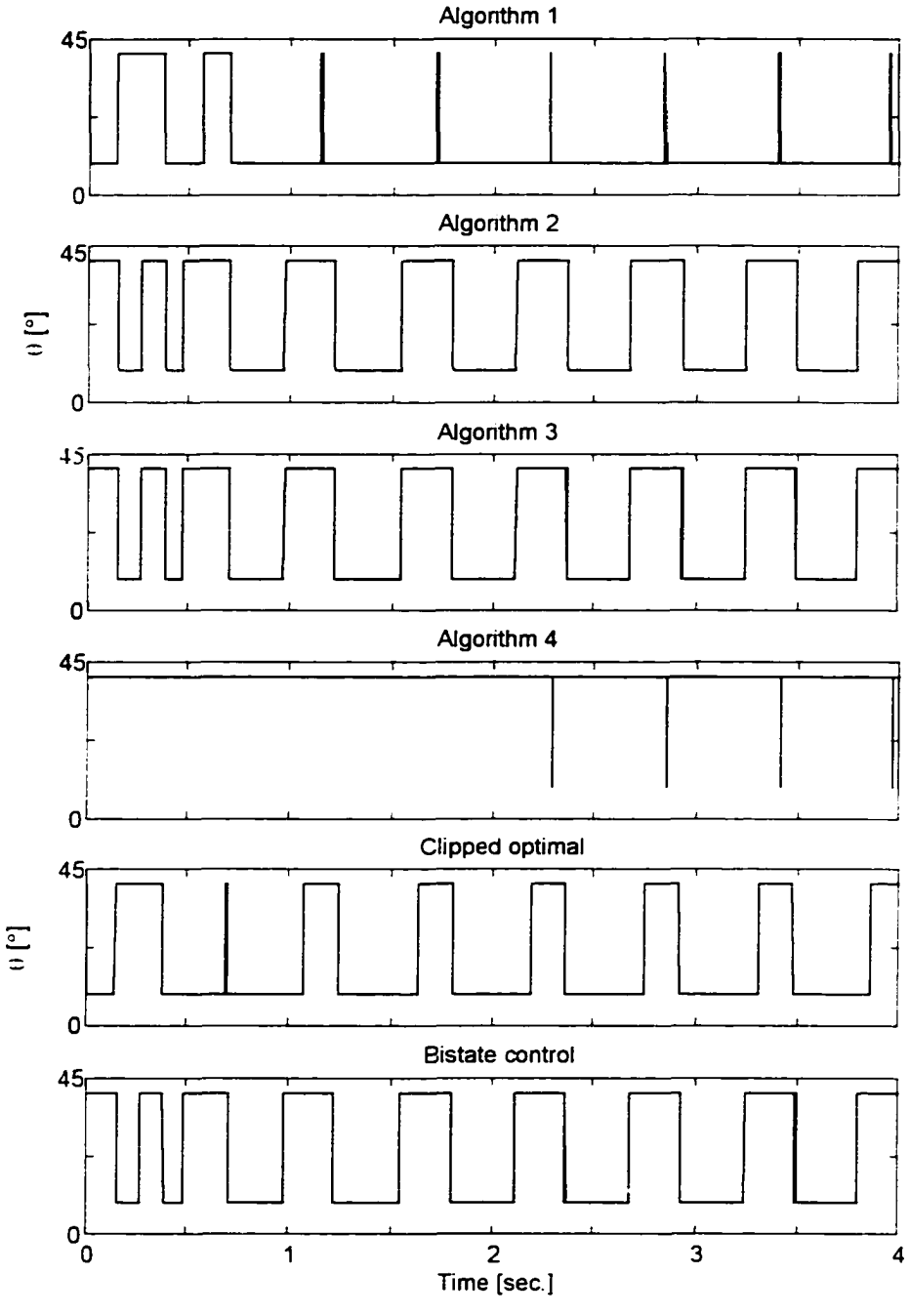

Figure 5.12 Comparison of valve action of four algorithms, clipped optimal and bistate controller with linearized spring for a bump roadway.

5.4 Control Response with Nonlinear Spring

Having established a control paradigm for the linear model of the ¼ truck chassis model, then a question remained regarding the effectiveness of the design to chassis that was characterized by nonlinear compliant elements. Recall that the linear model was identified from actual field data, and that for small perturbations one would expect the linearized model to mimic the linear model. On the other hand, it is reasonable to ask whether the controller "works" when the system undergoes large deviations from the nominal states. The following text examines that question by considering a more exact nonlinear model of the support springs in the chassis. The nonlinear spring model is then used in a simulation with the semiactive vibration absorber to determine the robustness of the SA controller design.

A typical hysteresis loop for a leaf spring is shown in Figure 5.13. The upper curve represents compression and the lower extension. The mathematical model of a leaf spring force is [Yi, et al, 1989, He, 1994]

$$F_t = F_{bt} - (F_{t-1} - F_{bt-1})\, e^{-\frac{\delta_t - \delta_{t-1}}{\beta_t}} \tag{5.13}$$

where

F_t represents the suspension force at the current simulation-time step,

F_{t-1} represents the suspension force at the last simulation-time step,

δ_t represents the suspension deflection at the current simulation-time step,

δ_{t-1} represents the suspension deflection at the last simulation-time step,

F_{bt} represents the force corresponding to the upper boundary when deflection δ increases (or, alternatively, the force corresponding to the lower boundary when deflection δ decreases) at δ_t, and

$$F_{bt} \begin{cases} K_{el}\delta_t + S_1 & when\ \delta_t < \delta_{t-1} \\ K_2\delta_t + S_2 & when\ \delta_t < \delta_{t-1} \end{cases} \quad (5.14)$$

Here, F_{bt-1} represents the force corresponding to the upper boundary when deflection δ increases (or the force corresponding to the lower boundary when deflection δ decreases) at δ_{t-1}, and β_l, β_u represents the friction parameter that characterizes the rate at which the calculated force approaches the upper (or lower) boundary.

In this case, K_{el} and S_1 represent the spring stiffness and intercept, respectively, of the lower portion of the envelope, while K_{eu} and S_2 represent the corresponding values for the upper portion. Next, both β_l and β_u provide vertical transitions between the upper and lower curves of the force-displacement diagram.

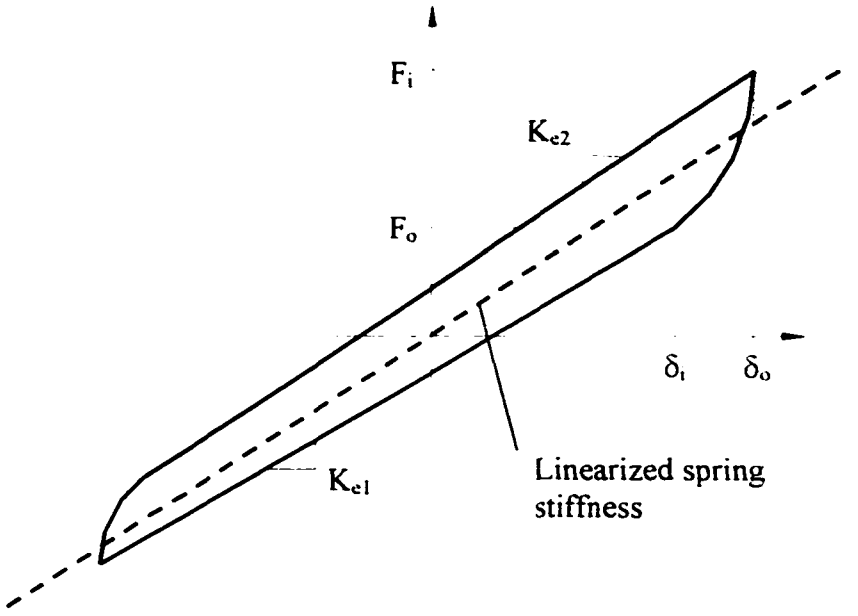

Figure 5.13 Typical force-deflection curve of a leaf spring

Table 5.7 Leaf spring parameters

Symbols	S_1	S_2	β_l, β_u	K_{e2}	K_{e1}
Unit	N	N	m	N/m	kN/m
Values	-500	500	0.0001	236	236

5.5 Truck Suspension Dynamics with a Leaf Spring

Figure 5.14 represents a schematic diagram of a quarter-car model with a leaf spring. This model consists of (1) sprung and unsprung mass, (2) a linear spring (instead of tire stiffness), (3) a nonlinear leaf spring for suspension and (4) a SAVA.

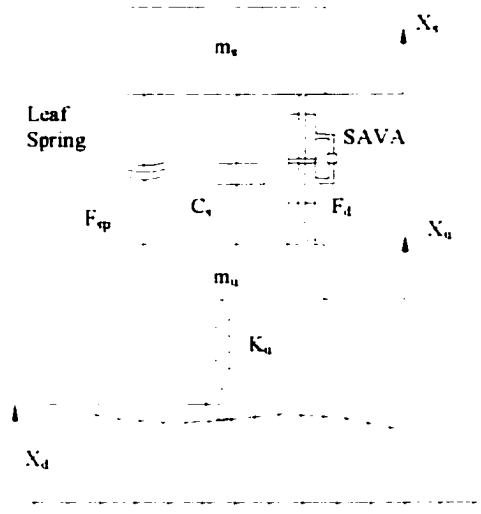

Figure 5.14 Schematic representation of quarter-car model with leaf spring and SAVA.

The equations of motion of the quarter-car model become

$$\begin{aligned} m_s \ddot{x}_s &= F_{sp} - c_s(\dot{x}_s - \dot{x}_u) - F_d \\ m_u \ddot{x}_u &= -F_{sp} + c_s(\dot{x}_s - \dot{x}_u) - k_u(x_u - x_d) + F_d \end{aligned} \tag{5.15}$$

where F_d represents the hydraulic force generated by SAVA and F_{sp} the nonlinear leaf spring force. The time variation of the hydraulic pressure within the SAVA can be rewritten as (see Equation 5.2)

$$\Delta\dot{P} = \frac{\beta(V_1 - V_2)}{V_1 V_2}\left(A_p(\dot{x}_s - \dot{x}_u) - sgn(\Delta P) C_d A_v \sqrt{\frac{2\ \Delta P}{\rho}} \right) \tag{5.16}$$

Define the state space vector as

$$X = [x_s \quad x_u \quad \dot{x}_s \quad \dot{x}_u]^T \tag{5.17}$$

then the state equations are

$$\dot{X} = AX + Bg(X) + EX_d + GF_{sp} \tag{5.18}$$

where

$$A = \begin{bmatrix} 0 & 0 & 1 & 0 \\ 0 & 0 & 0 & 1 \\ 0 & \frac{k_u}{m_s} & -\frac{c_s}{m_s} & \frac{c_s}{m_s} \\ 0 & -\frac{k_u}{m_u} & \frac{c_s}{m_u} & -\frac{c_s}{m_u} \end{bmatrix} \tag{5.19 a}$$

$$B = \begin{bmatrix} 0 & 0 & -\frac{A_p}{m_s} & \frac{A_p}{m_u} \end{bmatrix}^T, \quad E = \begin{bmatrix} 0 & 0 & 0 & \frac{k_u}{m_u} \end{bmatrix}^T \tag{5.19 b, c}$$

$$G = \begin{bmatrix} 0 & 0 & \frac{1}{m_s} & -\frac{1}{m_u} \end{bmatrix}^T, \quad g(X) = \Delta P \tag{5.19 d, e}$$

The reader is cautioned that given the nonlinear spring stiffness, then the system matrix A is singular, and the guarantees of asymptotic stability (see section 3.2) are lost.

The nonlinear model was used in a sequence of simulations to determine the extent to which those nonlinearities might effect the predicted open and closed loop performance of the truck suspension. The Lyapunov gains developed for the linear vehicle control were

used here to simulate the nonlinear response. The parameters that characterize the damper for a heavy truck are given in Table A.4 (see Appendix A). The examples of the open and closed loop performance for the "bump" are shown in Figures 5.15 through 5.17. For the random road profile, the RMS values of the sprung mass acceleration, the tire force and the rattle space deflection for each of the controllers and passive system are listed in Table 5.8. The maximum and RMS values of the sprung mass acceleration, the tire force and the rattle space deflection for bump road are listed in Tables 5.9 and 5.10.

Table 5.8 RMS reduction for a random displacement excitation with leaf spring

Control Algorithms	Acceleration of Sprung Mass	Tire Deflection	Suspension Deflection
Algorithm 1	15.5%	-9.4%	-3.8%
Algorithm 2	17.7%	-7.1%	-27.0%
Algorithm 3	16.0%	-6.4%	-32.5%
Algorithm 4	-0.2%	0.4%	11.7%
Clipped Optimal	15.6%	-12.7%	-79.3%
Passive (no SA)	31.3%	-64.6%	-71.7%
Passive (with SA)*	26.3%	-26.6%	-31.0%
Bistate Control	1.28	0.0035	0.011

Negative: worse than Lyapunov control. Positive: better than Lyapunov control.
*: with valve fully open ($A_{vmin} = 4.0\times10^{-6}\ m^2$, $\theta = 30°$).

Table 5.9 Maximum-peak reduction for a bump roadway with leaf spring

Control Algorithms	Acceleration of Sprung Mass	Tire Deflection	Suspension Deflection
Algorithm 1	-26.4%	-29.2%	22.3%
Algorithm 2	0.4%	1.2%	-0.4%
Algorithm 3	0.4%	1.2%	-0.4%
Algorithm 4	-3.3%	6.0%	-4.3%
Clipped Optimal	-30.0%	-30.0%	34.1%
Passive (no SA)	-4.7%	5.9%	-7.3%
Passive (with SA)*	-4.6%	5.9%	-7.1%
Bistate Control	1.33	0.003	0.033

Negative: worse than Lyapunov control. Positive: better than Lyapunov control.
*: with valve fully open (A_{vmin} 4.0×10^{-6} m^2, θ $30°$).

Table 5.10 RMS reduction for a bump roadway with leaf spring

Control Algorithms	Acceleration of Sprung Mass	Tire Deflection	Suspension Deflection
Algorithm 1	-0.4%	-2.2%	19.4%
Algorithm 2	0.3%	0.5%	-0.5%
Algorithm 3	0.3%	0.5%	-0.5%
Algorithm 4	-21.9%	-17.6%	-37.3%
Clipped Optimal	-15.8%	-16.5%	26.7%
Passive (no SA)	-26.8%	-22.1%	-46.3%
Passive (with SA)*	-26.4%	-21.8%	-45.7%
Bistate Control	0.35	0.00079	0.008

Negative: worse than Lyapunov control. Positive: better than Lyapunov control.
*: with valve fully open ($A_{vmin} = 4.0\times10^{-6}$ m^2, $\theta = 30°$).

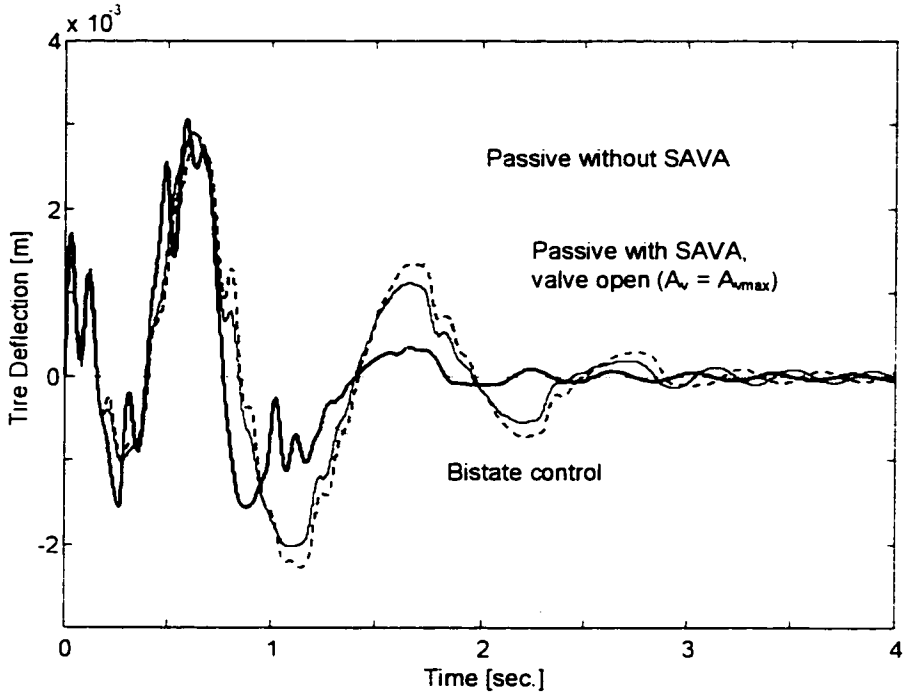

Figure 5.15 Comparison of tire deflection between bistate controller and passive with leaf spring for a bump roadway ($A_{vmin} = 4.0\times10^{-6}\ m^2$, $\theta = 30°$).

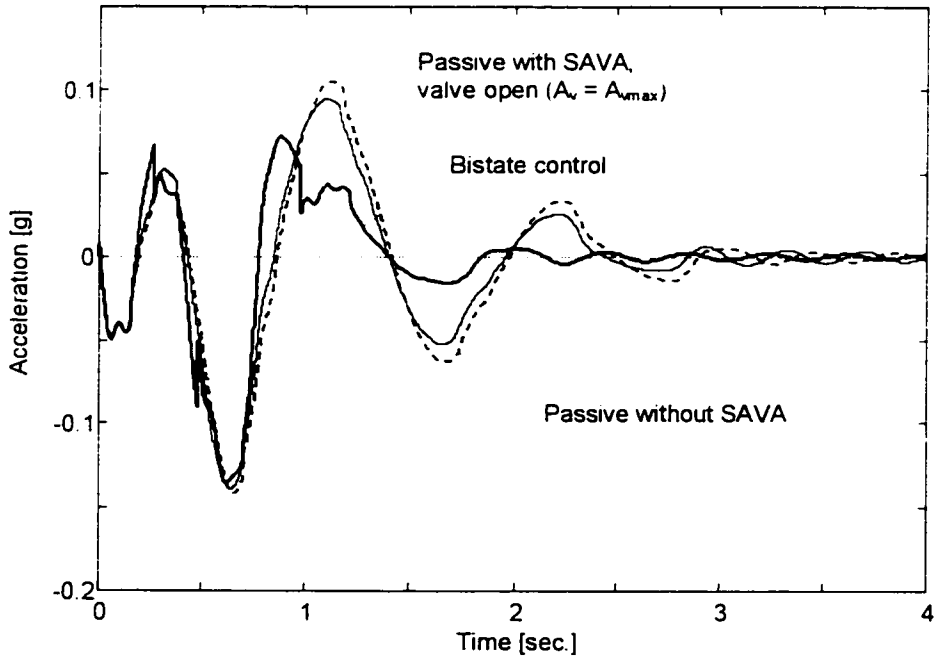

Figure 5.16 Comparison of acceleration of sprung mass between bistate controller and passive with leaf spring for a bump roadway ($A_{vmin} = 4.0\times10^{-6}\ m^2$, $\theta = 30°$).

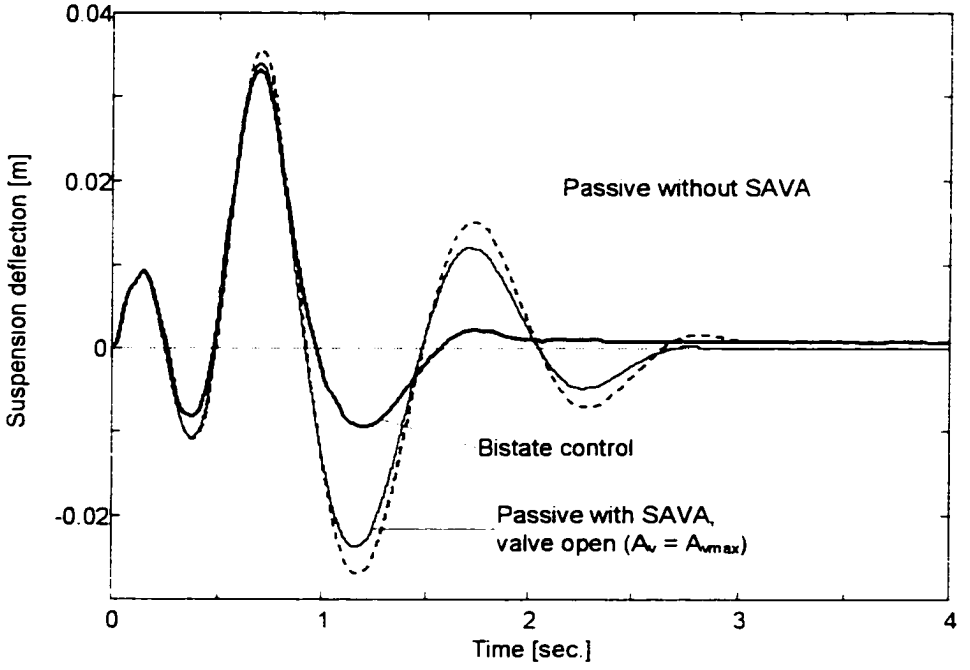

Figure 5.17 Comparison of suspension deflection between bistate controller and passive with leaf spring for a bump roadway (A_{vmin} 4.0×10^{-6} m^2, θ $30°$).

5.6 Conclusion

The results indicate that the Lyapunov control provides the best overall performance for a vehicle. The importance of each aspect of response (tire deflection, sprung mass acceleration and rattle space deflection) can on the other hand skew the apparent effectiveness of each of the controllers. In fact the measure of goodness (maximum values versus RMS values) can alter the outcome. For example, Algorithm 4 appears to be very competitive with the Lyapunov control when maximum output values (Table 5.4) are measured for the bump input. On the other hand, Algorithm 4 is apparently much less effectiveness when the RMS output of the system is measured (Table 5.5).

The response of the controlled system to a random displacement input (Figures 5.4 through 5.6) indicates that the Lyapunov controller provides the greatest amount of attenuation of the vehicle dynamics at the vehicles resonant frequencies.

Finally, the pressure responses for the Lyapunov control for the two different inputs (see Figures 5.7 and 5.11) indicate a reasonable level of acting pressure in SAVA actuator.

CHAPTER SIX

RECOMMENDATIONS

The purpose of this chapter is to provide the reader with an indication of additional research issues need to be explored with regard to the development of semiactive vibration mitigation systems.

The most obvious research question is how does one select (design) the semiactive hardware? A related and possible more important question is does the SA system design effect the performance of the control design. A review of the hydraulic Equations (Equations 2.9, 3.2) indicates that the control analysis must presume pre-selected values of the (double acting) face area of the piston in the actuator (A_p), the free stroke of the piston (l_p), the bulk modulus of the hydraulic fluid (β_o varies dramatically from one hydraulic fluid to the next) and the degree of air entertainment. The valve characteristics (A_{vmin}, A_{vmax}) are also presumed to have been pre-selected, as has C_d the discharge coefficient of the valve.

The work presented above relied on hardware configurations that adopted based on engineering estimates that lead in turn to an informed choice. For example, the SA actuator parameters used in the truck chassis analysis were based on a standard passive shock absorber. The valve characteristics employed reflect the properties of a readily available, inexpensive valve that was selected because it had very low rotational inertia making it ideal to applications requiring high bandwidth.

The need for thorough study of the design of semiactive systems is made evident with the following case study. When the author began his study of the SA seismic mitigation system, he presumed valves of the SA system parameters consistent with past work [Mo, 1996, He, 1994]. One assumption made was that A_{vmin} should be 45° (valve is fully closed). Simulations of the various bistate control laws indicated however that complete closure of the valve produced extremely high internal pressures. A study was then initiated to discover is a more suitable value of A_{vmin} might be determined. A random base excitation was used with an RMS amplitude of 0.0043 m and different A_{vmin} were incorporated. The study was based on the Lyapunov control design.

With the actuator mounted between the first floor and the second floor, then the predicted RMS displacements and accelerations were recorded and plotted (Figures 6.1 and 6.2). Figure 6.1 indicates that the SA system reduces deflection for the story on which it is mounted for all values of A_{vmin}. On the other hand, the displacement of the story not outfitted with a SA actuator increases as A_{vmin} decreases. While relative displacement is of prime importance for seismic isolation designs, the level of acceleration produced by the control action is also significant to the assessment of controller performance.

The acceleration amplitude (RMS) responses at each story for the various values of A_{vmin} used are shown in Figure 6.2. The graphical results indicate that when A_{vmin} is less than 14% of A_{vmax} then the trade off between reduced story height at the first and second floor becomes significant. That sensitivity study led to the selection of an A_{vmin} of 14% of the A_{vmax} of the valve used (See Table 4.3).

The sensitivity analysis of the design performance versus A_{vmin} clearly indicates that

the values of the SA system parameters used can effect the performance in a significant way. It is recommended that a thorough and systematic effort be undertaken to develop a means of optimizing the selection of SA system parameters in order to optimize the closed loop performance of the system. That task is not trivial. Design optimization methods for linear systems are well known. Design optimization techniques for nonlinear systems are less well developed.

Next, it is valuable to compare the performance of the different five control algorithms that effectively represent different performances for both displacement and acceleration. Chapter Two revealed that various physical parameters of SAVA affect the damping behaviors of a dynamic system. These parameters, of course, included piston effective area, discharge coefficient of the valve, valve area, etc. More importantly, when the hardware specifications of the SAVA are determined, the damping characteristics of the system then depend on the valve area to control. In investigating the effect of the change in valve area, one desires to know the effect of decreasing, as well as increasing, this area. The knowledge of both effects will, in turn, then provide much useful information as to the decision of optimal valve-opening area to obtain the overall performance desired with the given hardware of a SAVA. To this end, the TDOF system in Figure 4.1 with SAVA (Table 2.2 lists the physical parameters of SAVA) was used to the simulations in this work.

Figures 6.3 through 6.6 represent proper guidance options for the two decisions regarding (1) valve area to control and (2) the control algorithms themselves. Algorithm 4 and the bi-state controller represent a better performance (in terms of vibration

reduction) than that of Algorithms 2 and 3 for all cases. As seen in this chapter, various possible control algorithms should be tested and selected to obtain the best control performance when using "on-off" controllers. Techniques that automatically produce best solutions for the combined design and control of a nonlinear system is a virtually unexplored area of research. The challenge is therefore significant. The next chapter offers concluding comments.

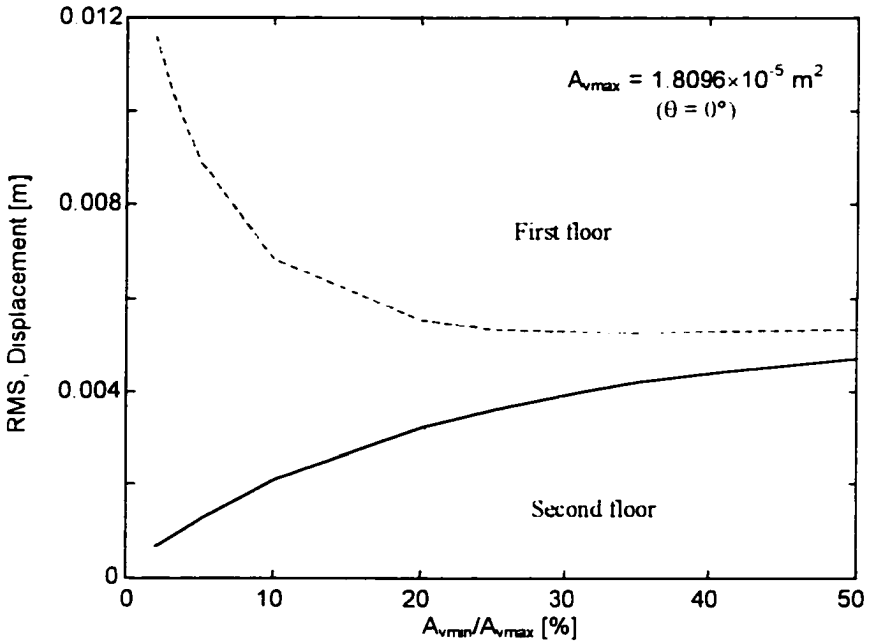

Figure 6.1 Relative displacement as a function of A_{vmin} for seismic protection (see Section 4.1).

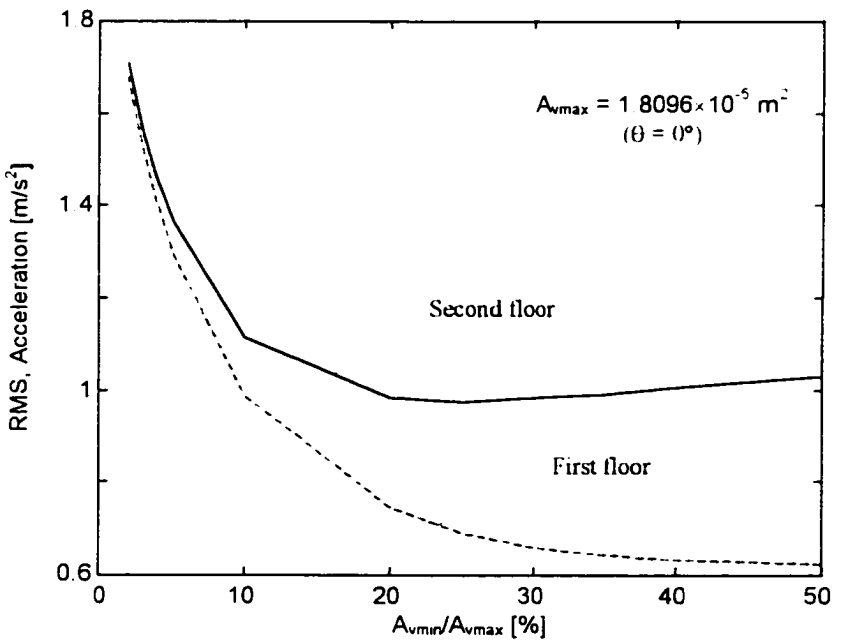

Figure 6.2 Absolute acceleration as a function of A_{vmin} for seismic protection.

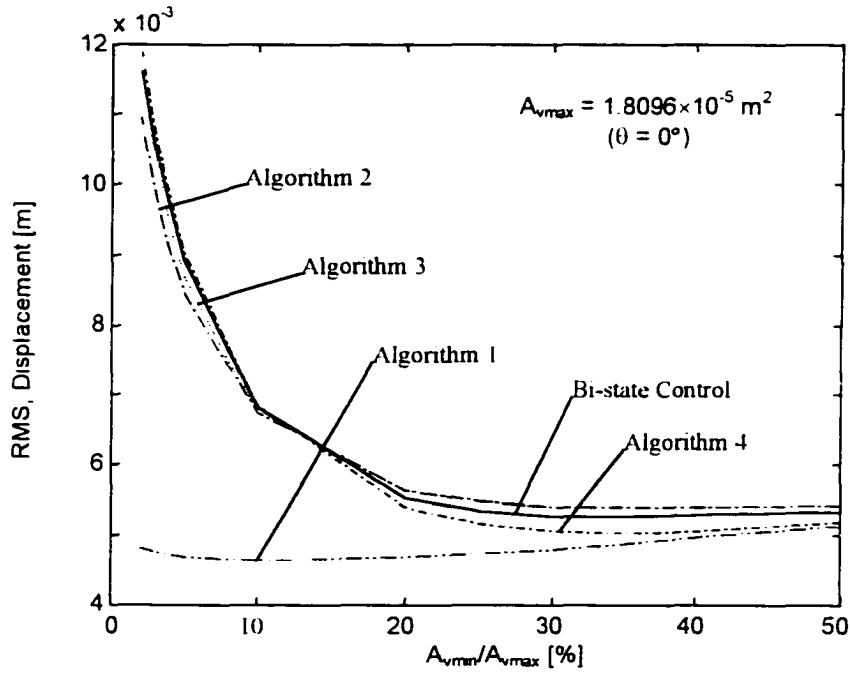

Figure 6.3 Comparison of relative displacement of the first floor as a function of A_{vmin} for various controllers.

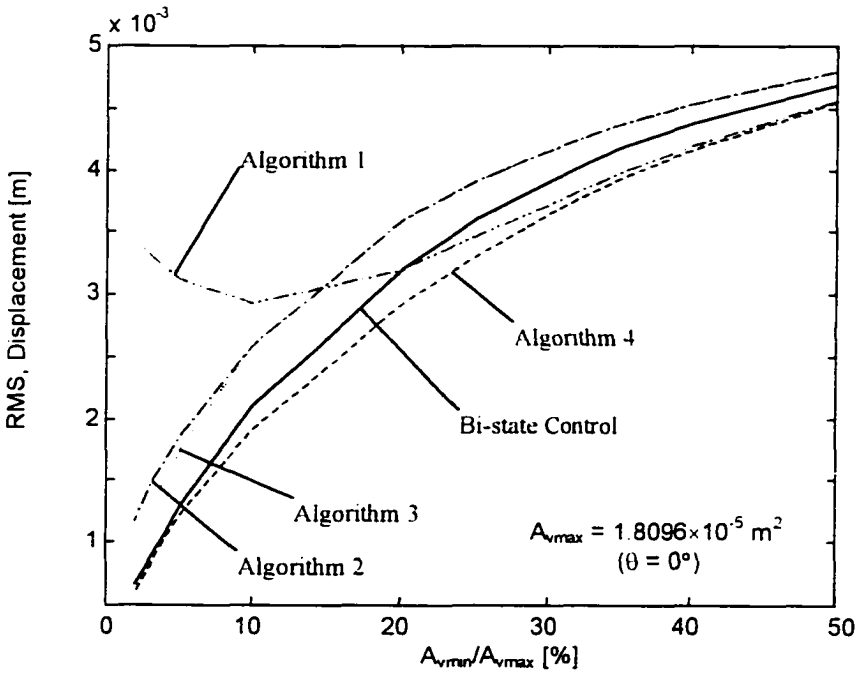

Figure 6.4 Comparison of relative displacement of the second floor as a function of A_{vmin} for various controllers.

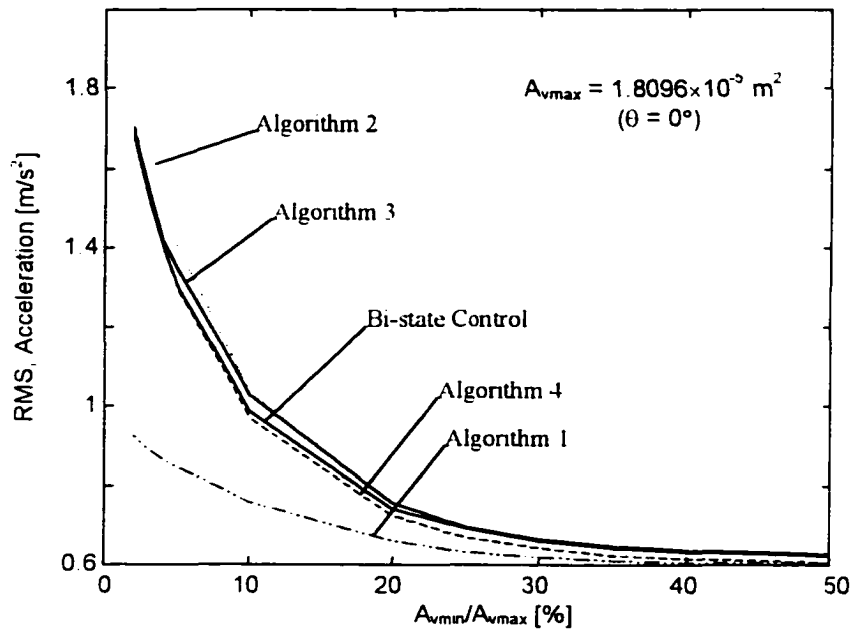

Figure 6.5 Comparison of absolute acceleration of the first floor as a function of A_{vmin} for various controllers.

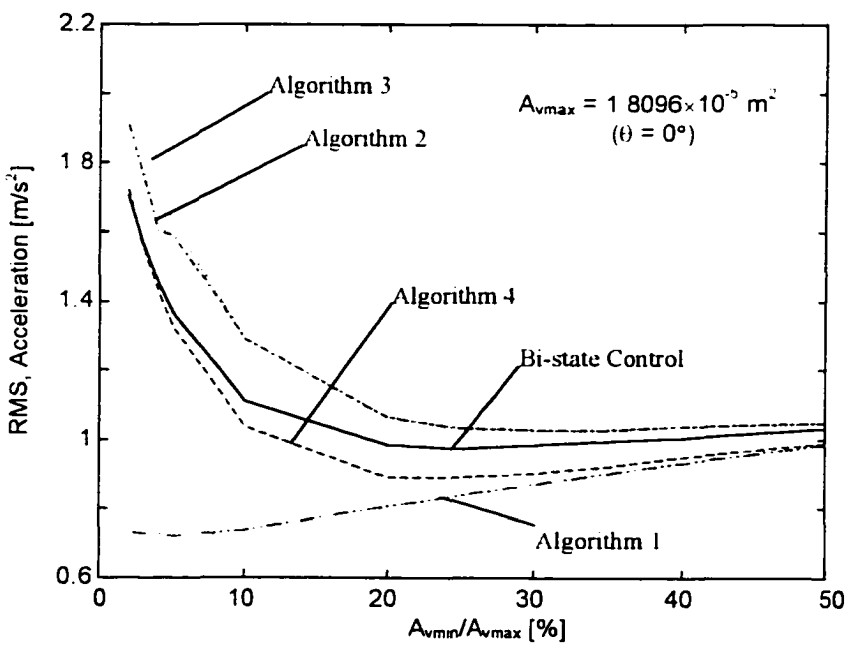

Figure 6.6 Comparison of absolute acceleration of the second floor as a function of A_{vmin} for various controllers.

CHAPTER SEVEN

CONCLUSIONS

The work reported in the dissertation provides heretofore-unavailable comparison of the effectiveness of various two states or bistate control algorithms for the operation of a hydraulic semiactive vibration mitigation system.

The study began with a detailed discussion of the various mechanisms that come into play when an adjustable hydraulic damper is utilized to absorb vibration. Chapter Two described an analytical and experimental effort to correlate the nonlinear dynamics of a semiactive actuator.

The next chapter (Chapter Three) provides a detailed review of the control approach that is used in most of the semiactive designs that have been developed at the University of Oklahoma's Center for Structural Control: the Lyapunov bistate control. While the dynamics of the SAVA system are demonstrably nonlinear, the actuator provides a straightforward proof of the stability of a Lyapunov control when applied to a stable linear system. The author also demonstrates that the Lyapunov design can be used directly to establish a state feedback law with fixed gains that provides a logical control decision: when to open, and when to close the by pass valve connecting the two hydraulic chambers of the semiactive actuator.

The actual comparison of different semiactive control laws is presented in Chapters Four and Five. Chapter Four reports the results of a variety of tests using competing

bistate control laws to govern the responses of a structure subjected to an earthquake. A two-story model of a structure was used in the analysis this made it possible to test two different actuator topologies. The results clearly indicate that the Lyapunov control and a special variant of that control (which relies on the velocity and differential pressure across the actuator) provide nearly identical levels of isolation. The other algorithms tested, including the clipped optimal control design provided much less protection.

The comparison of the performance of the various SA controllers was applied to a two-degree-of-freedom linearized suspension model of a vehicle. Two types of road input were assumed: a white noise displacement and a road swell. The comparisons included three criteria the same controllers were applied to a nonlinear model of the same vehicle (which included a leaf spring suspension). The comparative results of the different controllers were little different from those obtained with the linear model. The Lyapunov control provided the best overall performance. A possible drawback to the application of the Lyapunov control is that it assumes full state feedback that requires the construction of an estimator (or observer) to produce an estimate of the full state vector from the outputs, that need poses a problem when disturbances act on the system, because in order to provide an accurate estimate, one must supply information about the disturbance to the estimator.

Two approaches are possible: 1) rely only on the outputs and either use one of the "local" controllers (Algorithms 1 through 4) or deweight the gains in the Lyapunov controller that multiply states that are not readily available. The deweighting would have to be carried out indirectly by tuning the P matrix in the Lyapunov equation (Equation

3.9).

Finally, it is pointed out that the effectiveness of each of the algorithms tested could probably be improved by tuning each. No attempt was made hereto determine best gains for each controller because those "best" gains are likely to vary with different inputs to the system.

REFERENCES

[1] Alanoly, J., and Sankar, S., "A New Concept in Semi-Active Vibration Isolation," Transactions of the ASME, Journal of Mechanisms, Transmissions, and Automation in Design, Vol. 109, June 1987, pp. 242-247.

[2] Audenino, A. L., and Belingardi, G., "Modeling the Dynamic Behaviour of a Motorcycle Damper," Proc. Instn Mech Engrs, Vol. 209, Part D, 1995, pp. 249-262.

[3] Bandstra, J. P., "Comparison of equivalent viscous damping and nonlinear damping in discrete and continuous vibrating systems," Journal of Vibration, Acoustic, Stress, and Reliability in Design, Vol. 105, 1983, pp. 382-392.

[4] Barnett, S., and Storey, C., "On the general functional matrix for a linear system," IEEE Trans. Automatic Control, Vol. 12, 1967, pp. 436-438.

[5] Bartels, R. H., and Stewart, G. W., "Algorithm 432, Solution of the Matrix Equation AX+XB=C," Communications of the ACM, Vol. 15, No. 9, Sept. 1972, pp. 820-826.

[6] Bellman, R., "Stability Theory of Differential Equations," McGraw-Hill, 1953.

[7] Bellman, R., Glicksberg, I., and Gross, O., "On the "Bang-Bang," Control Problem," Quarterly of Applied Mathematics, Vol. 14, No. 1, 1956, pp. 11-18.

[8] Bingulac, S., "An alternate approach to expanding $PA+A^{\Gamma}P=-Q$," IEEE Trans. Automatic Control, Vol. 15, 1970, pp. 135-136.

[9] Butsuen, T., "The Design of Semi-active Suspension for Automotive Vehicles," Ph.D. Thesis, Department of Mechanical Engineering, MIT, 1989.

[10] Cebon, D., Besinger, F. H., and Cole, D. J., "Control strategies for semi-active lorry suspensions," Proc. Instn Mech Engrs., Part D, Vol.210, 1996, pp. 161-178.

[11] Chen, C. F., and Shieh, L. S., "A Note on Expanding $PA+A^{T}P=-Q$," IEEE Trans. on Automatic Control, 1968, pp. 122-123.

[12] Chen, C. T, Linear System Theory and Design, Holt, Rinehart and Winston, Inc., 1970.

[13] Cole, D. J., Cebon, D., and Besinger, F. H., "Optimisation of Passive and Semi-Active Heavy Vehicle Suspensions," SAE SP-1059, 942309, 1994, pp. 105-117.

[14] Crosby, M. J., and Karnopp, D. C., "The Active Damper - A New Concept for Shock and Vibration Control," The Shock and Vibration Bulletin, No. 43, Part 4., June 1973, pp. 119-133.

[15] Dulay, I.K. (Ed), with Fürész, F., Harkay, G. and J. Lukács, Fundamentals of Hydraulic Power Transmission, Studies in Mechanical Engineering, 7, Elsevier Science, N.Y, 1988.

[16] El-Demerdash, S. M., and Crolla, D. A., "Effect of non-linear components on the performance of a hydro-pneumatic slow-active suspension system," Proc. Instn Mech Engrs., Part D, Vol.210, 1996, pp. 23-34.

[17] Fancher, P. S., Ervin, R. D., MacAdam, C. C., and Winkle, C. B., "Measurement and Representation of the Mechanical Properties of Tuck Leaf Springs," SAE Paper No. 800905, 1980.

[18] Fodor, M., and Redfield, R. C., "Experimental Verification of Resistance Control, Semi-Active Damping," Vehicle System Dynamics, 1966, pp. 143-159

[19] Gajic, Z., and Qureshi, M. T. J., Lyapunov Matrix Equation in System Stability and Control, Mathematics in Science and Engineering, Vol. 195, Academic Press, 1995.

[20] Gillespie, T. D., "Fundamentals of Vehicle Dynamics," SAE Inc., 1992

[21] Gillespie, T. D., and Karamihas S. M., "Characterizing the Road-Damaging Dynamics of Truck Tandem Suspensions," SAE Paper No. 932994.

[22] Glasner, E. C., Göhring, E., Povel, R., and Schützner, P., "Analysis of Intelligent Suspensions for Commercial Vehicles," SAE Paper No. 933008.

[23] Green, M. F., and Cebon, D., "Dynamic Response of Highway Bridges to Heavy Vehicle Loads: Theory and experimental Validation," Journal of Sound and Vibration, Vol. 170, No.1, 1994, pp. 51-78.

[24] Hac, A., "Optimal Linear Preview Control of Active Vehicle Suspension," Vehicle System Dynamics, Vol. 21, 1992, pp. 167-195.

[25] Hac, A., and Youn, I., "Optimal Semi-active Suspension with Preview Based on a Quarter Car Model," Transaction of the ASME, Journal of Vibration and Acoustics, Vol. 114, 1992, pp. 84-92.

[26] Hatada, T. and Smith, H. A., "Development and Application of Nonlinear Controller Using Variable Damping Device," Proceedings of the American Control Conference, Albuquerque, NM, 1997, pp. 453-457.

[27] He, J., Semiactive Vibration Control with an Application to Automobile Leaf Spring Suspensions, MS Thesis, Aerospace and Mechanical Engineering, University of Oklahoma, 1994.

[28] Hedrick, J. K., and Karnopp, D. C., "Active and Semi-Active Suspensions - Theory and Application," Special Two Day Short Course sponsored by Monroe Auto Equipment Company, Feb. 8-9, 1988.

[29] Hrovat, D., Barak, P., and Rabins, M., "Semi-Active versus Passive or Active Tuned Mass Dampers for Structure Control," Journal of Engineering Mechanics, Vol. 109, No. 3, June 1983, pp. 691-705.

[30] Hrovat, D., and Hubbard, M., "Optimum Vehicle Suspensions Minimizing RMS Rattle space, Sprung-Mass Acceleration and Jerk," Transaction of the ASME, Journal of Dynamic Systems, Measurement, and Control, Dec. 1981, pp. 228-236.

[31] Hrovat, D., Margolis, D. L., and Hubbard, M., "An Approach Toward the Optimal Semi-Active Suspension," Transaction of the ASME, Journal of Dynamic Systems, Measurement, and Control, Vol. 110, Sept. 1988, pp. 288-296.

[32] ISO/CD 2631, "Third Committee Draft on Guide to the Evaluation of Human Exposure to Whole-body Vibration-Revision of ISO 2631," International Standards Organization, 1991

[33] Ivers, D. E., and Miller, L. R., "Semi-Active Suspension Technology: An Evolutionary View," Advanced Automotive Technologies, ASME-DE, Vol. 40, 1991, pp. 327-346.

[34] James, W. S., and Ullery, F. E., "An Automatic Shock Absorber," SAE paper, Vol. 30, No.5, May 1932, pp.185-191.

[35] Kalman, R. E., and Bertram, J. E., "Control System Analysis and Design via the Second Method of Liapunov: I. Continuous-time System; II. Discrete-time System," ASME, Journal of Basic Engineering, Vol. 82, 1960, pp. 371-393; 394-400.

[36] Kang, Young Kern, "Nonlinear Heavy Truck Shock Absorber Modeling and Its Application," MS Thesis, Department of Aerospace and Mechanical Engineering, University of Oklahoma, 1998.

[37] Karnopp, D. C., "Force Generation in Semi-Active Suspensions Using Modulated Dissipative Elements," Vehicle System Dynamics, Vol. 16, 1987, pp. 333-343.

[38] Karnopp, D. C., "Design Principles for Vibration Control Systems using Semi-Active Dampers," ASME, Journal of Dynamic Systems, Measurement, and Control, 1990, pp. 448-455.

[39] Karnopp, D. C., "Active and Semi-Active Vibration Isolation," ASME, Journal Of 50th Anniversary of the Design Engineering Division, Vol. 117, June 1995, pp 177-185.

[40] Karnopp, D. C., Crosby, M. J., and Harwood, R. A., "Vibration Control Using Semi-Active Force Generators," ASME, Journal of Engineering for Industry, Vol. 96, No. 2, 1974, pp. 619-626.

[41] Klinger, D. L., and Galzade, A. J., "A Pneumatic On-Off Vehicle Suspension System," ASME, Journal of Dynamic Systems, Measurement, and Control, 1977, pp. 130-140.

[42] Kobori, T., Takahashi, M., Nasu, T., and Niwa, N., "Seismic Response Controlled Structure with Active Variable Stiffness System," Earthquake Engineering and Structural Dynamics, Vol. 22, 1993, pp. 925-941.

[43] Krasnicki, E. J., "Comparison of Analytical and Experimental Results for a Semi-Active Vibration Isolator," Proceedings of the 50th Shock and Vibration Symposium, 1979, pp. 69-76.

[44] Krasnicki, E. J., "The Experimental Performance of an "On-Off" Active Damper," Proceedings of the 51st Shock and Vibration Symposium, 1980, pp. 125-131.

[45] Lefschetz, S., Differential Equations: Geometric Theory, 2nd ed., Dover Publications, Inc., 1977, originally published by Interscience Publishers in 1957.

[46] Leitmann, G., "Semiactive Control for Vibration Attenuation," Journal of Intelligent Material Systems and Structures, Vol. 5, Nov. 1994, pp. 841-846.

[47] Leitmann, G., and Reithmeier, E., "Semiactive Control of a Vibrating System by Means of Electrorheological Fluids," Dynamics and Control 3, 1993, pp. 7-33.

[48] Margolis, D. L., "The Response of Active and Semi-Active Suspensions to Realistic Feedback Signals," Vehicle Systems Dynamics, Vol. 11, No. 6, 1982, pp. 267-282.

[49] Margolis, D. L., "Semi-Active Control of Wheel Hop in Ground Vehicles," Vehicle System Dynamics, Vol. 12, 1983, pp. 317-330.

[50] Margolis, D. L., and Goshtasbpour, M., "The Chatter of Semi-Active On-Off Suspensions and Its Cure," Vehicle System Dynamics, Vol. 13, 1984, pp. 129-144.

[51] Margolis, D. L., Tylee, J. L., and Hrovat, D., "Heave Mode Dynamics of a Tracked Air Cushion Vehicle with Semi-Active Airbag Secondary Suspension," ASME, Journal of Dynamic Systems, Measurement, and Control, Vol. 47, Dec. 1975, pp. 399-407.

[52] Miller, L. R., and Nobles, C. M., "Methods for Eliminating Jerk and Noise in Semi-Active Suspensions," SAE 902284, 1990.

[53] "MATLAB® User's Manual for Personal Computer," The Maths Works, Inc., 1990.

[54] Merritt, H. E., Hydraulic Control Systems, Wiley & Sons, 1967.

[55] Mo, C., Lee, J., Kuehn, J., Khaw, C., and Patten, W. N., "Fluid Compressibility Effects in Semiactive Vibration Absorbers (SAVA)," DE-Vol. 93, ASME, International Mechanical Engineering Congress and Exposition, Atlanta, Georgia, 1996a, pp. 197-204.

[56] Mo, C., Lee, J., and Patten, W. N., "Semiactive Vibration Absorbers (SAVA) for Auto Suspensions," submitted to ASME, Journal of Dynamic Systems, Measurement, and Control, 1996b.

[57] Mohler, R. R., Nonlinear Systems-Dynamics and Control, Vol. 1 and 2, Prentice Hall, 1991.

[58] Nijmeijer, H. And Van der Schaft, A. J., Nonlinear Dynamical Control Systems, Springer Verlag, 1990.

[59] Ohta, M., Nishida, T., Suzuki, K., and Uehara, M., "The Influence of Tire Deformation on Ride Comfort of a Truck," SAE SP-843, 902268, 1990, pp. 37-45.

[60] Oueslati, F., and Sankar, S., "A Class of Semi-Active Suspension Schemes for Vehicle Vibration Control," Journal of Sound and Vibration, Vol. 172, No. 3, 1994, pp. 398-403.

[61] Patten, W. N. et al., "Semiactive Vibration Absorbers (SAVA) at the I-35 Walnut Creek Bridge," Final Report, No. 2125, FHWA, The Oklahoma Department of Transportation, and The University of Oklahoma, September, 1997.

[62] Patten, W. N., He, Q., He, J., and Hu, J., "A New Algorithm of Semiactive Control for Suspension with Nonlinear Leaf Spring," ASME Winter Annual Meeting, Chicago, IL, 1994a, pp. 147-156.

[63] Patten, W. N., He, Q., Kuo, K., Liu, L., and Sack, R. L., "Seismic Structural Control via Hydraulic Semiactive Vibration Dampers (SAVD)," 1st World Conf. on Structural Control, Vol. 3, FA 2, Los Angeles, CA, 1994b, pp. 83-89.

[64] Patten, W. N., Mo, C., Kuehn, J., Lee, J., and Khaw, C., "Hydraulic Semiactive Vibration Absorbers (SAVA): Separating Myth from Reality," 13th IFAC World Congress, Vol. L, San Francisco, CA, 1996a, pp. 157-162.

[65] Patten, W. N., Mo, C., Kuehn, J., and Lee, J., "A Primer on Design of Semiactive Vibration Absorbers (SAVA)," ASCE, Journal of Structural Engineering, Vol. 124, No. 1, 1998, pp. 61-68.

[66] Patten, W. N., Sack, R. L., and He, Q., "A Controlled Semiactive Hydraulic Vibration Absorbers for Bridges," ASCE, Journal of Structural Engineering, Vol. 122, No.2, 1996b, pp. 187-192.

[67] Rajamani, R., and Hedrick, J. K., "Semi-Active Suspension - A Comparison Between Theory and Experiments," Proc. 12th IAVSD Symposium on the dynamics of vehicles on roads and tracks, 1991, pp. 504-518.

[68] Rakheja, S., and Sankar, S., "Vibration and Shock Isolation Performance of a Semi-Active "On-Off" Damper," Transaction of the ASME, Journal of Vibration, Acoustics, Stress, and Reliability in Design, Vol. 107, Oct. 1985, pp. 398-403.

[69] Rose, N. J., "Theoretical Aspect of Limit Control," Report No. 459, Experimental Towing Tank, Stevens Institute of Technology, Nov. 1953.

[70] Sack, R. L., and Patten, W. N., "Semiactive Hydraulic Structural Control," Proc., Int. Workshop on Structural Control, 1993, pp. 417-431.

[71] Seayers, M., and Gillespie, T. D., "The Effect of Suspension System Nonlinearties on Heavy Truck Vibration," The Dynamics of Vehicles on Roads and on Tracks 7th, Proceedings, Sept. 1981, pp. 154-166.

[72] Segel, L., and Lang, H. H., "The Mechanics of Automotive Hydraulic Dampers at High Stroking Frequencies," Vehicle System Dynamics, Vol. 10, 1981, pp. 79-83.

[73] Singh, M. P., Matheu, E. E., and Suarez, L. E., "Active and Semi-Active Control of Structures under Seismic Excitation," Earthquake Engineering and Structural Dynamics, Vol. 26, 1997, pp. 193-213.

[74] Slotine, J. J. E., and Li, W., Applied Nonlinear Control, Prentice-Hall, Inc., 1991.

[75] Soom, A., and Lee, M. S., "Optimal Design of Linear and Nonlinear Vibration Absorbers for Damped Systems," Transaction of the ASME, Journal of Vibration, Acoustics, Stress, and Reliability in Design, Vol. 105, Jan. 1983, pp. 112-119.

[76] Symans, M. D., and Constantinou, M. C., "Seismic Testing of a Building Structure with a Semi-Active Fluid Damper Control System," Earthquake Engineering and Structural Dynamics, Vol. 26, 1997, pp. 759-777.

[77] Tseng, H. E., and Hedrick, J. K., "Semi-Active Control Laws-Optimal and Sub-Optimal," Vehicle Systems Dynamics, Vol. 23, 1994, pp. 545-569.

[78] Vidyasagar, M., Nonlinear Systems Analysis, Prentice-Hall, Inc., 1978.

[79] Wallaschek, J., "Dynamics of Non-linear Automobile Shock-absorbers," Int. J. Non-Linear Mechanics, Vol. 25, No. 2/3, 1990, pp. 299-308.

[80] Watton, J., Fluid Power Systems: Modeling, Simulation, Analog and Computer Control, Prentice-Hall, Inc., 1989.

[81] Whity "33" Series Multipurpose Ball Valves Catalog, A SWAGELOK COMPANY.

[82] Wu, Z., and Soong, T. T., "Modified Bang-Bang Control Law for Structural Control Implementation," Journal of Engineering Mechanics, Aug. 1996, pp. 771-777.

[83] Wu, H. C., Yan, W. Z., Mo, C., and Patten, W. N., "A Prototype Semiactive Damper," Advanced Automotive Technologies, ASME, Winter Annual Meeting, DSC-Vol. 52, 1993, pp. 51-57.

[84] Yi, K., and Hedrick, J. K., "Active and Semi-Active Heavy Truck Suspensions to Reduce Pavement Damage," SAE 892486.

[85] Yeaple, F., "Fluid Power Design Handbook," Third Edition, Revised and Expanded, Marcel Dekker, Inc., 1996

[86] Wilkinson, P. A., and Crolla, D. A., "Investigations into Alternative Suspensions for Commercial Vehicles," SAE 933048.

APPENDIX A

The specifications of the test rig are listed below:

Table A.1 Semi-Active Vibration Absorbers (SAVA)

Name	Model	Model Description	Manufacturer
Actuator	1.5KDXSR04.0	Bore size : 0.0381 m Rod diameter:0.0111m Effective piston area : 1.043×10^{-3} m^2 Stroke : $\pm$ 0.0508 m	Parker
Motor	RE035-071-33EAB200A	DC motor, Operating current : 3.06 A. Operating Voltage: 30V	Maxon motors
Flexible coupling	WAC22-4-6		Helical
Valve	SS-33VF4	Orifice dia.: 0.0048 m Flow coefficient : 0.9	Whitey Co.

Table A.2 Sensors, electronic circuit and hardware for the PC-based control system

Name	Model	Model Description	Manufacturer
LVDT #1	DLE-2000	Stroke : ±0.0508 m	Sensotec
LVDT #2	MDLC-1000	Stroke : ±0.0254 m	Sensotec
LVDT #3	AC100	Stroke : ±0.127 m	Solartron
LVDT modulator	1000-0012		Trans-Tek Corp.
Absolute pressure sensor	LM/2345-10	Pressure range : 6.9 MPa Output:21mV @6.9MPa	Sensotec
Accelerometer	3021-005-N	5g max. Output : 8 mv/g	IC Sensors
Encoder	HEDS-5540	Res.: 500 counts/rev.	Hewlett Packard
Current amplifier		2 channel	Controls Lab, OU
Voltage amplifier		8 channel	Controls Lab, OU
ADA board	ADA3100	AD : 8 channel, DA : 2 channel	RTD (Real Time Devices, Inc.)
HCTL2020 decoder board		Hewlett Packard HCTL2020 quadrature decoder/counter interface IC	Controls Lab, OU
DIO board	CIO-DIO 24	For HCTL2020 decoder board	Computer Boards, Inc

Table A.3 Active hydraulic power supply units and vibrating stand

Name	Model	Model Description	Manufacturer
Servo valve	76-263	Flowrate : 0.63 liter/sec	Moog
Actuator	2.5KJJ 2H KT24/24A-10	Bore size : 0.0635 m Stroke : $\pm$0.127 m	Parker
Electric motor	R-8905-01-436	15 HP, 260 V, 3 phase	US Motors
Hydraulic pump	AA10VSO28-DFR	Axial variable displacement piston pump Capacity : 0.8 liter/sec	Rexroth
Accumulator	A2A0058A1K	Piston type Capacity : 0.95 liter	Parker
Linear bearing	TWA 16	Low friction sliding unit	Nippon Bearing Co.
Self aligning coupler	FAC-1250-F	Compensate 2° angular error and 1/16 lateral misalignment	E&E Engineering Inc.

Table A.4 Parameters of SAVA for a heavy truck (Chapter Five)

Symbols	A_p	A_{vmax}	$V_{t,\ t=1,2}$	β
Unit	m^2	m^2	m^3	N/m^2
Values	1.824×10^{-3}	1.8096×10^{-5}	2.317×10^{-4}	8.61×10^{7}

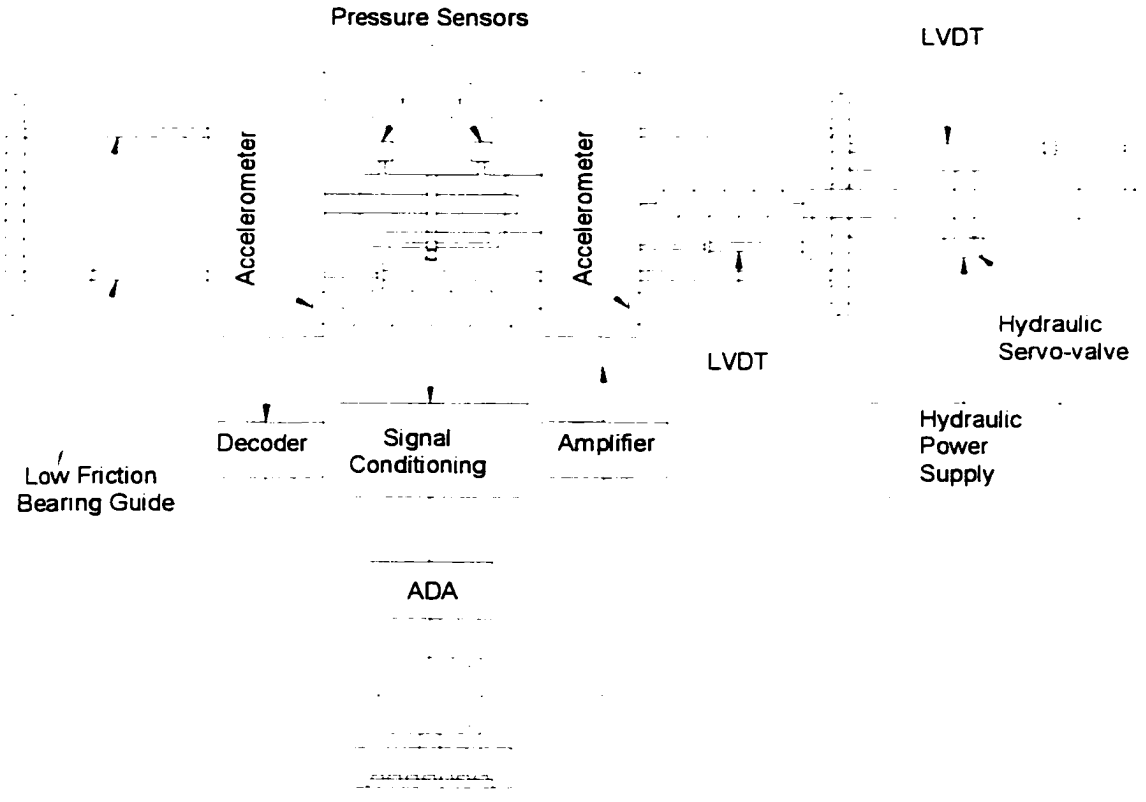

Figure A.1 Schematic representation of experimental setup

APPENDIX B

The performance index given by Equation (4.11) can be rewritten as;

$$J = \lim_{T \to \infty} \frac{1}{2} \int_0^T \{X^T Q X + 2X^T N f + f^T R f + 2X^T Q_2 X_d + X_d{}^T Q_1 X_d\} dt \qquad \text{(B.1)}$$

Matrix Q:

(1) for Cases (a) and (b) of Chapter 4

$$\begin{aligned}
Q(1,1) &= \rho_1 \frac{k_1^2}{m_1^2} + \rho_2 + \rho_3 \frac{k_1^2}{m_2^2} \\
Q(1,2) &= -\rho_1 \frac{k_1^2}{m_1^2} - \rho_2 - \rho_3 \left(\frac{k_1^2}{m_2^2} + \frac{k_1 k_2}{m_2^2} \right) \\
Q(1,3) &= \rho_1 \frac{k_1 c_1}{m_1^2} + \rho_3 \frac{k_1 c_1}{m_2^2} \\
Q(1,4) &= -\rho_1 \frac{k_1 c_1}{m_1^2} - \rho_3 \left(\frac{k_1 c_1}{m_2^2} + \frac{k_1 c_2}{m_2^2} \right) \\
Q(2,2) &= \rho_1 \frac{k_1^2}{m_1^2} + \rho_2 + \rho_3 \left(\frac{k_1}{m_2} + \frac{k_2}{m_2} \right)^2 + \rho_4 \\
Q(2,3) &= -\rho_1 \frac{k_1 c_1}{m_1^2} - \rho_3 \left(\frac{k_1 c_1}{m_2^2} + \frac{k_2 c_1}{m_2^2} \right) \\
Q(2,4) &= \rho_1 \frac{k_1 c_1}{m_1^2} + \rho_3 \left(\frac{k_1 c_1}{m_2^2} + \frac{k_1 c_2}{m_2^2} + \frac{k_2 c_1}{m_2^2} + \frac{k_2 c_2}{m_2^2} \right) \\
Q(3,3) &= \rho_1 \frac{c_1^2}{m_1^2} + \rho_3 \frac{c_1^2}{m_2^2} \\
Q(3,4) &= -\rho_1 \frac{c_1^2}{m_1^2} - \rho_3 \left(\frac{c_1^2}{m_2^2} + \frac{c_1 c_2}{m_2^2} \right) \\
Q(4,4) &= \rho_1 \frac{c_1^2}{m_1^2} + \rho_3 \left(\frac{c_1}{m_2} + \frac{c_2}{m_2} \right)^2
\end{aligned} \qquad \text{(B.2)}$$

(2) relative coordinates system, Equations (4.15) and (4.23)

$$
\begin{aligned}
Q(1,1) &= \rho_1\left(\frac{k_1^2}{m_1^2}+\frac{k_1^2}{m_1 m_2}+\frac{k_1^2}{m_2^2}\right)+\rho_2+\rho_3\frac{k_1^2}{m_2^2}\\
Q(1,2) &= -\rho_3\frac{k_1 k_2}{m_2^2},\quad Q(1,3)=\rho_1\frac{k_1 c_1}{m_1^2}+\rho_3\frac{k_1 c_1}{m_2^2}\\
Q(1,4) &= -\rho_3\frac{k_1 c_2}{m_2^2},\quad Q(2,2)=\rho_1\frac{k_2^2}{m_2^2}+\rho_3\frac{k_2^2}{m_2^2}+\rho_4\\
Q(2,3) &= -\rho_3\frac{k_2 c_1}{m_2^2},\quad Q(2,4)=\rho_3\frac{k_2 c_2}{m_2^2}\\
Q(3,3) &= \rho_1\left(\frac{c_1^2}{m_1^2}+\frac{c_1^2}{m_1 m_2}+\frac{c_1^2}{m_2^2}\right)+\rho_3\frac{c_1^2}{m_2^2}\\
Q(3,4) &= -\rho_1\frac{c_1 c_2}{m_2^2},\quad Q(4,4)=\rho_1\frac{c_2^2}{m_2^2}+\rho_3\frac{c_2^2}{m_2^2}
\end{aligned}
\tag{B.3}
$$

and

$$
\begin{aligned}
&Q(2,1)=Q(1,2),\quad Q(3,1)=Q(1,3),\quad Q(3,2)=Q(2,3)\\
&Q(4,1)=Q(1,4),\quad Q(4,2)=Q(2,4),\quad Q(4,3)=Q(3,4)
\end{aligned}
\tag{B.4}
$$

Matrices N and R:

(1) Cases (a)

$$
N=\begin{bmatrix}
\rho_1\dfrac{k_1}{m_1^2}+\rho_3\dfrac{k_1}{m_2^2}\\
-\rho_1\dfrac{k_1}{m_1^2}-\rho_3\left(\dfrac{k_1}{m_2^2}+\dfrac{k_2}{m_2^2}\right)\\
\rho_1\dfrac{c_1}{m_1^2}+\rho_3\dfrac{c_1}{m_2^2}\\
-\rho_1\dfrac{c_1}{m_1^2}-\rho_3\left(\dfrac{c_1}{m_2^2}+\dfrac{c_2}{m_2^2}\right)
\end{bmatrix},\quad R=\frac{\rho_1}{m_1^2}+\frac{\rho_3}{m_2^2}
\tag{B.5 a, b}
$$

(2) Cases (b)

$$N = \begin{bmatrix} \rho_3 \dfrac{k_1}{m_2^2} \\ -\rho_3\left(\dfrac{k_1}{m_2^2} + \dfrac{k_2}{m_2^2}\right) \\ \rho_3 \dfrac{c_1}{m_2^2} \\ \rho_3\left(\dfrac{c_1}{m_2^2} + \dfrac{c_2}{m_2^2}\right) \end{bmatrix}, \quad R = \frac{\rho_3}{m_2^2} \qquad \text{(B.6 a, b)}$$

(3) system (4.15)

$$N = \begin{bmatrix} -\rho_3 \dfrac{k_1}{m_2^2} \\ \rho_3 \dfrac{k_2}{m_2^2} \\ -\rho_3 \dfrac{c_1}{m_2^2} \\ \rho_3 \dfrac{c_2}{m_2^2} \end{bmatrix}, \quad R = \frac{\rho_1}{m_2^2} + \frac{\rho_3}{m_2^2} \qquad \text{(B.7 a, b)}$$

(4) system (4.23)

$$N = \begin{bmatrix} \rho_1 \dfrac{k_1}{m_1^2} + \rho_3 \dfrac{k_1}{m_2^2} & -\rho_3 \dfrac{k_1}{m_2^2} \\ -\rho_3 \dfrac{k_2}{m_2^2} & \rho_3 \dfrac{k_2}{m_2^2} \\ \rho_1 \dfrac{c_1}{m_1^2} + \rho_3 \dfrac{c_1}{m_2^2} & -\rho_3 \dfrac{c_1}{m_2^2} \\ -\rho_3 \dfrac{c_2}{m_2^2} & \rho_3 \dfrac{c_2}{m_2^2} \end{bmatrix} \qquad \text{(B.8)}$$

$$R = \begin{bmatrix} \rho_1\left(\frac{1}{m_1^2} + \frac{1}{m_1 m_2} + \frac{1}{m_2^2}\right) + \frac{\rho_3}{m_2^2} & -\frac{\rho_3}{m_2^2} \\ -\frac{\rho_3}{m_2^2} & \frac{\rho_1}{m_2^2} + \frac{\rho_3}{m_2^2} \end{bmatrix} \tag{B.9}$$

IMAGE EVALUATION
TEST TARGET (QA-3)

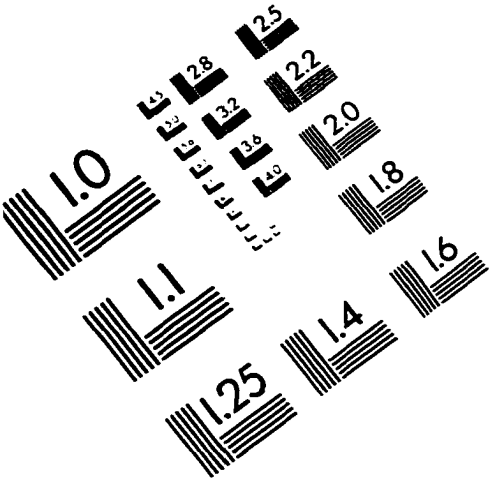

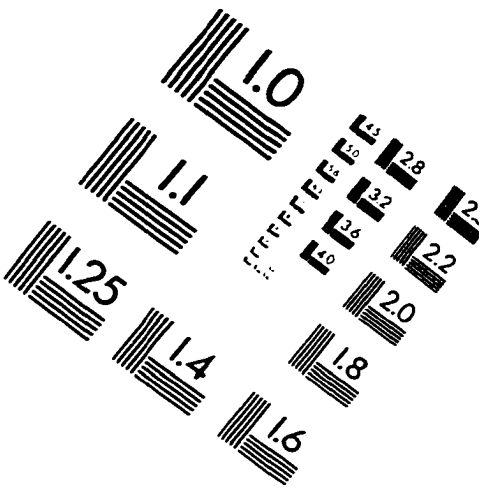

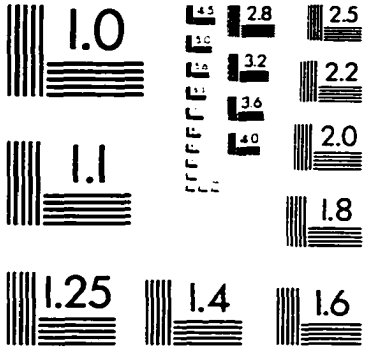

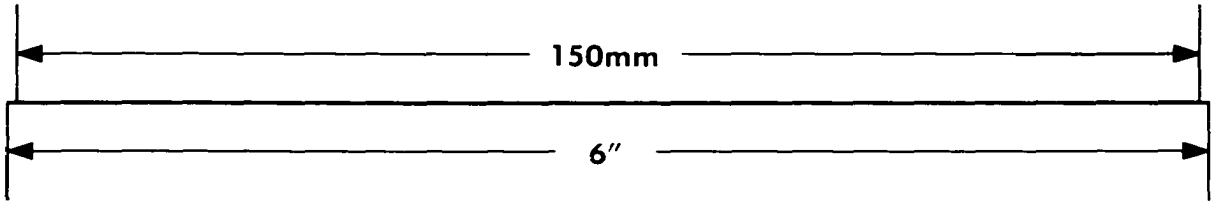

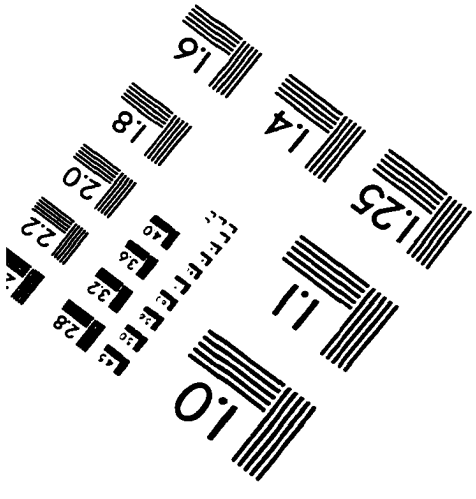

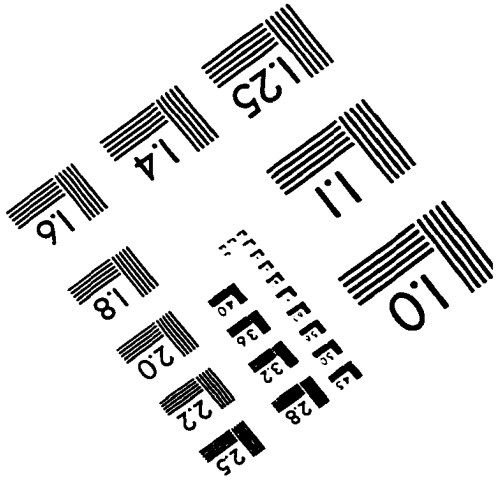

APPLIED IMAGE, Inc
1653 East Main Street
Rochester, NY 14609 USA
Phone: 716/482-0300
Fax: 716/288-5989